In presenting the dissertation as a partial fulfillment of the requirements for an advanced degree from the Georgia Institute of Technology, I agree that the Library of the Institute shall make it available for inspection and circulation in accordance with its regulations governing materials of this type. I agree that permission to copy from, or to publish from, this dissertation may be granted by the professor under whose direction it was written, or, in his absence, by the Dean of the Graduate Division when such copying or publication is solely for scholarly purposes and does not involve potential financial gain. It is understood that any copying from, or publication of, this dissertation which involves potential financial gain will not be allowed without written permission.

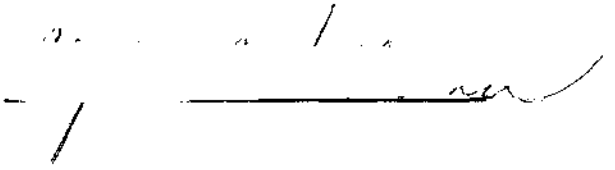

7/29/68

AN INVESTIGATION OF THE STRENGTH-DEFORMATION CHARACTERISTICS OF TWO SOILS TESTED UNDER HIGH CONFINING PRESSURES IN THE TRIAXIAL CELL

A THESIS

Presented to

The Faculty of the Graduate Division

by

Clyde Nelson Holland

In Partial Fulfillment

of the Requirements for the Degree

Doctor of Philosophy

in the School of Civil Engineering

Georgia Institute of Technology

January, 1971

AN INVESTIGATION OF THE STRENGTH-DEFORMATION CHARACTERISTICS OF TWO SOILS TESTED UNDER HIGH CONFINING PRESSURES IN THE TRIAXIAL CELL

Approved:

Dr. B. B. Mazanti, Chairman

Professor G. F. Sowers

Dr. C. Weaver

Date approved by Chairman: 8/11/72

ACKNOWLEDGMENTS

Grateful acknowledgment is expressed to all of those who participated in the development of this work.

In particular the writer wishes to thank Dr. B. B. Mazanti for his efforts.

Special thanks are extended to Professor G. F. Sowers, Dr. W. Brumund, Dr. R. Barksdale and Dr. C. Weaver who served as reading committee members, as well as to Mr. A. E. Jackson, Jr. who provided invaluable assistance in the laboratory phase of the work.

The financial assistance of the Corps of Engineers, Waterways Experiment Station, Vicksburg, Mississippi, is also acknowledged.

TABLE OF CONTENTS

LIST OF TABLES

LIST OF ILLUSTRATIONS

Figure Page

SUMMARY

The increasing use of high earth dams, heavy structures, and nuclear energy for excavation is placing demands on the soils engineer for information on the strength-deformation characteristics of soils under very high pressures.

For research and design the triaxial test with lateral pressures of 100 psi or less has to date been the major source of information. To supplement these data a program was completed wherein two soils were studied under triaxial loading conditions to lateral pressures of 10,000 psi.

The samples were formed in the partially saturated condition and all tests were undrained. The testing program included standard triaxial testing, standard triaxial testing with cycles of the confining pressure and/or the axial load, constant stress ratio tests and no-lateral-strain tests.

In the partially saturated condition the soil strength increased with increased confinement. Upon saturation the Mohr envelope became horizontal.

The samples tested under constant stress ratio conditions were, in general, weaker than similar samples tested under standard triaxial conditions.

The K_o values increased with confinement and reached a maximum value of approximately 0.9.

The results for the various tests were compared. No relationship between E, G and Poisson's ratio for the different test procedures was found.

CHAPTER I

STATEMENT OF THE PROBLEM

The history of soil mechanics can be divided into two periods--the time prior to 1920, and the years after.

Before the works of Terzaghi in the early 1920s, soils were utilized as an engineering material under all types of moisture and climatic conditions with little or no understanding of soil physics or soil mechanics other than empirical results collected by experience. During this first period there were few analytical and experimental techniques developed to explain the phenomena associated with the use of soils as an engineering material. The most significant early works produced in soil mechanics included those of Coulomb (1)[1] on earth pressure, Collin (2) on slope stability, Rankine (3) on earth pressures, and Atterberg (4) on the effect of water on soil properties. In general, these works represent investigations of a single problem. During this interval no concentrated effort was undertaken on the part of any individual or group to explain the physical and mechanical properties of soils.

With the advent of the second period of development, after 1920, came an increased interest in soil mechanics. To add to the knowledge previously collected concerning the strength properties, and to explain

---

[1]Numbers in parentheses indicate references in the Bibliography.

the mechanism of soil deformation and failure, many techniques as well as testing devices were developed. Most notable of the so-called strength testing devices were the direct shear test (5), the triaxial test (6), the torsion test (7), the vane shear test (8), and others such as the penetration test.

Each of these devices was developed to investigate one or more of the parameters associated with the strength and deformation properties of soils. Perhaps the most widely used, both for general design information as well as research, has been the triaxial test. Its advantages, including a wide range of controlled stresses as well as control over the soil water, account for its widespread use. One of the major disadvantages of the traixial test, however, is a nonuniform stress distribution throughout the sample resulting from end cap restraint. In the triaxial apparatus, normal practice utilizes lateral pressures of 100 pounds per square inch or less and gives no consideration to the effects of higher pressures on the properties of soils.

Present day practice, particularly in such practical problems as earth dam construction, bearing capacity of deep foundations, the use of nuclear energy for excavation, and the design of the national defense system requires a knowledge of soil properties (linear and bulk elastic moduli, tensile and compressive strengths, fatigue behavior, creep characteristics, and dynamic properties) under pressures greater than 100 pounds per square inch and far in excess of those capable of being generated and used in most existing laboratories. Since the direct measurement of the engineering properties of soils under conditions

simulating those encountered during nuclear blast is impractical, a concentration must be made on determining the mechanical properties under the maximum obtainable confining pressures. At the same time, an understanding of the mechanics of deformation must be obtained so that extrapolation to other stress states is possible.

It is believed that pressures of 10,000 pounds per square inch are the first practical step toward the explanation of soil properties in a high pressure environment. Thus, the intent of this research was to supply information on the compression and strength properties of two soils in the range of 100 to 10,000 pounds per square inch confinement.

The soils investigated were provided by the U. S. Army Corps of Engineers, Vicksburg, Mississippi; they were a clayey sand (SC) from New Mexico and a low plasticity clay (CL) from Canada. The investigation was conducted by forming samples of each soil and subjecting these samples to various stress states in a triaxial cell.

It was further intended that the project would provide basic information on materials and testing techniques so that additional work to pressures higher than 10,000 pounds per square inch could be conducted.

CHAPTER II

HISTORICAL REVIEW OF HIGH PRESSURE TESTING

The effect of pressures on the properties of materials has been of interest for centuries. One of the first recorded experiments involving pressure effects on material properties was in the year 1762 when Canton (9) published his experiments to prove that water was incompressible. From 1762, to the latter part of the 19th century, the volume change of liquids, namely water, occupied the thoughts of most of those who performed high pressure tests. This period produced some notable experimentors such as Perkins (10) and Parsons (11).

During the period after 1850, the range of interest spread from liquids to gases as well as to the effects of pressure on the conduction of electricity. Toward the latter part of the 19th century, the field of interest included not only liquids and gases, but solids and solutions.

The 20th century showed an increased interest in the effects of pressure on most materials of concern to the scientist and engineer and for the first time produced men who approached this problem as their primary interest, not as a single experiment. Richards (12) did much to advance the knowledge of high pressure effects. His papers and results were published mainly in conjunction with his students and covered the period from 1903 to 1928. In 1906, Bridgman, the century's leader in high-pressure research, began the work which was to continue

until the early 1960's. Several bibliographies have been prepared of Bridgman's publications, the most complete being that published by ASME (13).

In 1911 Von Karman (14) performed the first triaxial test, as we now recognize it, on rocks. Griggs (15) under the direction of Bridgman, continued the triaxial testing of rocks with essentially the same equipment designed by Von Karman. On the effects of both elevated pressures and temperatures, the work of Handin et al. (16), and Heard (17) are noteworthy. The tests of Handin and Heard were performed in the triaxial device. Schwartz (18) reports on an investigation of the strength of rock at confining pressures up to 10,000 pounds per square inch and pore pressures up to 5,000 pounds per square inch. Mazanti (19) reports on a series of tests on rock samples. The test specimens were hollow cylinders and were tested at pressures up to 15,000 pounds per square inch differential between the inside and outside. To date, no such tests have been reported for soil.

Since the latter part of the 1950s, there has been an increasing interest in the properties of soils under very high confining pressures. The following section reviews the works on this topic that have been published to date.

CHAPTER III

LITERATURE SURVEY--HIGH PRESSURE TESTING OF SOILS

Before 1945, no literature was found which reported on high pressure tests of soils. After this date, Ural (20) reported a series of tests investigating the compressibility of sands and remolded clays under high pressure. This work was performed in a consolidation device with a sample size of 1.50 in. diameter and 0.50 in. height. The consolidometer rested on a bed of springs and was loaded by means of a 25-ton screw jack. Ural reports:

> The void ratio *e*-log of pressure *p* curves for remolded clay leads to the following observations. The curve is not straight, but has a gently decreasing slope between values of pressure increasing from 1 to 2000 tons per square foot (27,800 pounds per square inch) although there is some indication that the slope may be constant at values of *p* about 2000 tons per square foot (27,800 pounds per square inch). There is no tendency at the greatest pressure observed for the curve to approach a horizontal tangent.

Terzaghi and Peck (21) discuss high-pressure consolidation tests, and report that the consolidation test of a remolded clay showed a void ratio *e* versus log of pressure *p* curve similar to a mixture of 90 per cent sand and 10 per cent mica, but that the void ratio of the clay at any given pressure is smaller than the corresponding void ratio of the sand-mica mixture. The curves for the soft clay were reported to start with a horizontal tangent and the slope of the middle part was observed to decrease so slightly throughout the range from about 1 to 2000 kilograms per square centimeter (28,446 pounds per square inch)

that the curve could essentially be regarded as a straight line. The curves were then reported to approach a horizontal tangent. Smith (22) investigated the Fort Union Clay shales. The material was tested in a specially-designed consolidation device to pressures of 500 tons per square foot (6950 pounds per square inch). The resulting void ratio *e* log of pressure *p* curves illustrated first a straight line section, then a curved section, and from 100 to 500 tons per square foot (6950 pounds per square inch) essentially a straight line with no indication of any horizontal inclination at the greatest loads. Esrig, Davison, and Peck (23) report on a series of tests investigating the consolidation of soils at pressures of 2000 tons per square foot (27,800 pounds per square inch). The samples tested were obtained from the Lake Maracaibo oil fields in Venezuela and ranged from heavily consolidated shales, to laminated sands and shales. The conclusions included the following:

1. At some pressure in the neighborhood of 100 TSF the compression index is appreciably reduced.

2. The test data indicated that the coefficient of consolidation C_v approaches a constant at high pressures.

Chilingar and Knight, 1960 (24), report on the consolidation of kaolinite, illite, and montmorillonite clays at pressures up to 200,000 pounds per square inch. The work was carried out to study the relationship between the water content and pressure in the above-mentioned materials. Samples of one-half-inch diameter and pressures from 40 to 200,000 pounds per square inch were employed. The authors did not

report on the consolidation characteristics in the form of a void ratio *e* versus log of pressure *p* plot, but they did illustrate plots of water content (percentage of dry weight) versus the load. The following conclusions resulted which indicated several factors concerning the consolidation characteristics.

1. From 40 to 200,000 pounds per square inch, a linear relationship exists between the moisture content (percentage of dry weight) and the logarithm of pressure for the kaolinite-illite clays. The curve for the illite clays has a steeper slope than that of the keolinite clay. The linear relationship possibly suggests that compaction is more or less a simple continuous process in this pressure range.

2. For montmorillonite clay, a break in the curve is present at about 1000 pounds per square inch. Above 1000 pounds per square inch and up to 200,000 pounds per square inch the moisture content versus logarithm of pressure curve is a straight line; however, its slope is steeper than that of either kaolinite or illite. Possibly up to 1000 pounds per square square inch a free liquid is squeezed out, whereas at higher pressures up to 200,000 pounds per square inch, an oriented water is being removed.

For a saturated sample, the relationship between the void ratio *e*, the volume of water V_w, the volume of solids V_s, is such that *e* equals V_w/V_s. This relationship suggests that the curves of water content (percentage of dry weight versus log pressure *p*) presented by Chilingar could indicate the general shape of the corresponding *e* versus log of pressure *p* curve. An inspection of these curves shows no

inclination of either of the clays to assume a horizontal shape at pressures up to 200,000 pounds per square inch.

DeBeer (25) discusses the results of tests on sand in a steel ring 2 centimeters in height with a diameter of 10 centimeters. The load was applied through a piston and was a maximum of 2,800 kilograms per centimeter squared (approximately 40,000 pounds per square inch). The results plotted in the form of load versus settlement indicate that from zero to 150 kilograms per square centimeter (2,135 pounds per square inch), the gradient of settlement increases when the unit pressure increases, and from 350 kilograms per centimeter squared (4,980 pounds per square inch), the gradient of settlement regularly decreases with increasing unit pressure.

High pressure triaxial testing of soil is a relatively recent development. As previously reported, high-pressure triaxial devices (14) have been in use since the early days of the century, but their application to a study of soil mechanics did not develop until the late 1940s and early 1950s.

Blanks and McHenry (26) report a triaxial device capable of lateral pressures of 125,000 pounds per square inch with large samples (6 in. diameter x 12 in. height). This device was designed primarily to test concrete and rock but tests on soils were anticipated. To date, no such results or data on soil tests employing this device are available. Golder and Akroyd (27) announced the construction of a triaxial device capable of lateral pressures of 1000 pounds per square inch and designed to test hard soils and soft rocks. The authors state

that a wide range of materials including soft to hard sandstone, clay shale, shale, limestone, artificially cemented sand and compacted stabilized soil had been successfully tested in the apparatus. The results presented were Mohr's circles for a soft sandstone with lateral pressures up to 80,000 pounds per square foot (555 pounds per square inch), a soil consisting of 78 per cent sand, 22 per cent clay with lateral pressures up to 120,000 pounds per square foot (approximately 835 pounds per square inch) and crushed stabilized rock to lateral pressures of 80,000 pounds per square foot (555 pounds per square inch). The first two plots indicate a straight line envelope, and in the third, no envelope was drawn. The results of all tests were too limited to allow any conclusions concerning the properties of the materials tested.

From 1954 to 1963, there were no published reports on high pressure triaxial testing of soils found in the literature. In 1963, several efforts in this area were reported. These included an unpublished series of tests by Hirschfeld (28). This report involves the testing of undisturbed silt samples, 3.58 centimeters in diameter with a height of 8.5 centimeters, at pressures up to 40 kilograms per centimeter squared (570 pounds per square inch) in the triaxial *S* or slow test. These results indicated that the Mohr envelope was curved over the entire range of lateral pressures employed and that the slope of the envelope decreased with increasing lateral pressure, that the volume change characteristics depend on the confining pressures; for low confining pressures, all specimens expanded near failure, while at

high confining pressures, they contracted. Hirschfeld and Poulos, (1963 (29), reported on triaxial *S* or slow tests on a compacted sand and an undisturbed silt to confining pressures of 40 kilograms per centimeter squared (570 pounds per square inch). For both soils, the *S* envelope was curved; both soils exhibited a net increase in volume during shear at low confining pressures and a net decrease in volume during shear at high confining pressures. The curvature of the envelope illustrated the perils of interpolating from tests at low confining pressures and was attributed to the effects of volume changes which occurred during shear. It is interesting to note that the failure strain (axial strain corresponding to maximum deviator stress, sigma one minus sigma three) increased slightly with confining pressures. Further, at strains larger than the failure strain, the deviator stress decreased. This article also describes the high pressure triaxial cell employed for this series of tests.

Hall and Gordon (30) report on high pressure (650 pounds per square inch maximum confining pressure-specimen: maximum diameter - 12 in) triaxial tests on the proposed embankment material for the Oroville Dam. The equipment employed in these tests is described in reference (31). The testing program instigated the following conclusions:

1. The slope of Mohr's failure envelope for sandy and gravelly soils tested in this program decreased with increasing lateral pressure.

2. The decrease in slope is inferred to be principally related to particle breakdown. Most of this breakdown occurs under shearing strains, with minor effects occurring during compaction and consolidation.

3. Particle degradation is a function of the gradation of the individual soils with the better-graded soil displaying the least degradation.

4. Within the range of pressures used in this program, no similar decrease in slope of the Mohr envelope with increase in lateral pressure was noted for clayey and silty materials, even with a substantial percentage of plus No. 4 sieve sizes.

Volume change in all tests were as previously described by Hirschfeld, and Hirschfeld and Poulos (28,29).

Barksdale (32) at the Georgia Institute of Technology, Atlanta, Georgia, performed a series of tests on sand at high confining pressures. Sample size was 2.22 centimeters in diameter and 4.5 centimeters in height, with a maximum confining pressure of 648 kilograms per centimeter squared (approximately 9200 pounds per squareinch). This work was presented at the conference on Laboratory Shear Testing of Soils at Ottawa, Canada, in September of 1963, by Vesic and Barksdale (33). Essentially, the results correspond with those of Hirschfeld (28) and Hirschfeld and Poulos (29). However, Vesic and Barksdale noted that the stress-strain curves under both high and low confining pressures were of the same shape; that all samples failed in bulging without pronounced ruptured surface; that there was a decrease in volume under the initial confining stress, and, with high confining pressures, this decrease was noted throughout the test. Unlike Hirschfeld and Poulos (29), Vesic and Barksdale found Mohr's envelope to be composed of essentially two straight lines with a transition at approximately 50

kilograms per centimeter squared (6950 pounds per square inch) confining pressure. It is interesting to note that with the sand tested at a constant mean stress of 48.3 tons per foot squared (671 pounds per square inch), there was little if any volume change throughout the test. The conclusion derived by the reporting authors are as follows:

1. The well-known phenomenon of dilatancy of dense cohesionless materials occurs at low pressures only. Beyond a certain critical pressure, which in the case of Chattahoochee River sand is about 50 kilograms per centimeter squared, the shear is made possible by crushing and breaking of soil particles.

2. The frictional component of the shear strength of the sand tests appears to be proportional to the normal stress in the entire range tested (up to 9900 pounds per square inch). The dilatance component of the strength, however, appears to reach a peak at about one-half the critical pressure and to vanish at the critical pressure.

Clough (34) reports on triaxial tests of sands to pressures of 10,000 pounds per square inch. This work is quite thorough and includes not only normal triaxial tests, but tests with a constant octahedral stress. The conclusions derived by Clough are as follows:

1. The strength envelope for dense sand has significant curvature between 0 and approximately 700 psi due primarily to dilatation.

2. The strength envelope for both loose and dense sand in the pressure range from 700 psi to 9000 psi may be approximated by a straight line and has a slope angle of 32.4 degrees.

3. Initial void ratio ceases to affect shear strength characteristics above 700 psi, and volume change characteristics above 2800 psi.

4. Crushing of grains becomes an important phenomenon at chamber pressures as low as 300 psi and increases, but not linearly, with confining pressure. Crushing of grains is increased by application of shearing forces to an isotropically confined sample.

5. Volume change throughout shear for loose sands is a decrease from chamber pressures of 0 to 9000 psi; whereas, for a dense sand volume increases from chamber pressures of 0 to about 425 psi and decreases past 425 psi.

Patterson (35) reports on triaxial tests at confining pressures up to 10,000 kilograms per centimeter squared (142,200 pounds per square inch). The testing program included samples of copper, cast iron, limestone, marble, granite, sandstone, and serpentinite. No tests were performed on soil samples of any kind. Bishop (36) discusses the design of a triaxial cell for lateral pressures of 1,000 pounds per square inch. This work also describes very limited drained test results obtained from a stiff fissured clay and a sand. Vesic and Clough (37) arrived at essentially the same conclusions as Clough (34).

A careful review of the existing work on soil properties in a high pressure environment indicates that knowledge in this area is lacking. In instances where data are available, there is often conflicting observation. Ural (20) reports that in a consolidation test on remolded clays, the void ratio e-log of pressure p curve is not straight and, at

a pressure of 27,800 psi, there is no tendency for the curve to approach a horizontal tangent. Terzaghi and Peck (21) report the opposite and state that to 28,400 psi pressure a remolded clay will have a void ratio e-log of pressure p curve which can be considered straight. Chilingar and Knight (24) report results which suggest that the void ratio e-log of pressure p plot for kaolinite, illite, and montmorillonite, would be a straight line to pressures of 200,000 psi and that at this pressure there is no tendency for the plot to approach a horizontal tangent. Smith (22) and Esrig, Davison, and Peck (23) agree on the shape of the void ratio e-log of pressure p plot for shales and indicate that to 27,800 psi pressure, the materials display a straight line section followed by a curved section then a straight section with no tendency to approach a horizontal tangent.

Under triaxial test conditions, published results indicate that the Mohr envelope for sands is not straight and that its slope decreases with increasing confining pressures, that there is a volume decrease throughout the entire triaxial test under high confining pressures; that the phenomenon of dilatancy does not occur at high confining pressures. For silts under slow triaxial test conditions, it is reported that the Mohr envelope is curved and that the slope of the envelope decreases with increased confining pressures, that the volume change characteristics are a function of pressure with all specimens increasing in volume at failure for low confining pressures and decreasing in volume for high confining pressures. For clays, only one series of tests (consolidated undrained) have been completed; these were at 900 psi confinement,

Bishop (36). It is reported that the Mohr envelope appears to be sensitive to confining pressure levels, decreasing in slope with increasing confinement, that at low confining stress levels the samples failed at 2 to 3 per cent axial strain, after which the axial load decreased sharply, and at high confining stress levels the samples continued to shear at an almost constant stress level. Bishop (36) also reports that at high confining stress levels the clay showed a volume decrease throughout the test.

Past work on soils under high confining pressures in the triaxial cell have been concerned with dry and saturated sands (32,33,34), saturated silts (28,29), and one series of tests on a saturated clay (36). No work has been reported on partially saturated soils.

CHAPTER IV

TESTING PROGRAM

The purpose of this work was to investigate the strength deformation characteristics of two soils under high confining pressures in the triaxial cell. The samples were molded and partially saturated in the as-formed condition. All tests were undrained; thus, it was expected that, depending on the test procedure, the samples would be partially saturated or saturated.

The bulk modulus properties were investigated by a series of hydrostatic tests. The strength-deformation characteristics, modulus of deformation, and ratio of lateral strain to axial strain characteristics were measured under standard triaxial loading conditions.

To determine the effect of cyclic load applications, a series of tests were performed wherein the deviator stress was applied, removed and reapplied. In another test series and as a first step toward studying the effect of stress path on the strength-deformation characteristics, loads were applied such that the ratio σ_r/σ_a was constant.

This latter test series was followed by a loading sequence wherein the confining pressure was applied in such a fashion that the lateral strain was zero.

A description of each test procedure follows:

1. Standard triaxial tests were performed, wherein the shear load was applied after the application of a predetermined value of

confining pressure. Loading was continued to a desired strain value or to failure.

2. Tests were completed with cyclic loading of the hydrostatic compression phase and/or the triaxial shear phase. For the hydrostatic compression phase, the confining pressure was applied in increments to the maximum, then removed in the same increments, and reapplied. In the triaxial shear phase, loads were applied, removed and reapplied at the same strain rate. In the hydrostatic cycling tests, the number of cycles never exceeded two. For the shear phase, the cycles varied generally from one to four with several to nine cycles.

3. Constant stress ratio tests were performed wherein the axial and confining loads were applied such that a constant ratio existed between the lateral and vertical stresses. These tests were carried out with initial confining pressures varying between zero and 3200 psi.

4. No lateral strain tests were completed by increasing the vertical load and adjusting the lateral pressure so that the specimen center diameter remained constant. These tests were carried out in the range of initial confining pressures from zero to initial confining pressures of 3200 psi.

With the exception of some constant stress ratio tests and some no-lateral-strain tests, all samples were subjected to a hydrostatic compression phase prior to the application of a shearing load. In all tests the load rate was 0.015 inches/minute and all were performed in an unconsolidated, undrained manner.

CHAPTER V

INSTRUMENTATION AND EQUIPMENT

The major portion of the equipment used on this project was designed, fabricated, and instrumented in the School of Civil Engineering at Georgia Institute of Technology.

Triaxial Cell

The triaxial cell, Figure 1, was designed to allow the testing of specimens up to two inches in diameter and with lengths up to five inches. The maximum hydrostatic working pressure of the cell is 10,000 psi. It consists of four basic parts: (1) the base, (2) the cylinder, (3) the gland, and (4) the load piston.

The base was machined from naval brass with a tensile yield strength of approximately 24,000 psi. The base diameter is eight inches with a threaded pedestal two inches in diameter. Two pressure ports are provided through the base. One port is for the confining pressure, while the second allows either the application of a pore pressure, the measurement of pore pressures, or drainage of the specimens.

The cylinder is of cold drawn seamless steel tubing with a yield strength of 55,000 psi. It screws to the base and is sealed by an O-ring between the pedestal and the cylinder. The internal diameter is 3-1/2 inches, the wall thickness is 13/16 inches, and the length is 12-13/16 inches. Two ports were provided in the cylinder wall. One was

used as either a pressure port or as an air escape port when filling the chamber with oil. The other port allowed the attachment of an electrical-lead manifold.

The gland screws into the top of the cylinder and serves as a guide for the piston. It is made of naval brass. Sealing is accomplished by means of an O-ring between the gland and the cylinder as well as between the gland and the piston. Although three O-ring grooves were provided for sealing the piston, it has been found satisfactory to use only one. A different gland was used for each of the two piston sizes.

The pistons are of polished alloy steel with a yield strength of approximately 150,000 psi. The diameters were 7/8 inch and 1.40 inch.

Pressure Generating System

For undrained compression and shear testing, the pressure generating and regulating system used is shown schematically in Figure 2. An air-operated hydraulic pump is used as the prime pressure source. The pump is essentially a pressure intensifier which is valved so that it is capable of re-cycling when the stroke limit is reached. The pump used is made by SC Hydraulic. It is a Model 10-500-16, and has a minimum fluid pressure capacity of 27,500 psi. The output pressure depends upon the applied air pressure and is continuously variable from approximately zero. The major disadvantage of the pump is that it can only "unload" a negligible amount.

In order to accurately control the confining pressure, there is included, in the line, a piston-cylinder arrangement. The piston is positioned by a bolt reaction member. The adjustment of the bolt either

forces the piston into the cylinder or allows it to move outward, thus causing the pressure in the line to increase or decrease, respectively.

In the constant stress ratio and no lateral strain tests it was necessary to rapidly adjust the confining pressure. In those cases, a manually-operated 10,000 psi hydraulic pump was utilized.

Confining pressures were measured by means of Heise Pressure Gages. The following set of gages was used:

Pressure Range	Accuracy, Percentage Full Scale
0-200 psi	0.5
0-400 psi	0.5
0-1,000 psi	0.5
0-20,000 psi	0.1

The gages were periodically checked against a standard transfer gage accurate to 0.1 per cent Full Scale. The standard gage was calibrated with a precision 20,000 psi dead load tester.

Auxiliary Equipment

Load Cells

Three different load cells were used to measure axial loads on the specimens. All were commercial load cells of the bonded wire, electric resistance type. For loads up to 2.5 kips, a Strainsert flat load cell was used. This cell has a nominal diameter of 2-1/4 inches and a thickness of 3/4 inches. Linearity of the cell as reported by the manufacturer is within 0.10 per cent. Full Scale and repeatability is 0.20 per cent Full Scale.

For loads up to 10 kips, a BLH load cell was used. The cell is approximately 4 inches in diameter by 6 inches in length. Linearity and repeatability are reported by the manufacturer to be equivalent to that given for the 2.5K load cell.

For loads up to 25 kips, a Strainsert flat load cell was used. The cell is 4-1/8 inch in diameter by 1-3/8 inch thick. Linearity and repeatability are as indicated for the 2.5K cell. All load cells were installed on the testing machine and then calibrated by proving rings. Total calibrations were performed at the beginning and end of any test series and when changing the load cell. Spot calibrations were performed every two weeks.

Strain Gage Indicator

All strain gage circuits were fed into a BLH Model 120C strain gage indicator. Those signals being recorded were re-transmitted through the scope output to the recorder.

Linear Motion Transducers

Linear motion transducers (LVDT's) were used for the measurement of axial deformations of the specimens. The devices are excited by an external 24 V.D.C. source and the output signal is sufficiently strong to go directly to a recorder. The LVDT's used were made by G. L. Collins Corporation, Model SS207, with a stroke length of ±1.00 inches. Linearity for these instruments is reported by the manufacturer to be 0.27 per cent.

The linear motion transducers were calibrated in place by using a special micrometer attachment. The micrometer read directly to 1/1000

inch. The output of these transducers was recorded. Check calibrations were run at least once per month.

The axial deformation of the sample was measured by two linear motion transducers mounted 180° apart on the testing machine outside the cell, Figure 3. Due to the mounting arrangement, the transducers recorded not only the sample deformation, but the combined deformation of the load cell piston, and the testing machine. The amount of equipment deformation was determined experimentally by assembling the cell and using a metal specimen. Loads were applied to this specimen under all proposed test conditions and the total deformation recorded. The deformation of the dummy specimen was calculated by the theory of elasticity and subtracted from the total deformation. The remainder was taken as the combined deformation of the equipment and was used as a correction factor in data reduction.

Prior to and after testing, the sample height was measured manually using calipers reading directly to 3/1000 inch.

Recorder

A Hewlett-Packard Model 135 Recorder was used for all automatic recording. This is a multi-range, general purpose X-Y plotter with ranges from 0.5 mv/inch to 50 v/inch. Accuracy, as reported by the manufacturer, is 0.2 per cent Full Scale and linearity is 0.1 per cent Full Scale.

Electrical Lead Manifold

This manifold was made of steel, yield strength of 150,000 psi, and contained electrical lead plugs manufactured by the Fusite

Corporation, Figure 4. These lead plugs or terminals were aluminum alloy, threaded with 1/16 inch pipe threads, the center conductor was separated from the housing by fused glass. Each manifold contained eight terminals.

Sample Membranes

The membranes were standard 1.40 inch diameter by 0.028 inch thick rubber. A single membrane was used up to 4 times.

The Lateral Deformeter

The deformation of the sample in a transverse direction was monitored by a lateral deformeter developed for this study. The deformeter consists of a ring attached to a sample base with three arms as shown in Figure 5. The arms are fixed to the base and bear against the sample at its initial mid-height. Each arm contains two strain gages fixed with Eastman 910 cement. The strain gages on the inner side of the arms are connected in series as are the outer gages. The output of the gages is read on a BLH 120C Readout Unit.

The lateral deformeter was calibrated by means of the step blocks shown in Figure 5. The blocks were machined so that the deformeter was calibrated over a diameter range of 1.20 to 1.70 inches. Calibration of the deformeter by step blocks indicated that 13.27 micro-inches was equivalent to 0.0001 inch diameter change.

The influence of pressure on the deformeter was determined by placing the deformeter in the triaxial cell and applying pressure to the confining fluid. The deflection of the rubber membrane was determined by:

1. Placing the deformeter in the cell with a standard size steel specimen and pressurizing.

2. Placing a rubber membrane over the steel specimen with the deformeter in contact with the membrane and pressurizing. The combined effect of pressure and membrane compression is shown in Figure 6. These effects result in a correction factor which indicates a diameter decrease.

The sample diameter before and after testing was obtained manually using calipers reading directly to 3/1000 inch.

Instrumentation and Measurements

Those calibrations and measurements necessary to the testing, data collection, and data processing not previously mentioned are discussed in this section. Table 1 lists the accuracy of each measurement.

It was a general laboratory procedure that all samples were measured for weight and volume before and after each test. After testing, selected samples were measured for shape changes; then the entire sample was used for a water content determination.

During hydrostatic compression, the sample height and diameter was recorded manually at the completion of each pressure increment. While applying the shearing load, the change in sample height was continuously recorded, and the sample diameter was noted and recorded manually at selected stress levels.

Piston Friction

In most tests, the influence of piston friction was nullified by the method of processing data. Prior to a shear test, the piston was above the sample top cap a sufficient distance so that a constant friction force had been generated as the piston moved down and touched the sample top cap, Figure 7. For data processing, the load, indicated by the load cell, at contact between piston and the sample top cap was subtracted from the total load as recorded by the load cell during the test. In those instances when it was necessary to account for the piston friction, it was determined by a loading test where the piston was forced into the cell at the desired confining pressure. Piston friction was checked every two weeks.

Load Rate

The load rate of the testing machine, 0.015 inches per minute, was checked by clock two times per month.

Sample Weight

The sample weight was determined by using a set of triple beam balances reading directly to 1/10 gram. The balances were zeroed prior to each weighing. With an average sample weight of 125 grams, the accuracy is 0.08 per cent.

Sample Volume

The sample volume before and after testing was determined by mercury displacement. See Figure 8. The displaced mercury was weighed on scales reading directly to 1.0 gram. The scales were zeroed prior to each weighing. With an average weight of displaced mercury being 1800 grams, the accuracy is 0.05 per cent.

Sample Shape

The sample shape after testing and pressure release was determined by placing it in a horizontal position on the bed of a milling machine and plotting points taken every 5/100 inch along its length using a 1/10,000 inch dial gage. The accuracy of measurement was a function of degree of curvation of sample shape, length of dial gage shoe, and degree of smoothness of the sample surface. It is estimated that the true diameter was within +0.10 per cent of the reported diameter.

Equipment Assembly

For the undrained testing program, specimens were selected at random from those previously formed. The one to be tested was removed from its wrappings, measured for length and diameter, and weighed. The volume was determined by mercury displacement.

The specimen was placed on the sample base and enclosed in a single rubber membrane (0.028 inches thick). Rubber bands sealed the membrane to the base.

The lateral deformeter, Figure 5, was carefully lowered over the specimen and attached to the base by screws. The top cap was placed on the sample and the membrane pulled taut over it and made secure by rubber bands. The assembly was then checked for vertical position and firm seating.

The triaxial cell, Figure 4, was attached to the cell base and internal electrical connections made and checked. Oil (SAE 20) was poured in the cylinder and the gland was screwed in place. To insure

that no air was entrapped, the oil level in the cell was such that oil was forced out as the piston guide was secured.

The load piston as inserted into the cell through the guide and onto the sample top. As the piston was forced into the cell, fluid drainage was allowed through a valve at the top of the cell.

This completed the assembly, and the unit was then manually transported to the loading machine and all electrical leads checked, Figure 9. A 2.0 psi seating load was applied to the fluid and initial reading recorded. The piston was then put in contact with the sample top cap, and the test was carried out.

CHAPTER VI

SAMPLE PREPARATION AND PROPERTIES

All soils used in this program were subjected to preliminary classification tests with the results as noted in Figures 10 and 11. The procedure for molding the samples prior to testing follows.

Prior to forming, all the soil was air dried, passed through a No. 4 sieve and the minus No. 4 sieve size was thoroughly mixed. This mixing was accomplished in a mechanical mixer with a final mixing performed manually.

Following the preliminary mixing, the desired quantity of water was added, the soil and water thoroughly mixed manually, mechanically, and finally manually. The moist soil was sealed in plastic bags and placed in a constant humidity room to cure. The curing lasted for at least seven days, after which the samples were formed.

The forming mold was a stainless steel tube with an ID of 1.385 inches and a wall thickness of 1/8 inch. The pistons used for compacting the sample were of aluminum and were machined to have a diameter 5/1000 inch less than the mold ID.

The actual molding of the 1.4 inch diameter by 3 inch high samples was accomplished by calculating the weight of soil required to yield a predetermined density. After obtaining this value, the weight required for each sample was measured. The mold was placed in an upright position with a bottom piston extending approximately 1/2 inch

into the mold. A machined brass funnel was placed on the mold top and the soil was poured into the mold through the funnel. All the soil required for a sample was placed in one operation. The top piston was put into position and the entire assembly was placed in a loading frame, Figure 12. A hydraulic jack was used to load the pistons so as to yield the desired length of sample. The length was measured by using a 1/1000 inch dial gage. During the application of load both the top and bottom piston moved into the mold while the load was rotated to minimize friction. At the proper length, the load was allowed to remain on the sample for a period of 30 seconds. After this time interval, the load was released, the forming pistons removed, mold inverted, the extruding piston inserted and the sample extruded from the mold by hydraulic power.

The sample was then weighed, measured for parallel ends, height and diameter. Each sample was wrapped in Saran wrap, placed in three plastic bags (each bag individually sealed) and stored in a constant humidity room until testing.

Sample Properties

Average index properties of the as-formed samples are given in Figures 10 and 11.

The density variation throughout the length of the samples was determined. For each soil type, samples were selected at random, measured for diameter and height using calipers reading directly to 0.01 centimeter (0.0039 inch). The samples were then weighed on scales reading directly to 0.10 gram and the volume determined by mercury

displacement. The sample was cut (perpendicular to the long axis) into thirds, and on each portion the above measurements were taken. The water content of each portion of the sample was then determined.

The McCormick Ranch Soil had an average dry density in the center section which was 5 per cent less than the average dry density of the end sections. The Watching Hill Soil had an average dry density in the center section which was 5.6 per cent less than the average dry density of the end sections.

Rotating the mold during the forming process did not minimize the reported density variations.

The moisture content-unit weight relationship for each soil is shown in Figure 13.

CHAPTER VII

RESULTS

Sample Deformation

McCormick Ranch Clayey Sand

Following hydrostatic compression the McCormick Ranch clayey sand samples were of the shape shown in Figur 14. For an average distance of 0.15 inches from either end the sample diameter remained constant and equaled the as-formed diameter. At distances greater than 0.15 inches from either end the sample diameter reduced and this reduction reached a maximum value at the sample mid-height. Each sample was symmetrical about a horizontal plane at its mid-height and the shape was the frustrum of a right cone.

Average values of axial and radial strains as functions of confining pressure during hydrostatic compression are shown in Figure 15.

The standard triaxial test, increasing the axial stress while maintaining a constant confining pressure, showed an increase in the sample diameter at mid-height for all values of axial load and confining pressures.

All samples tested under standard triaxial conditions failed by bulging with the maximum bulge occurring at the samples mid-height. There were no visible shear planes in any sample tested. Tension cracks were visible in all samples which were tested to axial strain values exceeding 12 per cent.

Samples tested under constant stress ratio conditions (σ_r/σ_a = constant) deformed and failed in the manner previously described for the standard triaxial test.

Watching Hill Clay

Following hydrostatic compression the Watching Hill clay samples were of the shape shown in Figure 16. The dimensions shown in this figure were used to calculate the sample volume. Those dimensions, excepting the diameter at mid-height, which were functions of confining pressure are listed in Table 2.

For all test conditions other than hydrostatic, the clay samples reacted to load and failed exactly as described for the McCormick Ranch sand samples under standard triaxial test conditions. A photograph of a typical sample of clay following the standard triaxial test at 6400 psi confinement is shown in Figure 17. Average values of axial and radial strain as a function of confining pressure are shown in Figure 18.

Volume Change

Average values of volumetric strain as a function of confining pressure are given in Figures 19 and 20. The data were obtained principally from volume measurements after load application. The plots show that the major volume reductions had occurred prior to the application of the 1600 psi confinement.

Hydrostatic Stress Cycling

Random samples of Watching Hill clay were subjected to one load-unload-reload cycle of hydrostatic stress. Testing involved the use of at least three separate samples for each value of confining

pressure. The process for each sample was to load in increments (100, 200, 400, 800, 1200, 1600, 3200, 6400, 10,000 psi) of pressure to a predetermined maximum value and then unload-reload in the same increments. Average results for the first load application are shown with volumetric strain as a function of confining pressure, Figure 20. Typical results for stress cycling using the same variables are given in Figure 21. Because of the difficulties of measuring small volume changes at high pressures, the reload data in Figure 21 is not considered accurate and is intended to show the trend only.

Standard Triaxial Tests

Standard triaxial tests, wherein the confining pressure was held constant while the axial load increased, were performed on the soils previously described. All such tests were undrained with no pore pressure measurements, and with a strain rate of 0.015 inches per minute. For each confining pressure used, at least three samples were tested. The results reported herein are averages.

McCormick Ranch Sand

Plots of total deviator stress (σ_a-σ_r) versus axial strain, ϵ_a, are presented in Figures 22 and 23.

Watching Hill Clay

Plots of total deviator stress (σ_a-σ_r) versus axial strain, ϵ_a, are presented in Figures 24, 25 and 26.

With regard to the plots in Figures 22-26, none displayed a decrease in deviator stress (σ_a-σ_r) with increases in axial strain. Rather, as the axial strain increased, there was a small increase in

deviator stress, $(\sigma_a-\sigma_r)$. To investigate this, one sample at each confining pressure was tested to 30 per cent axial strain and the same trend continued. Typical deformed conditions are shown in Figure 27.

Because of this phenomenon, there was no well-defined failure point for any sample tested. However, if a straight line is fitted to the points corresponding to high axial strains, the point of tangency of this straight line and the initial portion of the curve will be defined as the failure point; the corresponding strain will be denoted as ε_{af}.

Mohr's Envelope

The plotting of a Mohr's envelope for the tests described in the previous section requires a definition of failure. An axial strain of 1.5 per cent is hereby defined as ε_{af}. The envelopes on Figures 28 and 29 are constructed for axial strain values of 0.5 and 1.5 per cent. The axial strains are noted on the plots.

Cycling the Axial Load in the Standard Triaxial Test

A series of standard triaxial tests were performed wherein the axial load was continued to stress values corresponding to 35 per cent and 75 per cent of the stress at ε_{af}, then released to zero and immediately reapplied. The load and unload rate was constant at 0.015 in/min. These tests were performed on samples which had previously been subjected to a single cycle of hydrostatic stress as well as on samples where the hydrostatic stress was not cycled.

McCormick Ranch Sand

The test series on the sand involved testing different samples at 35 per cent and 75 per cent failure stress levels. No samples were subjected to a hydrostatic stress cycle prior to the application of the shear load.

Typical results presented as plots of total deviator stress ($\sigma_a - \sigma_r$) as a function of axial strain, ε_a, are given in Figures 30-34.

Watching Hill Clay

The test procedures on the clay samples involved cycling the axial load at 35 and 75 per cent of defined failure stress on the same sample. Tests were performed on samples with one cycle of hydrostatic stress. Figure 35 is the average results obtained.

Constant Stress Ratio Tests

Tests were performed on both soils wherein the ratio of σ_r to σ_a was maintained at a constant value. The values of the constant were 0.4, 0.6 and 0.8.

The condition of the samples prior to the application of the constant stress ratio loading varied and included the application of such loading to samples with no previous load history, as well as samples subjected to hydrostatic stress values of 100, 800, 1600 and 3200 psi.

For those samples subjected to initial hydrostatic stress loads, the constant stress ratio loading was such that the confining pressure was increased as a constant function of the applied axial stress (the

axial stress, above that equal to the confining stress) rather than the total axial stress.

The results of these tests are presented in the form of plots of total deviator stress as a function of axial strain. See Figures 36-41. Note that the plots are averages of at least three separate tests and that the conditions prior to the application of the constant stress loading are stated on each plot.

No-Lateral-Strain Tests

Samples of the Watching Hill clay were subjected to loading conditions wherein the axial loading was applied at a strain rate of 0.015 inches per minute and the lateral confinement was applied so that the diameter of the sample at mid-height remained constant. Such tests are called no-lateral-strain tests or K_o tests.

Test results are presented in Figure 42. The points are averages of at least three tests and the initial confinement values are noted on each plot. From Figure 42 it is seen that the higher the initial level of confinement, the greater the deviator stress for a given value of axial strain.

Bulk Modulus

The compressibility of a material is defined as the relative change in volume-per-unit change in pressure, and is denoted as:

$$\beta = \frac{\Delta v}{v} \cdot \frac{1}{\Delta p}$$

where Δv = change in volume under the application of pressure change.

v = original volume.

Δp = pressure change.

The bulk modulus K_B is defined as the reciprocal of β.

With the data in Figures 19 and 20, it is possible to calculate K_B values for the soils tested. The results are presented in Table 3.

Modulus of Deformation

The modulus of deformation is defined as the slope of the total deviator stress versus axial strain plot. This slope taken at axial strain values of 0.1 per cent is E_i, at any other value of axial strain E_t; the slope of a line through the origin of the axis system and any point on the above-mentioned plot, E_s. For cyclic loading, the slope of the reload curve is E_c.

Table 4 tabulates E_i values calculated from Figures 22-26. Due to the shape of the plots (Figures 22-26) it is clear that the values of E_t and E_s will be less than E_i, and that they will be a decreasing function of axial strain. Figure 43 is a plot of E_s versus axial strain, ε_a, and illustrates the rapid decrease in the modulus values with axial strain. The plot is typical and shows that after axial stains of approximately 3 per cent the rate of change of E_s with E_a is greatly reduced.

Ratio of Lateral-to-Axial Strain

Z is defined as the ratio of lateral strain to axial strain and will hereafter be referred to as Poisson's ratio. For hydrostatic loading, Z varied as the hydrostatic stresses ranged to 1600 psi, Figures 15 and 18. During standard triaxial testing, Z was not constant

over the entire test but was constant over several separate ranges of axial strain. Figure 44 is typical of the results obtained. It is to be noted that the position of Points A and B on this type of plot was shifted to the left as the confining pressure increased. Table 5 tabulates the average values of Z over the ranges O-A and A-B for the soils tested in the standard triaxial test.

Shear Modulus G

The value G is calculated as one-half the slope of the $(\sigma_a-\sigma_r)$ versus $(\varepsilon_a-\epsilon_r)$ plots. For proof of this relationship, by elastic theory, see Appendix C.

Average plots of total deviator stress $(\sigma_a-\sigma_r)$ versus the axial and lateral strain differences $(\varepsilon_a-\epsilon_r)$ are shown in Figures 45 and 46. The values of shear modulus G for $(\varepsilon_a-\epsilon_r)$ equivalent to 0.1 per cent are given in Table 6. Typical variations of G with axial strain are shown in Figure 47.

CHAPTER VIII

DISCUSSION

Hydrostatic Loading

The application of a hydrostatic load resulted in a volume and shape change in all samples. The shape change was different for the two soils as is shown in Figures 14 and 16.

During hydrostatic loading there are two distinct portions of each sample; the end sections in contact with the metal load caps and the center section.

For the McCormick Ranch soil the diameter of the sample in contact with the end plates did not change a measurable amount. For the Watching Hill Soil the diameter of the sample in contact with the end plates reduced with the application of hydrostatic loads as follows:

Hydrostatic Load (psi)	Diameter Reduction of Sample at Contact with End Plates After the Application of Hydrostatic Load:
100	0.021 in.
200	0.028 in.
400	0.060 in.
800 and Greater	0.065 in.

Measured along the longitudinal center line of the sample, the length of the zones influenced by the end caps were:

Hydrostatic Load (psi)	Length of Zone Influenced by End Caps as Measured from One End Only: McCormick Ranch Soil	Watching Hill Soil
100	0.15 in.	1.20 in.
200	0.15 in.	0.75 in.
400	0.15 in.	0.75 in.
800 and Greater	0.15 in.	0.75 in.

Due to low densities, the central portion of each sample experienced the greatest volume change during hydrostatic loading and thus had a lower void ratio than the remainder of the sample.

As previously noted, the as-formed samples consisted of aggregates of particles and were partially saturated with S = 41.7 per cent for the Watching Hill soil and S = 80.6 per cent for the McCormick Ranch soil.

To accommodate the volume change under hydrostatic loads, the aggregates changed in shape. The result was a reorientation of the mineral grains within each aggregate. Assuming the individual grains to be compressible leads to the concept of volume change or reorientation as largely a slipping or shearing action of one particle over its neighbor to reform the group into a denser structure. The aggregates change shape as a result of particle movement within an aggregate, but the sample remains in an aggregated state.

In theory there are no shear stresses in a body loaded hydrostatically. For soils this is approximately true only when large areas are considered. In the samples tested it is visualized that the

resisting shear stresses and the structural resistance of the framework combats the volume-reducing effect of the applied load. When the sample's resistance to load is overcome, the particles move and reach a state of equilibrium at a reduced void ratio. This movement and reorientation of grains is not independent of time. The time factor was accounted for by applying the load at the same rate and taking all readings at the time of load application.

The samples tested were a closed system and during load application it is assumed there was no escape of soil air or water. The consequence was that each increase in hydrostatic load resulted in an increased degree of saturation. The point of complete saturation is of interest.

Examining the results as given in Figures 19 and 20 indicates a marked difference in the soils' response to load at 1600 psi confinement. Confining pressures greater than 1600 psi resulted in a very small increase in volumetric strain.

At 1600 psi confinement the volumetric strain was 25.13 per cent for Watching Hill soil and 4.14 per cent for the McCormick Ranch soil. With the data from Figures 10 and 11 the average volume change for the McCormick Ranch and Watching Hill soils was 3.05cc and 18.3cc, respectively. Comparing these figures with the average volume of air for the as-formed samples, Figures 10 and 11 indicate that at 1600 psi the degree of saturation was 96+ per cent for both soils. It is concluded that the samples will behave as if saturated at confining pressures of 1600 psi and higher; and, that at confining pressure less than 1600 psi, they will behave as if partially saturated.

The samples not being fully saturated at 1600 psi means that there is still some undissolved air present and this could account for the trend of a volumetric strain increase upon reloading in the hydrostatic cycling sequence. Figure 21 indicates approximately a 1 per cent increase in volumetric strain after the second application of 1600 psi confinement.

Partially-Saturated Range--Hydrostatic Loading

For a discussion of the factors affecting air and water in a partially-saturated soil and an explanation of the symbols used herein, see Appendix A. The increase in the degree of saturation to 96+ per cent from initial values of 80.6 and 41.7 for the McCormick Ranch and Watching Hill soils, respectively, is brought about by the void ratio decrease under the applied hydrostatic loads. The relationship between the soil air and soil water during this change in degree of saturation is of interest.

For the no-load, as-formed condition, the effective stress throughout the sample is

$$\bar{\sigma} = -u_c$$

where

$$u_c = -T_s\left[\frac{1}{r_1} + \frac{1}{r_2}\right]$$

For a loading phase where air but no water is allowed to escape, the values of r_1 and r_2 become larger as the void ratio decreases. That

is, u_c becomes less negative and approaches zero or atmospheric pressure. The effective stress $\bar{\sigma}$ increases due to the applied load. When the volume of voids is equivalent to the volume of water, the water is a continuous phase, r_1 and r_2 are infinite, and u_c is zero. The water is under atmospheric pressure. Increased hydrostatic loads, unless large enough to compress the water, will not increase the effective stress. For the undrained condition the effective stress has reached its maximum value.

If the air is not allowed to escape, the pressure in the air u_a increases as the volume decreases. At the interface of the air and water, the pressure in the water is u where

$$u = u_a + u_c$$

For the no-load, as-formed condition, when the air is under atmospheric pressure, u_c is negative. As the hydrostatic load increases, u_a increases; air is dissolved in the water, and r_1 and r_2 increase. The value of u_c changes due to changes in r_1 and r_2 and increased air pressure. It is possible for u_a to exceed u_c and for u to be positive if the water is saturated with air at the pressure u_a. For the latter case, due to the compressibility of air, $\bar{\sigma}$ would increase; due to the positive value of u_c, $\bar{\sigma}$ would decrease. Until all the air is dissolved in the water, there would be a net increase in $\bar{\sigma}$. However, the net increase in $\bar{\sigma}$ per unit of applied hydrostatic pressure would reduce as the quantity of free air approached zero. When the quantity of free air

equals zero, water is the continuous phase and the water pressure is that necessary to dissolve all the air. With additional pressure, $\bar{\sigma}$ can only increase if the load is sufficient to cause a volume change in the water.

Volume changes in the samples tested, at 1600 psi confinement, were such that the measured degree of saturation was 96+ per cent. With increases in hydrostatic stress above 1600 psi, there would be additional volume change but the magnitude would be very small compared to that which occurred prior to a confinement of 1600 psi. The assumption of complete saturation at 1600 psi is not in serious error. By Equation (20) the air pressure required to dissolve all the air is 180 psi for the McCormick Ranch soil and 1100 psi for the Watching Hill soil. Under these conditions at the point of saturation, the effective stress in the McCormick Ranch soil is 1420 psi and in the Watching Hill soil 500 psi. To evaluate the effective stress at hydrostatic pressures less than 1600 psi would require measuring the pore water and the pore air pressure or solving Equation (21) and calculating values of u_c. Both suggested solutions are involved problems and were not attempted in this study.

Saturated Range--Hydrostatic Loading

A saturated soil is a two-phase system composed of soil grains and water. Information available from low-pressure, undrained triaxial tests on normally consolidated saturated soils shows that the soil water carries all the applied load (45). There is no increase in effective pressure. These results are generally true if there is no volume change. Under the conditions as stated, volume changes can occur only

if the applied stresses are large enough to compress the soil water. For normal triaxial testing, 100 psi or less confinement, this is not likely to occur. High pressure triaxial testing may result in such a volume change.

Water is compressible. As is true for most materials, the compressibility of water decreases as the pressure increases. At atmospheric pressure the bulk modulus of water is 3.0×10^5 psi. The change in bulk modulus with pressure is given below:

Confining Pressure (psi)	Bulk Modulus of Water (psi) (41)
100	3.0135×10^5
200	3.0270×10^5
400	3.0540×10^5
800	3.1080×10^5
1200	3.1620×10^5
1600	3.2160×10^5
3200	3.3420×10^5
6400	3.5340×10^5

For the soils tested, assume that at 1600 psi confinement saturation is complete and that the soil water carries no load. Further, assume that the soil water carries all load in excess of 1600 psi. The volumetric strain for water at confining pressures of 1600, 3200, 6400 and 10,000 psi are as shown:

Confining Pressure (psi)	Volumetric Strain (%)
1600	0
3200	0.52
6400	1.49
10,000	2.50

The Watching Hill clay would have a volumetric strain, due to compression of the soil water, as shown:

Confining Pressure (psi)	Volume Change (cc)	Volumetric Strain (%)
3200	0.07	0.13
6400	0.20	0.37
10,000	0.34	0.63

If the soil structure assumed any of the applied load, then the volumetric strains would be less than those noted above. For confining pressures in excess of 1600 psi, the increases in volumetric strains above that which had occurred at 1600 psi confinement are noted below:

Confining Pressure (psi)	Watching Hill Clay Increase in Volumetric Strain Above That Which Had Occurred at 1600 psi
3200	0.4%
6400	0.8%
10,000	0.8%

The fact that the soils were not completely saturated at 1600 psi would account for a portion of the above increase in volumetric strain. For the work reported, it is not believed that volume change in the soil water significantly affected the results.

Triaxial Tests

A soil's strength characteristics differ depending on the degree of saturation (46). This fact divides soils into two groups: partially saturated and saturated.

Loading a normally consolidated, saturated soil under low pressure triaxial conditions will not increase the effective stress nor will there be a volume change. As a consequence the Mohr envelope will be horizontal (45).

A partially saturated soil's effective stress, in a low pressure triaxial test, depends on the value of confinement and the deviator stress. Thus, the strength and stress deformation characteristics must be a function of the confining stress. The Mohr envelope for partially saturated soils under low pressure triaxial testing is not a horizontal line as for saturated soils (47).

High pressure triaxial test results for undrained tests are presented in Figures 22 to 27.

Partially Saturated Condition (σ_r < 1600 psi)

The strength and deformation characteristics are a function of confining pressure; the soils become stronger as σ_r increases.

The axial strain at failure, ε_{af}, reduced with increases in confinement. This is in conflict with the high pressure work of Hirschfeld

and Poulos (29) and Vesic and Barksdale (33) wherein both report that the value of ε_{af}, which they define as the value of axial strain at peak effective deviator stress, increased with increased confinement. The difference is due to the conditions of drainage during testing. The reference works were drained triaxial tests.

The general shape of the stress-strain curves are similar to Types I and IV described by Casagrande (48) for low-pressure triaxial tests on partially saturated fine-grained soils. This work by Casagrande classifies the shape of stress strain curves resulting from low-pressure triaxial tests on partially saturated and saturated soils (see Figure 63).

Saturated Condition (σ_r > 1600 psi)

At confining pressures in excess of 1600 psi the strength-deformation characteristics are less sensitive to confining pressures and the plots, Figures 21 through 26 for a given soil tend to converge.

The effective stress in a soil has been given in Equation (2), Appendix A, as

$$\bar{\sigma} = \sigma - u.$$

The convergence of the plots of total deviator stress as a function of axial strain at values of confinement suggest that $\bar{\sigma}$ is independent of confinement and that for the high-pressure triaxial tests reported, Equation (2) is valid.

For confining pressures greater than 1600 psi the failure strain ε_{af} is approximately constant and thus independent of confinement. At strains less than ε_{af} the plots of total deviator stress versus axial strain are approximately the same (Figures 23 and 26). Thus it is indicated that the deformation characteristics of the soils tested at high confining pressures in the standard triaxial test are independent of the level of confinement.

General Observation--Saturated and Partially Saturated Condition

For both soils, a portion of each sample near the end caps had no measurable volume change until the axial strains were approximately 12 per cent. These dead zones are illustrated in Figure 27 which shows the sequence of shape change during the triaxial test for different samples of Watching Hill soil at 3200 psi confinement.

During triaxial loading, all samples, regardless of the confining pressure, had a diameter increase at the center of the sample. With increased axial strain, this diameter increase progressed toward the sample ends (Figure 27).

All samples failed plastically by bulging with no visible shear planes. Several samples were tested to axial strain values greater than 25 per cent with the same results. After approximately 12 per cent axial strain, the saturated samples had vertical tension cracks (Figure 17). These cracks started at the center of the sample and advanced toward both ends as the axial strain increased.

At axial strain values in excess of ε_{af} all samples showed a small increase in total deviator stress with axial strain. For a given

test, the value of $\frac{d(\sigma_a-\sigma_r)}{d\varepsilon_a}$ at $\varepsilon_{af} > \varepsilon_f$ was approximately constant, but decreased with confining pressures. Bishop (36) in reporting his high-pressure work on clay, makes note of the same phenomenon.

For the partially saturated samples the axial strain exceeded the lateral strain numerically. However, the ratio $\frac{\varepsilon_r}{\varepsilon_a}$ increased with confining pressure. For both soils in the saturated condition, the axial strain exceeded the lateral strain numerically; for the Watching Hill soil the ratio $\frac{\varepsilon_r}{\varepsilon_a}$ seemed to be independent of σ_r.

In all samples there was a volume change during triaxial loading. The partially saturated samples had a volume decrease. The saturated samples had a very small volume change which tended toward a reduction.

Cyclic Loading

For both soils the deviator stress was cycled at approximately 35 and 75 per cent of the failure stress as determined by ε_{af}. For the McCormick Ranch soil for a given sample the deviator stress was cycled at one stress value only (either 35 or 75 per cent of the failure stress, but not both); the hydrostatic stress was not cycled. For the Watching Hill Soil, the hydrostatic stress was cycled followed by a deviator stress cycle at both 35 and 75 per cent of the deviator stress at failure on the same sample. Typical plots of total deviator stress as a function of axial strain with the cycles shown are given in Figures 31-33. Average plots of total deviator stress as a function of axial strain without the cycle shown are given in Figures 34-36.

For the McCormick Ranch soil with no cycling of the hydrostatic stress, the average plots of deviator stress as a function of axial

strain for both the cyclic and standard triaxial tests are the same up to the deviator stress at which the cycle occurred. Following cycling there was an increase in the deviator stress for the cycling as compared to the standard triaxial test. After cycling the soils were slightly stronger (see Figures 22, 23 and 34). The increase in strength of the soils cycled compared to those under standard triaxial tests was greatest for low values of confinement and was a constant increase. That is, the plots were parallel after cycling. The strength increase due to cycling was not greater than 2 per cent.

The Watching Hill samples for the hydrostatic cyclic test had for any given value of axial strain a larger deviator stress than for the triaxial test (compare Figures 25 and 35). However, there does not appear to be any significant increase in strength in the samples cycled at 75 per cent of the failure deviator stress as compared to those cycled at 35 per cent of the failure deviator stress.

Cycling the hydrostatic stress prior to the application of the deviator stress resulted in a soil more resistant to deviator stress (compare Figures 24 and 35). The increase in strength was greater at low values of confining pressure and for the Watching Hill soil was negligible after full saturation. The strength increase due to hydrostatic cycling only was less than 3 per cent. Cycling the deviator stress with or without a cycle of hydrostatic stress resulted in a stronger sample. The strength increase due to cycling the deviator stress only was less than 2 per cent. In all cases it is concluded that the strength increase is due to a change in soil structure resulting

from cyclic loads. In all tests where the deviator stress was cycled, the stress strain curve, for that test (total deviator stress versus axial strain), after cycling had points which fell on an extension of the plot prior to cycling (see Figures 31-33).

The results of high pressure triaxial tests wherein cyclic loads are applied give qualitatively the same results as similar tests on soils tested under low pressure triaxial conditions.

Mohr's Envelope

Mohr's envelopes for the soils tested are shown in Figures 28 and 29. Due to the range in confining pressures, several plots are given for each soil.

The envelopes are curved over the range of partial saturation (confining pressures σ_r < 1600 psi) and approximately horizontal after saturation. Similar plots have been reported for low-pressure triaxial tests.

In reviewing the stress-strain curves (Figures 21-26) and Mohr's envelopes, it is concluded that the compressive strength of partially saturated soils under high confining pressures increases with cell pressure. The increase in strength becomes progressively smaller as the soil air is compressed and passes into solution and ceases when the stresses are large enough to cause full saturation. At full saturation the pore water pressure is positive and equals the pressure required to completely dissolve the air. Upon complete saturation the ϕ equal zero condition is applicable.

For undrained triaxial tests under partial saturation at high confining pressures, the failure envelope expressed in terms of total stress is not linear. For undrained triaxial tests at high confining pressures under complete saturation, the failure envelope will be approximately horizontal.

Comparing these results with those reported from low-pressure triaxial testing brings the conclusion that regardless of the level of confinement, high or low, a partially saturated soil will behave in essentially the same fashion. After saturation, the same statement applies.

Constant Stress Ratio Tests

To collect soil properties for design, the triaxial test is performed wherein, generally, two principal stresses are constant and the third is varied. For example, the standard triaxial tests reported here were completed with $\sigma_3 = \sigma_2 =$ constant while σ_1 was increased.

In practical situations such as a roadway embankment, or rigid foundation, all principal stresses change--usually not at the same rate. Therefore the standard triaxial procedure may not closely simulate actual field conditions.

An initial study to investigate the performance of soils when the principal stresses σ_a and σ_r were changing at the same time was completed. This was done under high-pressure triaxial test conditions and is reported here as the result of a series of constant stress ratio tests, $\frac{\sigma_r}{\sigma_a} = \frac{\sigma_3}{\sigma_1} = K$.

In a natural deposit at depth D, a soil element will be acted upon by a vertical stress $\sigma_v = \gamma D$ and a horizontal stress of $\sigma_h = K_o'\gamma'D' + \gamma_w D$. The at-rest ratio of effective horizontal to effective vertical stress is K_o', γ' is the submerged unit weight and γ_w the unit weight of water. Approximating that γ_w and γ' are equivalent, then $\gamma = 2\gamma_w$.

The ratio of total stress $\frac{\sigma_r}{\sigma_a}$ is K. With the conditions as stated, $K = \frac{1 + K_o'}{2}$. For K_o' values of 0 and +0.9, K is 0.5 and 0.85. Results of K tests at 0.4, 0.6, and 0.8 are reported.

Stress Conditions During the K Test

For undrained triaxial loading the maximum total shear stress on a soil element is $\tau = \frac{\sigma_a - \sigma_r}{2}$; the corresponding total normal stress is $\sigma = \frac{\sigma_a + \sigma_r}{2}$. For the K test, $\sigma_r = K\sigma_a$. Then $\tau = \frac{\sigma_a(1-K)}{2}$ and $\sigma = \frac{\sigma_a(1+K)}{2}$. A saturated soil has $\bar{\sigma}_a = \sigma_a - u$ and $\bar{\sigma}_r = \sigma_r - u$, $\bar{\sigma}_a$ and $\bar{\sigma}_r$ the major and minor effective principal stress with u the pore water pressure. The ratio K is

$$K = \frac{\bar{\sigma}_r}{\bar{\sigma}_a}$$

The maximum effective shearing stress is

$$\tau = \frac{\bar{\sigma}_a - \bar{\sigma}_r}{2}$$

$$= \frac{\bar{\sigma}_a - K\bar{\sigma}_a - (Ku - u)}{2}$$

$$= \frac{(\bar{\sigma}_a+u) - K(\bar{\sigma}_a+u)}{2}$$

but $\bar{\sigma}_a + u = \sigma_a$.

$$\tau = \frac{\sigma_a(1-K)}{2} .$$

Defining a pore pressure parameter A as the ratio of $\Delta u/(\sigma_a-\sigma_r)$, by the procedure shown above $(\Delta\sigma_a-\Delta\sigma_r) = \Delta\sigma_{a(1-K)}$; then

$$A = \frac{\Delta u}{(\Delta\sigma_a-\Delta\sigma_r)} = \frac{\Delta u}{\Delta\sigma_a(1-K)} .$$

Thus, in a saturated undrained shear test where $K = \frac{\sigma_r}{\sigma_a}$ the undrained strength and pore water pressure are functions of the value of K. The larger K values increase the total major principal shear stresses and pore water pressures, but not the effective shear stresses.

A partially saturated soil tested under K conditions would have an increase in the major principal effective shear stresses until saturation; then the above statements for the saturated conditions would apply.

Representing the stress path for K test by plotting the maximum shearing stress and corresponding normal stress in an element gives the results shown in Figure 60. These stress paths indicate that shearing stress at a given value of normal stress increases as the ratio K decreases. At low values of K the stress-strain plots $(\sigma-\sigma_r)$ vs. ε_a should be higher than the corresponding plots at high K values.

Results of K tests are given in Figures 36-41.

McCormick Ranch--Constant Stress Ratio Tests

For this soil, K tests with initial confinement of zero were performed. Results in the form of total deviator stress as a function of axial strain are given in Figure 36. Lateral strain as a function of axial strain for different K loadings are given in Figures 50-51.

Comparing Figures 22 and 23 for the standard triaxial test with Figure 36 shows that the shape of the stress-strain curves are functions of the method of loading. Computing E_i at 0.1 per cent axial strain yields E_i values of 20×10^3, 10×10^3 and 5×10^3 psi for K loadings of 0.4, 0.6 and 0.8, respectively. Table 4 shows E_i values of 25×10^3 and 30×10^3 psi for the standard triaxial test under initial confining pressures of 100 and 200 psi, respectively.

In Figure 36 the curves tend to converge at a shear stress value of approximately 90 psi and an axial strain value of 2.7 to 3.0 per cent. Following this, the K = 0.4 series is less resistant to shear stresses than the K = 0.6 or K = 0.8 series.

From Figure 50 and 51, during the initial stages of loading the lateral strain is very close to zero and in this respect the samples are similar to a one-dimensional consolidation test. The K = 0.6 and 0.8 series had a reduction in the central diameter which peaked at approximately 2.7-3.0 per cent axial strain, then started to increase. The K = 0.4 series did not have a reduction in the central diameter; rather up to axial strains of approximately 1 per cent the central diameter strain was less than 0.1 per cent after which it increased as a constant function of the axial strain (Z = 0.47).

Watching Hill--Constant Stress Ratio Tests

For this soil, results, in the form of total deviator stress as a function of axial strain plots are given in Figures 36-40. Representative plots of lateral strain as a function of axial strain are given in Figures 52-54. The K = 0.4 series had a central diameter increase throughout each test. The K = 0.6 and 0.8 series with zero initial confinement, had a central diameter decrease which continued up to axial strain values of approximately 4 per cent, after which the diameter appeared to remain constant for the 0.8 series and increase for the 0.6 series.

For initial confining values greater than zero, the lateral strain was zero or very small at small values of axial strain; however, as the axial strain increased, a linear relationship between axial and lateral strain was noted.

The relative position of the stress-strain plots in Figures 37-41 indicate that the strength-deformation characteristics are functions of the loading and that the magnitude of K value has a different effect depending on whether the soil is partially saturated or saturated. In general the writer believes that the higher the stress ratio the quicker the breakdown in structure and thus the higher the pore water pressures.

As previously shown for the McCormick Ranch Soil, the initial E values are lower for the K tests than for the triaxial tests. To further investigate the E values for the two test types, E was calculated for the value of deviator stress at which the two stress paths intersected (see Figure 55 for typical results). For this case, E was

calculated as the slope of a straight line extending from the origin of the deviator stress versus axial strain plot to the value of deviator stress corresponding to the intersection of the stress paths.

For the McCormick Ranch soil with all K tests having initial confining stresses of zero, the results show that as K increases, E for the triaxial test increases for any given value of confining pressure. For K constant, as the confining pressure increases, E for the triaxial test increases but E for the K test decreases.

If the initial confinement is greater than zero, the limited data available from the Watching Hill soil indicate that with K constant at 0.8, E for the triaxial test is greater than E for the K test, and that E values for both tests increase as the confining pressure increases.

The above observations with regard to E are not in keeping with the relationships derived in Appendix B wherein the constant-stress ratio tests were evaluated based on a purely elastic sample. By this latter investigation it was shown that for a purely elastic material the modulus E_k was a function of Young's modulus E divided by (1-2ZK). This would indicate that theoretically E_k should exceed E.

While both soils did not display purely elastic properties, they did show the same trends as the analysis based on elastic theory; that is, a variation in E_k with K and a more pronounced change in mechanical properties when K is greater or less than 0.6.

No-Lateral-Strain Tests

Consider an element of soil at a depth Z below the surface of a uniform deposit. Let the effective vertical pressure by $\bar{\sigma}_a$ and the

effective horizontal pressure be $\bar{\sigma}_r$.

If the mass is loaded under conditions of no lateral strain ($\varepsilon_r = 0$), then the ratio of $\bar{\sigma}_r$ to $\bar{\sigma}_a$ is called K_o, the coefficient of lateral earth pressure at rest. The value of K_o may be determined under triaxial test conditions where the confining pressure is applied so that there is no lateral strain. The results are reported as ratios of effective stress or in the case of quick and undrained triaxial tests, as ratios of total stress.

Several writers have reported results of tests to evaluate K_o. Sowers (49) reports the following:

Type Soil	K_o Effective, Drained	K_o Total, Undrained
Soft Clay	0.6	1.0
Hard Clay	0.5	0.8
Loose Sand	0.6	
Dense Sand	0.4	

On the Watching Hill clay, a series of no-lateral-strain tests with different values of initial confinement were performed. In the case of initial confining pressures greater than zero, all applied stresses in excess of the confinement were measured with the value of confinement taken as the reference. The results in the form of total deviator stress as a function of axial strain are given in Figure 42. In terms of relative positions, these plots are similar to the standard triaxial results in Figures 24-26.

Average plots of σ_r versus σ_a are presented in Figure 56.

From the plots the ratio of total stresses $\frac{\sigma_r}{\sigma_a} = K_o$ is obtained. The results are tabulated below:

Initial Confining Pressure (psi)	K_o
0	0.63
100	0.66
200	0.67
400	0.748
800	0.892
1600	0.848

For high-pressure triaxial tests under partially saturated conditions (σ_r < 1600 psi), the values of K_o are sensitive to σ_r and increase with σ_r, but not linearly. For the same test conditions as above, saturated soils have values of K_o higher than those of partially saturated soils and the K_o values for saturated soils are not nearly so sensitive to confining pressure.

For the soils tested it is concluded that the maximum value of K_o for total stress conditions is approximately 0.9. Also from Figure 42 it is seen that the total deviator stress at any value of axial strain increases sharply as the value of initial confinement is increased, the most drastic change occurring at confining pressures greater than 100 psi.

Modulus of Deformation

The modulus of deformation is defined as E, where

$$E = \frac{(\sigma_a - \sigma_r)}{\varepsilon_a} .$$

Different values of E which depend on the selection of $(\sigma_a - \sigma_r)$ and ε_a have been previously defined. In general soil mechanics practice, E values are necessary to determine stress distribution and deformation in soils.

Frequently, the triaxial test at low pressure is used to determine values of E. Reports of results obtained in such a manner are in reference (50). The reported values of E vary considerably within a soil type as well as for different soils. It is well known that the modulus E of a soil for undrained loading (low confining stresses) is not a unique property, but varies with disturbance, type of loading, stress history, etc. For high-pressure work, Vesic and Barksdale (33) report that initial tangent modulus values for sand increase linearly with confining pressure. Hirschfeld and Poulos (29) report that for the sands and silts tested, the initial tangent modulus values increased with increased confinement but not linearly.

For this work, initial tangent modulus values, E_i, were calculated at 0.1 per cent axial strain from Figures 24-26. The results are shown in the plot of Figure 57. It is seen that the E_i values are sensitive to the value of confining pressure up to saturation, after which it is approximately constant. In the partially saturated range,

E_i values vary approximately linearly with pressure over two ranges of confining pressure: 100-800 and 800-1600 psi (see Figure 57). From Figure 57 an approximate relationship between E_i and confining pressure is

E_i = cp + y.

c and y = constants.

p = confining pressure in psi.

For each soil, the values of c and y are tabulated below:

Range of Confining Pressure (psi)	Watching Hill Soil		McCormick Ranch Soil	
	c	y	c	y
0-800	65.0	0	112.5	12,500
800-1200	5.0	45,000	4.5	65,000
1200- -	0		0	

The variation of E_i with pressure is not unexpected considering the reports previously mentioned. The magnitude of the values of E_i are compared to those in references (29) and (33) in Figure 57.

The variation of the tangent and secant modulus with axial strain is of importance. Figure 43 is representative, showing that the modulus values may be approximately 1/5 of their initial values at axial strains greater than 3 per cent. Cycling the axial load, regardless of the value of confinement, increased the modulus values. Taking the slope of the straight line portion of the reload curve, $(\sigma_a-\sigma_r)$ vs. ε_a, showed an increase of at least 1.5 over the initial tangent modulus values. Figure 48 illustrates the variation of E_c as a function of confining pressure.

The results for E_i presented for high-pressure triaxial tests compare favorably in a qualitative sense with those of low-pressure triaxial testing. It is to be noted that for partially saturated soils under high confinement, E_i is approximately a linear function of confinement. However, the E_i values for each soil will be different. After saturation E_i is independent of pressure.

Ratio of Lateral-to-Axial Strain

Similar to the modulus of deformation E, a value for the ratio of lateral strain to axial strain is often required to calculate the stress distribution or settlement in a soil mass. The ratio of lateral strain to axial strain will be designated Z.

Typical plots of lateral strain versus axial strain are shown in Figure 58. It is significant to note for partially saturated soils at very low values of axial strain the plot of ε_r vs. ε_a is approximately horizontal. This suggests that up to axial strain values of a few tenths of a per cent, the triaxial specimen behaves essentially as a one-dimensional consolidation test. Similar results for sands at low confining pressures have been reported by Chen (51).

All of the data collected showed that the plots of ε_r versus ε_a were linear over several ranges of ε_a. Ignoring the initial small values of ε_a where ε_r was approximately zero, then the ranges of axial strain over which the ratio $\varepsilon_r/\varepsilon_a$ was linear, will be denoted as O-A and A-B as shown in Figure 44. Table 5 tabulates the range of axial strains for O-A and A-B, as well as the corresponding values of Z.

For the partially saturated region the values of Z for both soils in the range O-A increase with confining pressure, but are generally less than 0.5 for the McCormick Ranch soil and are less than 0.5 for the Watching Hill soil (Table 5).

In summary, the results of the standard triaxial tests show that Z is sensitive to the type of load, that Z is constant over several different ranges of axial strain, that Z increases with increasing axial strain, that the first region of axial strains over which Z is constant reduces with increasing pressures.

Shear Modulus G

Initial values of G, taken from Figures 45-46 at 0.1 per cent axial strain, are given in Table 6. It is to be noted that the modulus G values, similar to the E_i values, are sensitive to confining pressure and increase, but not linearly with σ_r. By elastic theory, the relationship between the constants G, E and Poisson's ratio is

$$G = \frac{E}{2(1+Z)} .$$

Taking G and E from the test results presented and solving for Z or Poisson's ratio, then comparing this value with the Z values from the tests presented, gives no correlation. It is then concluded that the soils tested do not obey elastic theory and that the values G, E and Z must be determined for each soil under specific test conditions.

General Discussion of Results

The results reported herein were collected by subjecting two soils to various stress states in the triaxial cell. The stress conditions for the standard triaxial test will be discussed by considering an element loaded as shown in Figure 59(a) where σ_1, σ_2 and σ_3 are principal stresses. The Mohr's circle for planes perpendicular to the 1-2 plane are shown in Figure 59(b). For this case the maximum shear stress is

$$\tau_{1\text{-}2} = \frac{\sigma_1 - \sigma_2}{2}$$

Similarly, Figures 59(c) and 59(d) show the Mohr's circles for planes perpendicular to the 1-3 and 2-3 planes, respectively. The maximum shear stress for each case being

$$\tau_{1\text{-}3} = \frac{\sigma_1 - \sigma_3}{2}$$

and

$$\tau_{2\text{-}3} = \frac{\sigma_2 - \sigma_3}{2}$$

In Figure 59(e), all cases are combined to give the complete Mohr diagram for triaxial loading. The stresses on any plane perpendicular to one of the principal planes can be found by using the corresponding Mohr's circle or analytically. For example, the stresses on a plane perpendicular to the 1-2 plane may be found by

$$\sigma = \frac{\sigma_1 + \sigma_2}{2} + \frac{\sigma_1 - \sigma_2}{2} \cos 2\phi$$

$$\tau = \frac{\sigma_1 - \sigma_2}{2} \sin 2\phi$$

where σ is the normal stress and τ the shearing stress on a plane perpendicular to the 1-2 plane at angle ϕ from the 2 axis. The general procedure in soil testing is to assume that $\sigma_2 = \sigma_3$; hence the outer circle in Figure 56 is used.

Hydrostatic compression is a state of stress that exists in a body surrounded by a fluid or gas under pressure p. The pressure p is always normal to the surface on which it acts and is the same in all directions. Theoretically, no shearing stresses are possible because the shearing resistance of the fluid is zero. The Mohr's circle for this case is a point at $\sigma_1 = \sigma_2 = \sigma_3 = p$. In standard triaxial testing the usual procedure is to subject the sample to a hydrostatic stress which is maintained constant while the vertical axial stress is increased.

The soils tested were in some cases subjected only to a hydrostatic stress. The result was a shape change, indicating that shear stresses were acting in the sample. The volume change of the samples under a hydrostatic stress state continued to confining values of 1600 psi, after which it was so small that accurate measurements were difficult. It is emphasized that volume changes were measured by mercury displacement after the sample was removed from the cell. While it is recognized that some expansion occurred upon removal of the load, it was

not possible to accurately measure this volume change by monitoring the sample dimensions inside the cell.

The volume decrease under hydrostatic stress was as expected, since most engineering materials will undergo a volume change when subjected to such a stress. The relationship between applied stress and volumetric strain is generally taken as the bulk modulus K_B, previously defined. Experiments with materials under high confining pressures (52) have shown that K_B is not a constant. Rather, a plot of applied stress p versus volumetric strain $\Delta V/V$ is of the form shown in Figure 61(a). It is to be noted that after a given value of p the upward curvature of the plot becomes pronounced. This same trend was found and noted for the soils tested; that is an abrupt change in the plot of p versus $\Delta V/V$ at confining pressures in excess of 1600 psi. For a homogeneous, isotropic material the change in shape of the p versus $\Delta V/V$ plot is thought due to the increased repulsion of the atoms in the material as they are pushed closer together. For the soils tested, the change is due to the material going from three phase to two phase. That is, at 1600 psi all the air is dissolved and the sample is then composed of soil grains and water.

For the soils tested, the bulk modulus was calculated by the expression

$$K_B = \frac{\Delta\sigma}{\Delta V/V}$$

where $\Delta\sigma$ was an increment of hydrostatic stress (say 200 psi to 400

psi, then $\Delta\sigma$ = 200 psi) and $\Delta V/V$ was the corresponding volumetric strain over that increment. The values of K_B for confining pressures in excess of 1600 psi are not considered accurate due to the difficulties in measuring the small volume change at these pressures. For comparison, in materials such as steel or aluminum, the bulk modulus may be approximated by the modulus of elasticity E for that material.

The assumption was made that the testing was done in a closed system. That is, once the loading started there was no loss of soil water or air. Checking the membranes before and after testing confirmed the assumption of no water loss. The assumption of no air loss through the membrane may be in error. However, by volume measurements of the samples after hydrostatic loading, it was found that the total volume change at 1600 psi confinement was approximately equivalent to the original volume of air in the sample. If there was no air loss, then by Henry's law--assuming it to be a linear function of pressure in the air phase--it was shown that all the air would be dissolved in the soil water at a confining pressure of 1600 psi. The procedure used in this phase of the study was primarily that proposed by Hilf (44).

The soils were assumed saturated when the confinement reached a value of 1600 psi. Any error in this assumption is not considered significant for the results presented. At confining pressures of less than 1600 psi the volume change was assumed due to the air being compressed and a portion of the air going into solution in the water. Over this same pressure range the soil water pressure increases and the net effective stress between the soil particles increases, the result being

that in the partially saturated state the soil strength increases as the confining pressure increases. This increase in strength is reflected in the Mohr's envelope which is concave down over the range of partial saturation. The strength increase with pressure decreases as saturation is approached. This is reflected in the curvature of the Mohr envelope at pressures close to 1600 psi. These observations indicate that partially saturated soils tested under high values of confinement follow the same trend as partially saturated soils under low values of confinement.

In the standard triaxial test, as has previously been stated, the strength of the samples increased as the level of confinement increased to 1600 psi. This strength increase is due to the increase in effective stress and is reflected in the relative positions of the total deviator stress versus axial strain plots. At confining values greater than 1600 psi the total deviator stress versus axial strain plots tend to converge. The scatter is likely a result of incomplete saturation at the time of test. It is not believed that for this series of tests the volume change of the soil water, if such occurred, was a significant factor in the results.

The results of the standard triaxial tests expressed in the form of a Mohr's envelope showed that at values of confinement in excess of 1600 psi the envelope was horizontal, again confirming saturation at 1600 psi.

The constant stress ratio loading was carried out by keeping the confining stress ($\sigma_3=\sigma_r$) a constant portion of the applied axial stress

($\sigma_1=\sigma_a$). In this work, constant stress ratio tests were carried out with K values of 0.4, 0.6 and 0.8, and with different initial conditions. Standard triaxial tests were also carried out for different initial conditions.

For a discussion of the constant stress ratio test and its relation to the standard triaxial test, see Appendix B.

Figure 49 is a diagram illustrating the total stress paths for several different loading conditions. Note that Q is $\frac{\sigma_a - \sigma_r}{2}$ and P is $\frac{\sigma_a + \sigma_r}{2}$ where σ_a and σ_r are total stresses. The soils tested did not have a failure stress in terms of a peak value of deviator stress in the plot of total deviator stress as a function of axial strain. Thus, failure conditions must be described in terms of some limiting value of deviator stress or axial strain. With failure defined, then the Mohr envelope can be superimposed on Figure 49 and the tests compared.

Figure 55 shows the total-stress paths (Q vs. P) for the constant stress ratio and standard triaxial tests on the McCormick Ranch soil. On this same plot is the Mohr envelope for 0.5 per cent axial strain in the standard triaxial test. For this envelope the K = 0.4 test is weaker than the standard triaxial test at 100 psi; the K = 0.6 test, at failure, is comparable to the standard triaxial test at 200 psi, while the K = 0.8 test, at failure, is comparable to a standard triaxial test with σ_r = 1350 psi. The relative position of the K tests on the plot of total deviator stress as a function of axial strain (Figure 36) does not influence the relative position of the corresponding stress paths in Figure 55.

Figure 60 shows stress paths (Q vs. P) for the constant stress ratio and standard triaxial tests on the Watching Hill soil. Of particular interest are the K tests with initial stress values of 1600 and 3200 psi. Figures 40 and 41 indicate that at any given value of axial strain the K = 0.6 test has a higher value of shear stress than the K = 0.8 or K = 0.4 test series. Similarly, at any given value of axial strain the K = 0.8 series has a higher stress value than the K = 0.4 series. These results suggest that after saturation the deformation characteristics in terms of shear stress for a given value of axial strain are different than those prior to saturation. Skempton (53) has defined pore pressure coefficients A and B such that the pore water pressure Δu is:

$$\Delta u = B[\Delta\sigma_3 + A(\Delta\sigma_1 - \Delta\sigma_3)]$$

$\Delta\sigma_1$ and $\Delta\sigma_3$ are total stresses.

For the K test where $\sigma_1 = \sigma_a, \sigma_3 = \sigma_r$ and $K = \frac{\sigma_r}{\sigma_a}$, then $\sigma_r = K\sigma_a$. The pore water increase $\Delta u = BK\Delta\sigma_a + AB\Delta\sigma_a(1-K)$. For saturation B is unity (53). If A is less than 1, then Δu is a function of K such that the lower K the less the pore water increase due to any increment of stress $\Delta\sigma_a$; similarly, the larger K the larger Δu. Should A be greater than unity, Δu will increase as K gets smaller.

For the case of the K test starting at confining pressures of 1600 psi, it is conceivable that as the shear stress (τ is greater for small K values) increases due to K loading, the A parameter exceeds

unity. For such a case the K = 0.4 test series would be less resistant to deviator stress than the K = 0.6 or 0.8 series and hence the change in position of the plots in Figures 39, 40 and 41.

Comparing the triaxial and K tests through the plots of total deviator stress versus axial strain (Figures 24-26 and 37-41) shows in general that for the same initial confining pressure (up to 800 psi) the deviator stress required for any given value of axial strain is larger for the standard triaxial test than for the K tests. At an initial confinement of 1600 psi, comparing the same parameters, the K = 0.6 is stronger than the standard triaxial specimens and for the K = 0.4, 0.8 series, the triaxial specimens are stronger. Without measurements of pore-water pressures an explanation for this behavior is difficult if not impossible. However, considering the relationship $\Delta u = BK\Delta\sigma_a + AB\Delta\sigma_a(1-K)$ with B constant for the standard triaxial test as $\Delta\sigma_a$ increases K decreases. Considering K only, the first term decreases and the second term increases. Recalling that there was a general volume decrease during the application of deviator stress suggests that AB increases.

The expression above applies equally well to the K test. For this case K = constant; therefore, the first term will increase as a constant portion of $\Delta\sigma_a$; likewise for the second term. The factor A must be considered. If A is a constant and is equal for both the K and the triaxial test, then the increase or decrease in Δu would be the same for both types of tests. From the results presented, it is obvious that A is not the same for both tests. The implication is that in general

A is less for the triaxial loading than for the K loading.

The no-lateral-strain test is an excellent means of checking the point of complete saturation in a sample. Bishop and Henkel (54, p. 141) state that when the K tests are performed on partially saturated soils, as full saturation is approached the increase in pressure necessary to maintain zero lateral strain rapidly increases. For such a test the axial strain is equivalent to the volume change. The plot (Figure 42) tends to verify that the samples are very close to saturation at 1600 psi confinement.

Comparing the plots of total deviator stress for no lateral strain and constant stress ratio tests gives an indication of how sensitive the soils are to increases in lateral strain. There is little information available with which to compare the reported results. Casagrande and Hirschfeld (50) report that for a clay at constant water content, approximately the same relation between pore water pressure and total major principal stress was obtained for hydrostatic, K, and uniaxial loading. They state that when testing specimens compacted at high water contents (small air contents), one observes that for low pressures the curve of pore pressure vs. applied stress starts out slightly flatter than 45 degrees; but under a relatively small applied stress the small quantity of air contained in the specimen is driven into solution and the remainder of the curve is a straight line with a 45 degree slope. In contrast, when testing specimens compacted at low water contents (high air contents) this curve is very flat (very small pore pressure buildup) and approaches a 45 degree slope only under high

pressure. The volumetric strain relations to confining pressure reported herein for high pressure triaxial tests follow the same trend.

Lee and Haley (55) after testing partially saturated kaolinite soil in the undrained triaxial condition report that beyond a certain confining pressure (250 psi) all of the pore air becomes dissolved, resulting in a saturated sample. Tests at higher confining pressures gave essentially the same stress-strain curves. The data reported herein follows the same trend.

Bishop (36) reports that for a clay sample under high confining pressures the soil continued to shear under very nearly a constant total axial stress. On several tests he states that the value of $(\sigma_1-\sigma_3)$ continued to increase with axial strain values even to the limit of the piston travel. The same trend was noted for the tests reported herein.

Hirschfeld and Poulos (29) on testing a sand silt under triaxial slow conditions report a drop in the axial stress $(\sigma_1-\sigma_3)$ at failure. The strain corresponding to the peak value of $(\sigma_1-\sigma_3)$ increased with increased confining pressures. In the test series reported herein, it has been shown that at higher confining pressures the samples became stiffer and thus did not follow the described pattern.

With regard to volume changes during the application of the shearing stress, Vesic and Clough (37), Hirschfeld (28), and Hirschfeld and Poulos (29) and Bishop (36) all report a volume decrease throughout the test. This same general pattern was observed for the McCormick Ranch clayey sand and the Watching Hill clay for σ_r values less than 1600 psi.

With regard to sample shape change during the application of the shear load, all the authors cited in the previous paragraph note that the soils tested failed by bulging, and there was no clearly defined shear planes at any axial strain value. The soils tested for this study followed essentially the same pattern.

Bishop and Bjerrum (47) state for undrained tests on partially saturated cohesive soils the compressive strength increases with increases in all-around pressure. The increase in strength becomes progressively smaller as the air passes into solution and ceases when the stresses are large enough to cause full saturation, ϕ approximating zero. The failure envelope expressed in terms of total stress is thus not linear. This same statement applies to the high-pressure triaxial tests reported herein.

A relationship between the various tests was not found. It was shown that in the standard triaxial test under high confining pressures the soil properties, in terms of strength, E, G and Poisson's ratio, increased with confinement to saturation. Upon saturation, regardless of the level of confinement, these same properties tended to converge. At all levels of confinement, as the axial strain increased there was a marked decrease in E and G while Poisson's ratio increased.

Due to the similarity of the test procedures, the standard triaxial and cyclic tests may be compared directly. Basically the same observations made with regard to the standard triaxial tests are applicable to the cyclic tests. In evaluating the cyclic test it was found that cycling the hydrostatic phase and/or the axial load increased the

strength and the E and G values. The same trend as noted above for these values was observed following cycling.

A method for comparing the standard triaxial test and the constant stress ratio test has been presented. It was shown experimentally that the constant stress ratio loading yielded a weaker sample than the standard triaxial loading. This may be due, in part, to the difference in structure imparted to the sample by the difference in the stress paths.

By elastic theory the relationship between E_K and E was found to be

$$E_K = \frac{E}{(1-2ZK)} .$$

Using E_i and Z from the standard triaxial test and calculating E_K for the K test showed no correlation of results. The trend was for the calculated value of E_K to exceed by at least a factor of 3 the test value of E_K.

From the work presented it is clear that soils subjected to high confining pressures act essentially in the same fashion as soils under low confining pressures. However, as in the low confining pressure ranges, little or no correlation has been found between the design parameters E, G and Z; the same is true for high pressure work. Thus, to obtain accurate parameters for design, it is necessary to test the soils under conditions in which they will be used.

CHAPTER IX

CONCLUSIONS

High-pressure undrained triaxial tests wherein the confining pressure varied from 100 to 10,000 psi were performed on two soils, a SC and a CL. From the results of this testing the following conclusions were drawn.

1. The undrained compressive strength of partially saturated soils under high confining pressures increases as the confinement increases. The increase in undrained strength becomes smaller as the pore air is compressed and dissolved in the pore water, and ceases when the total stresses are large enough to cause saturation. Therefore, the Mohr envelope for total stress is non-linear for the partially saturated range.

2. Where saturation is complete there is little if any increase in undrained strength due to higher confining pressures. Therefore the Mohr envelope is approximately horizontal after saturation is complete.

3. The shape of the total stress-axial strain curves at low and high confining pressures are the same for the standard triaxial test.

4. The shape of the total stress-axial strain curves are sensitive to the loading procedure.

5. The failure mode of all samples was a bulging failure with no well-defined failure planes. At high values of axial strain the total deviator stress increased slightly with increased axial strain.

6. Cycling the hydrostatic load prior to the application of the shear load increased the strength of the samples. The strength increase decreased as the degree of saturation increased and was negligible after complete saturation.

7. Cycling the shear load increased the strength of the sample. The strength increase decreased as the degree of saturation increased.

8. For any given cyclic test, after cycling the shear load, the total stress axial strain plots were always smooth extensions of the total stress axial strain plots prior to cycling.

9. The strain at failure, ε_{af}, reduced with confinement to the point of saturation, then remained constant.

10. The initial modulus values E_i increased with confinement to saturation and then remained constant. The increase was approximately linear with pressure to saturation. Cycling the deviator stress at any level of confinement resulted in E_c values greater than 1.5 times the initial E_i values for the same sample.

11. The modulus values E_i, E_c and G dropped rapidly with increased axial strain and at approximately 3 per cent axial strain are less than 20 per cent of their original values.

12. The ratio of lateral-to-axial strains for a given level of confinement was constant over several different ranges of axial strains. For axial strain values greater than ε_{af}, the ratio of lateral-to-axial strain approached or exceeded 0.5.

13. The bulk modulus increased as a nonlinear function of the confinement. There was no apparent relationship between the bulk modulus values for the two soils tested.

14. The coefficient of earth pressure at rest was 0.63 under a confining pressure of zero, and increased nonlinearly with confining pressure and approached 0.9 at a confining pressure of 1600 psi.

15. No relationship between the modulus of deformation E, shear modulus G, and the ratio of lateral to axial strain Z was found between any test types.

16. The strength-deformation characteristics of the soils tested differ for the constant stress ratio test and the triaxial condition. In general, for the partially saturated case the soils were weaker during the constant stress ratio type loading than for the standard triaxial loading.

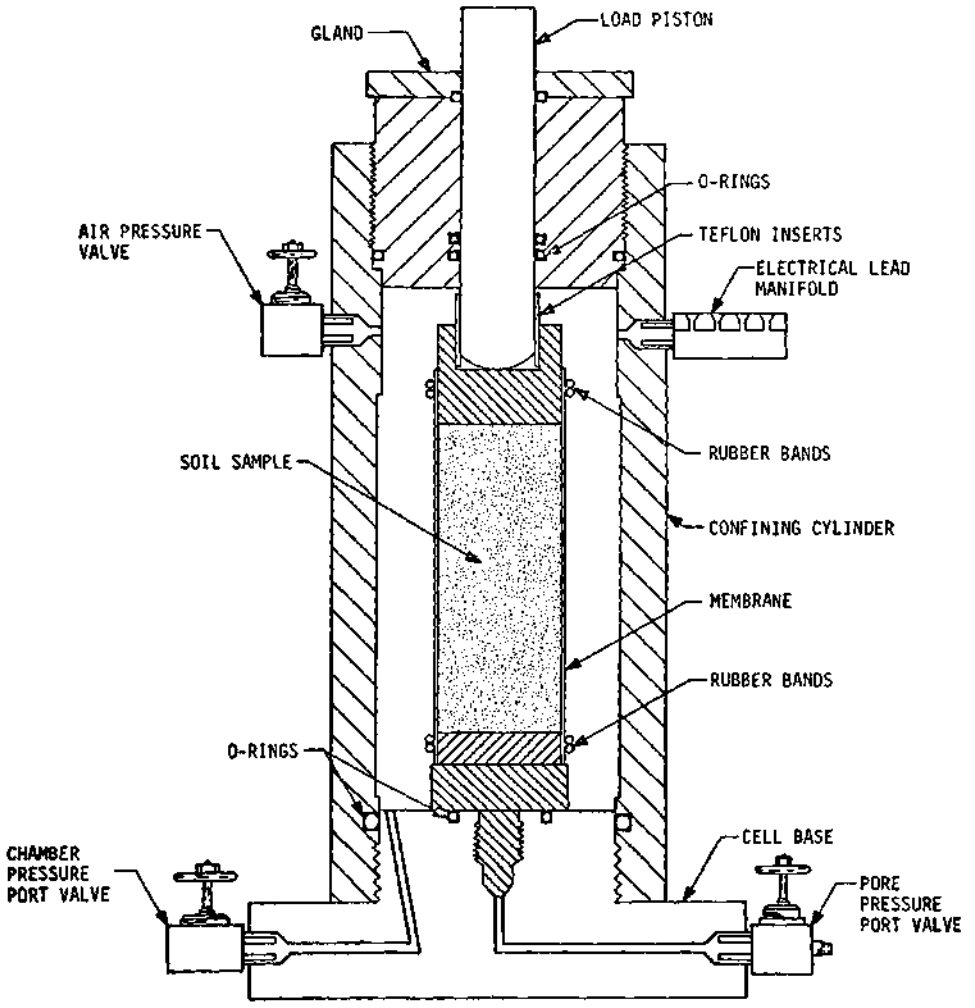

Figure 1. Triaxial Cell

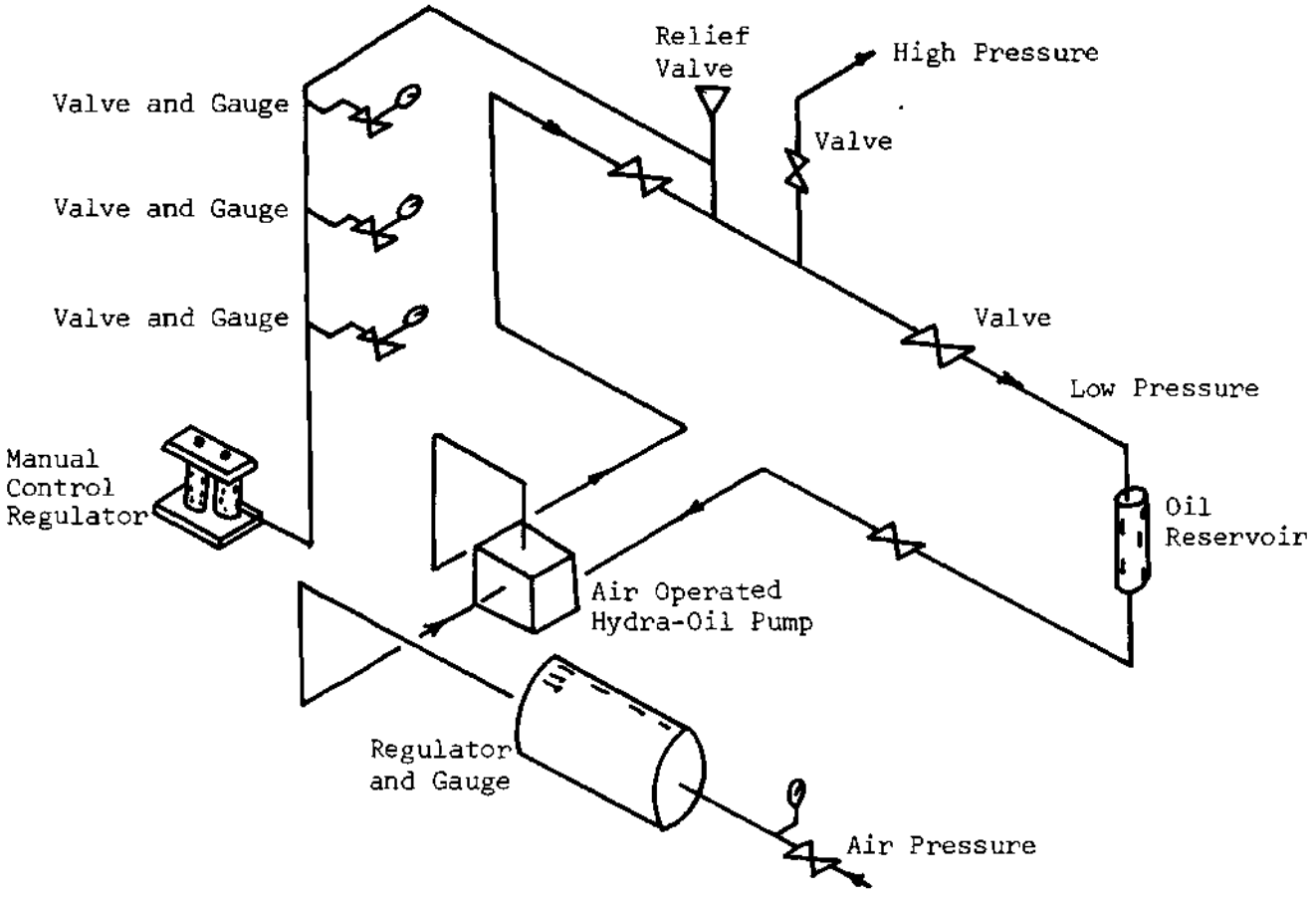

Figure 2. Pressure Generator and Controls

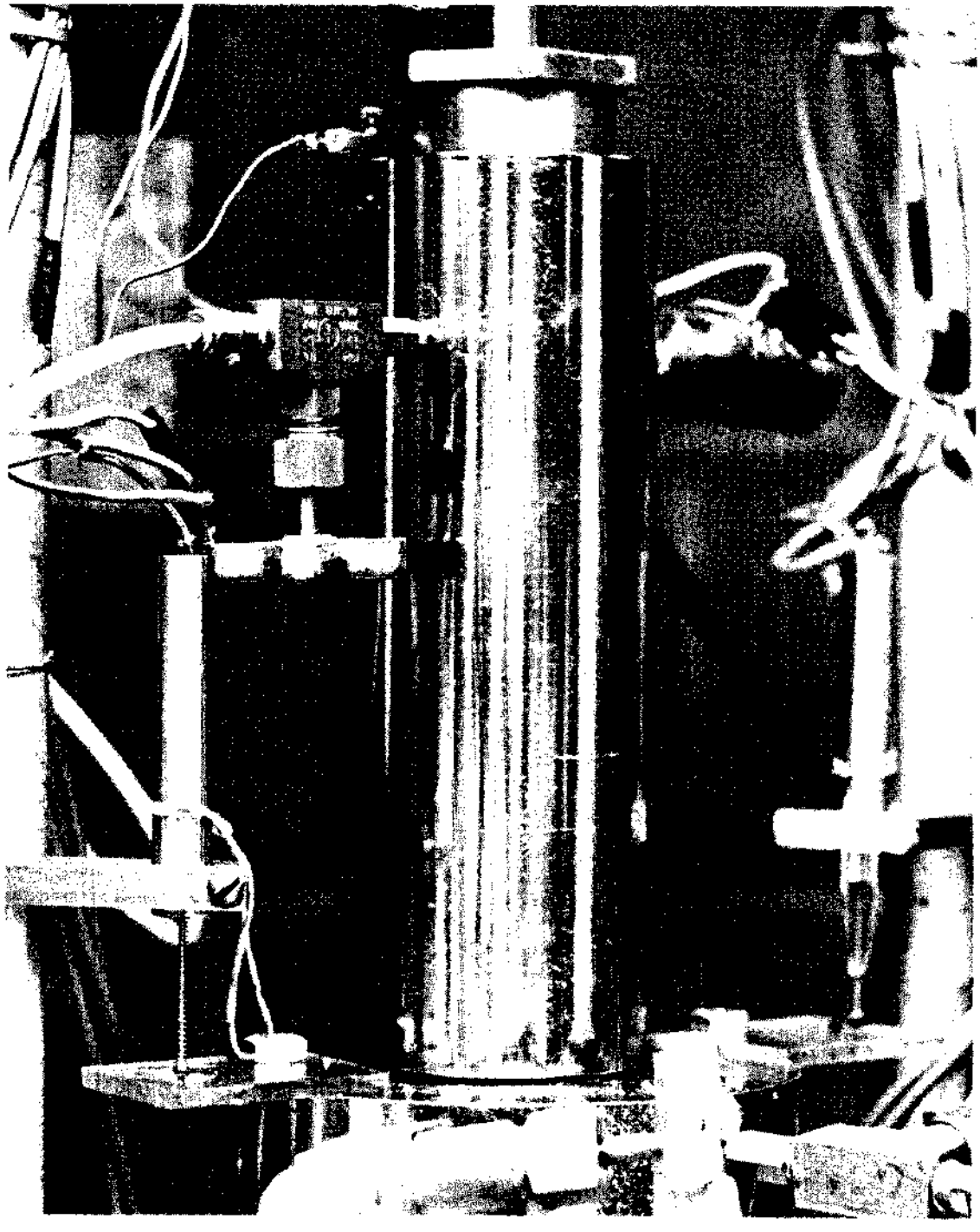

Figure 3. Location of the Linear Motion Transducer on the Exterior of the Triaxial Cell

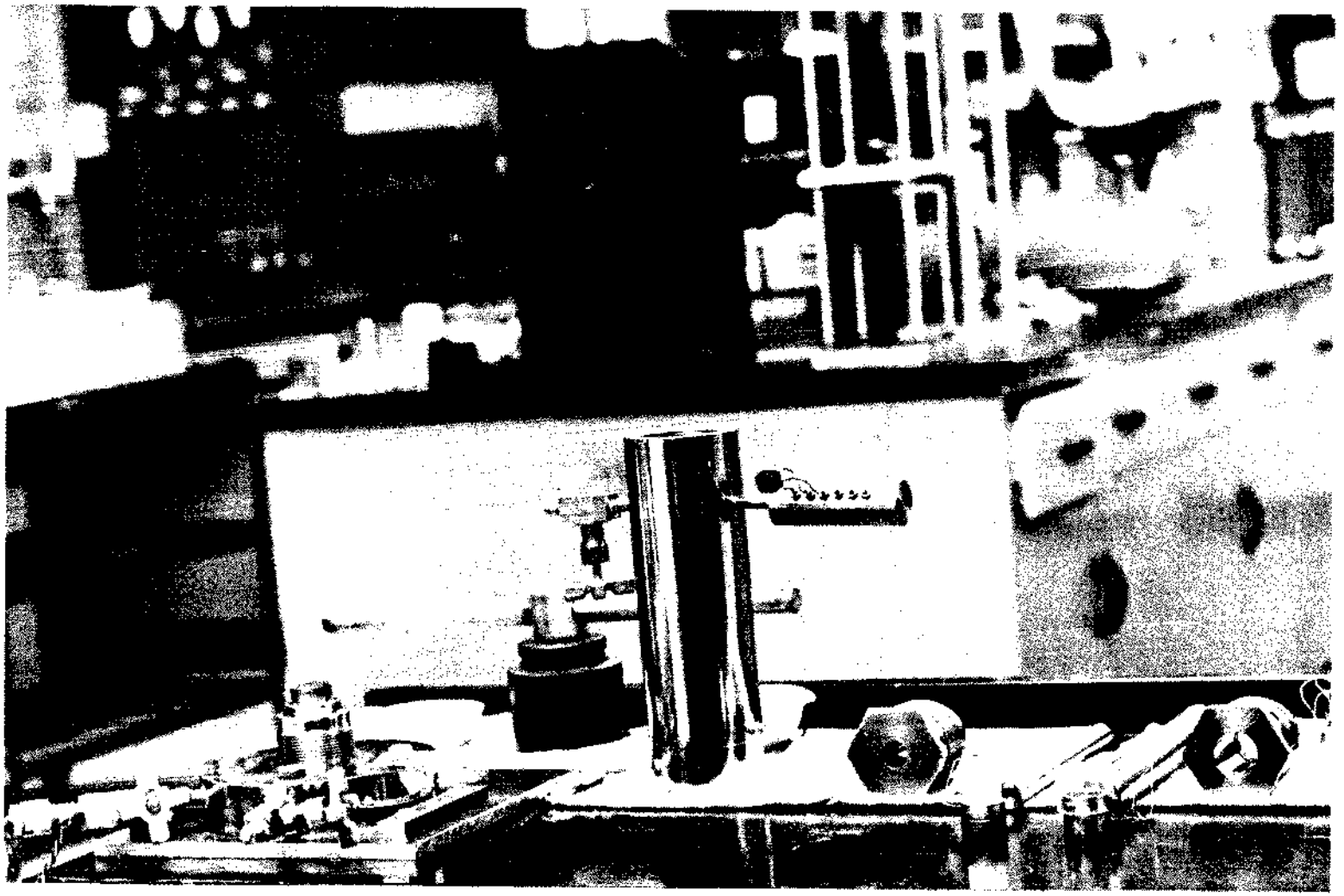

Figure 4. Triaxial Cell and Components--Unassembled

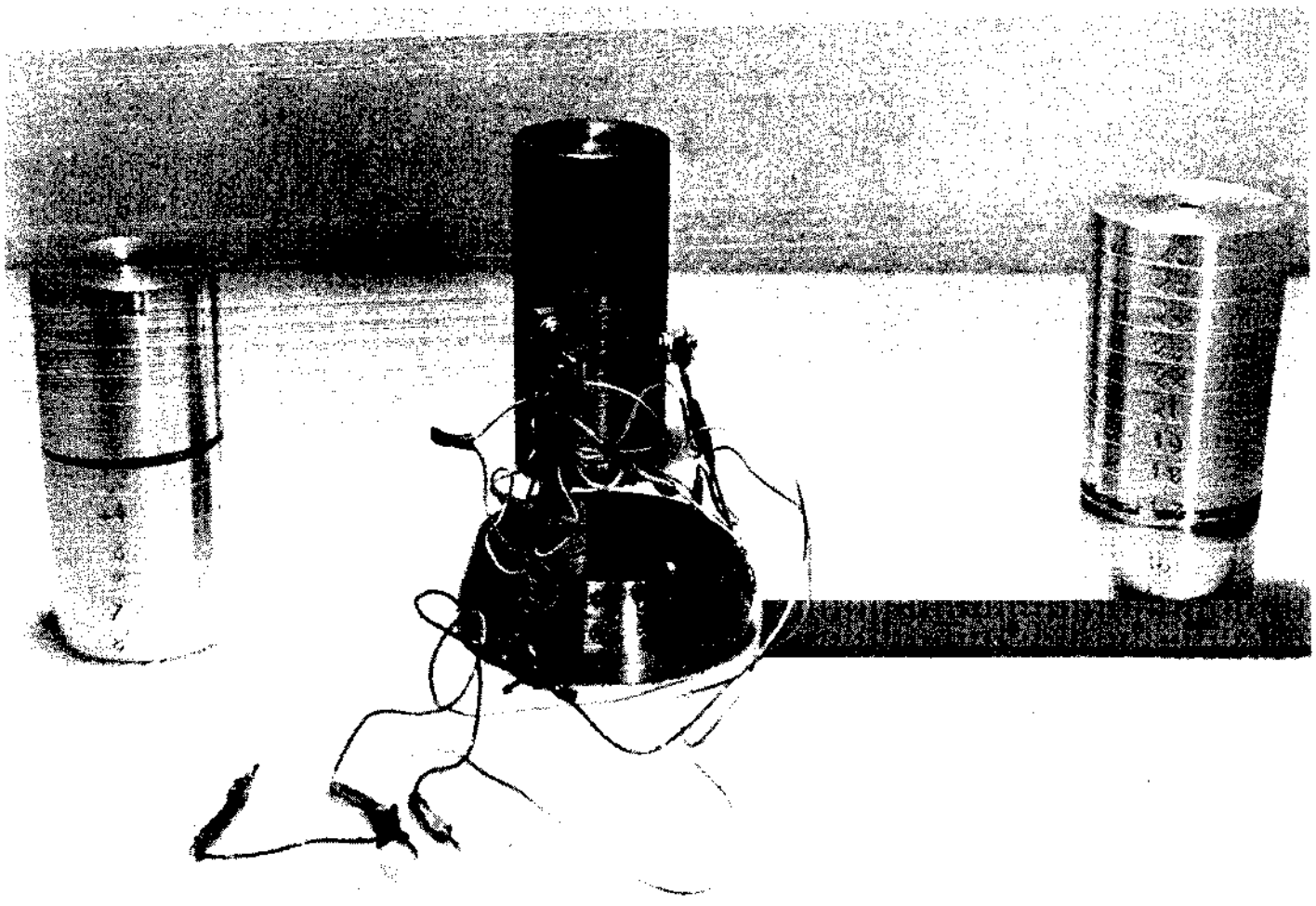

Figure 5. Lateral Deformeter with Step Blocks for Calibration

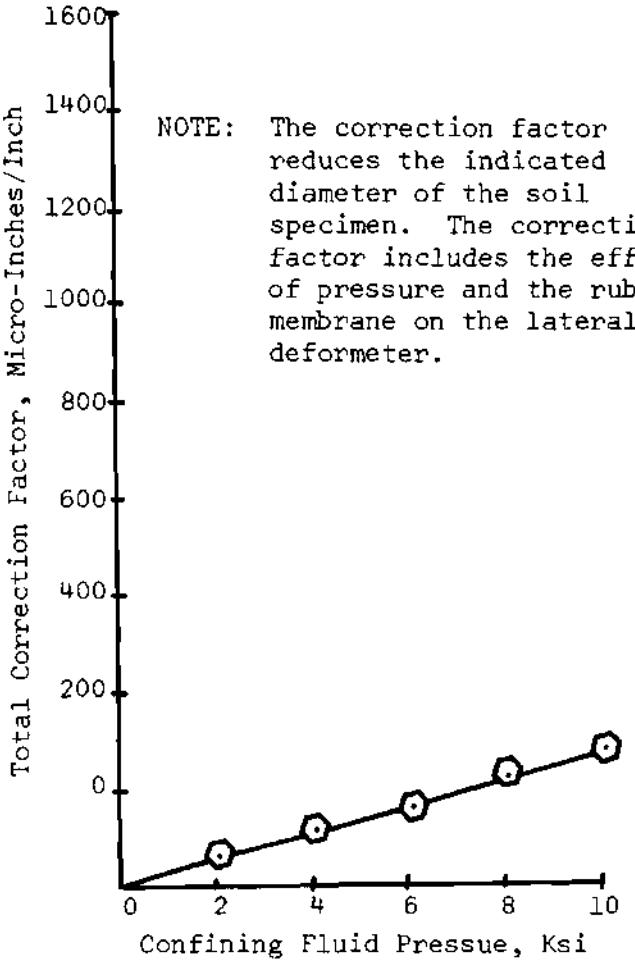

Figure 6. Total Correction--Lateral Deformeter

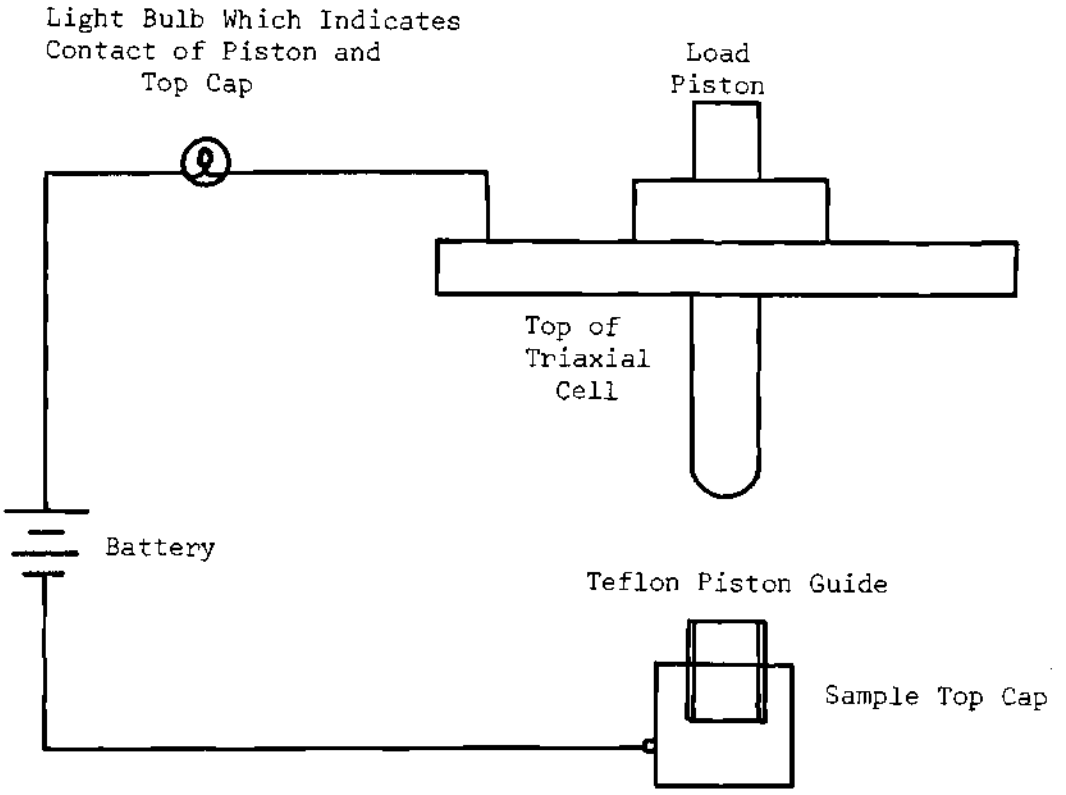

Figure 7. Wiring Diagram Between Piston and Top Cap

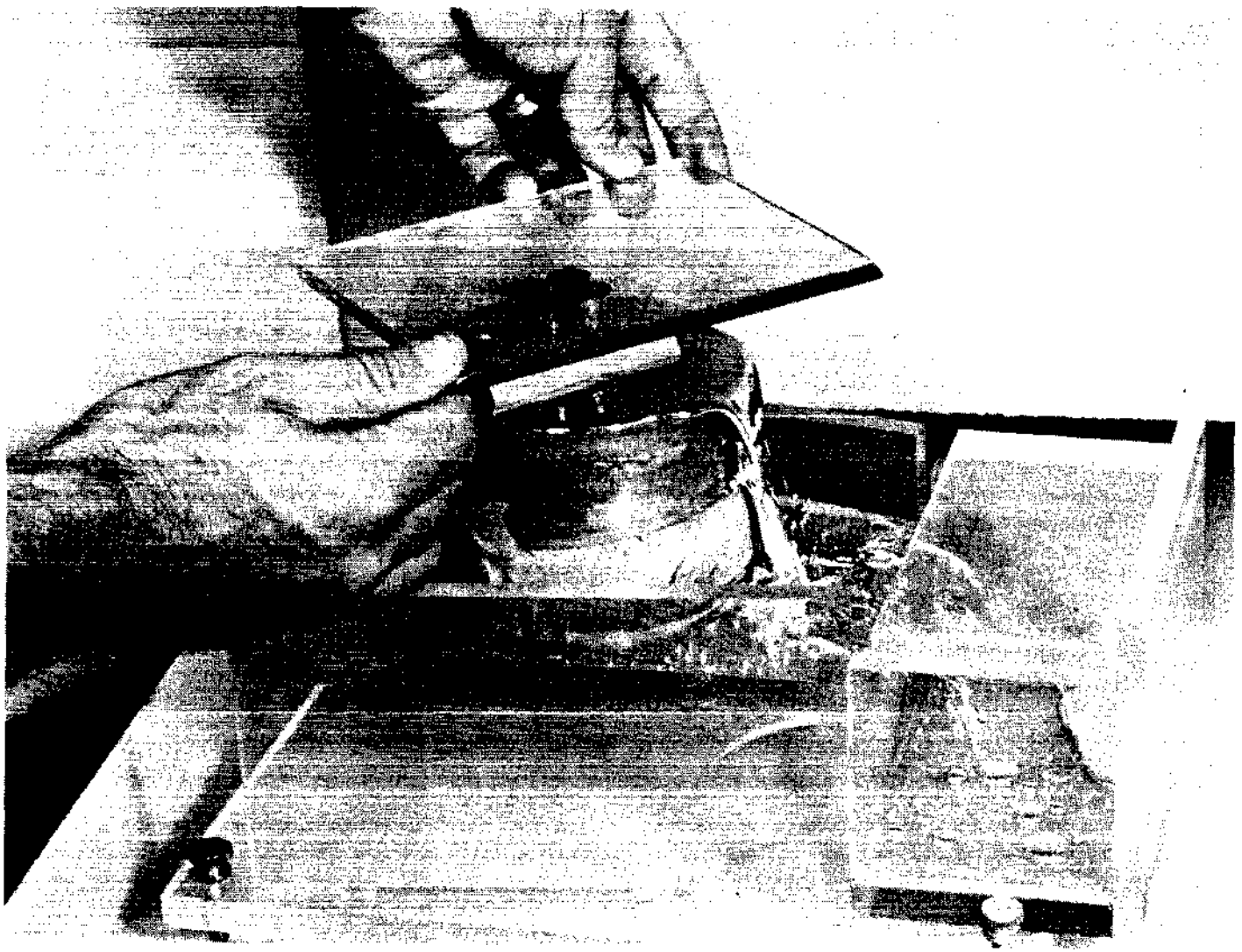

Figure 8. Sample Volume Determination by Mercury Displacement

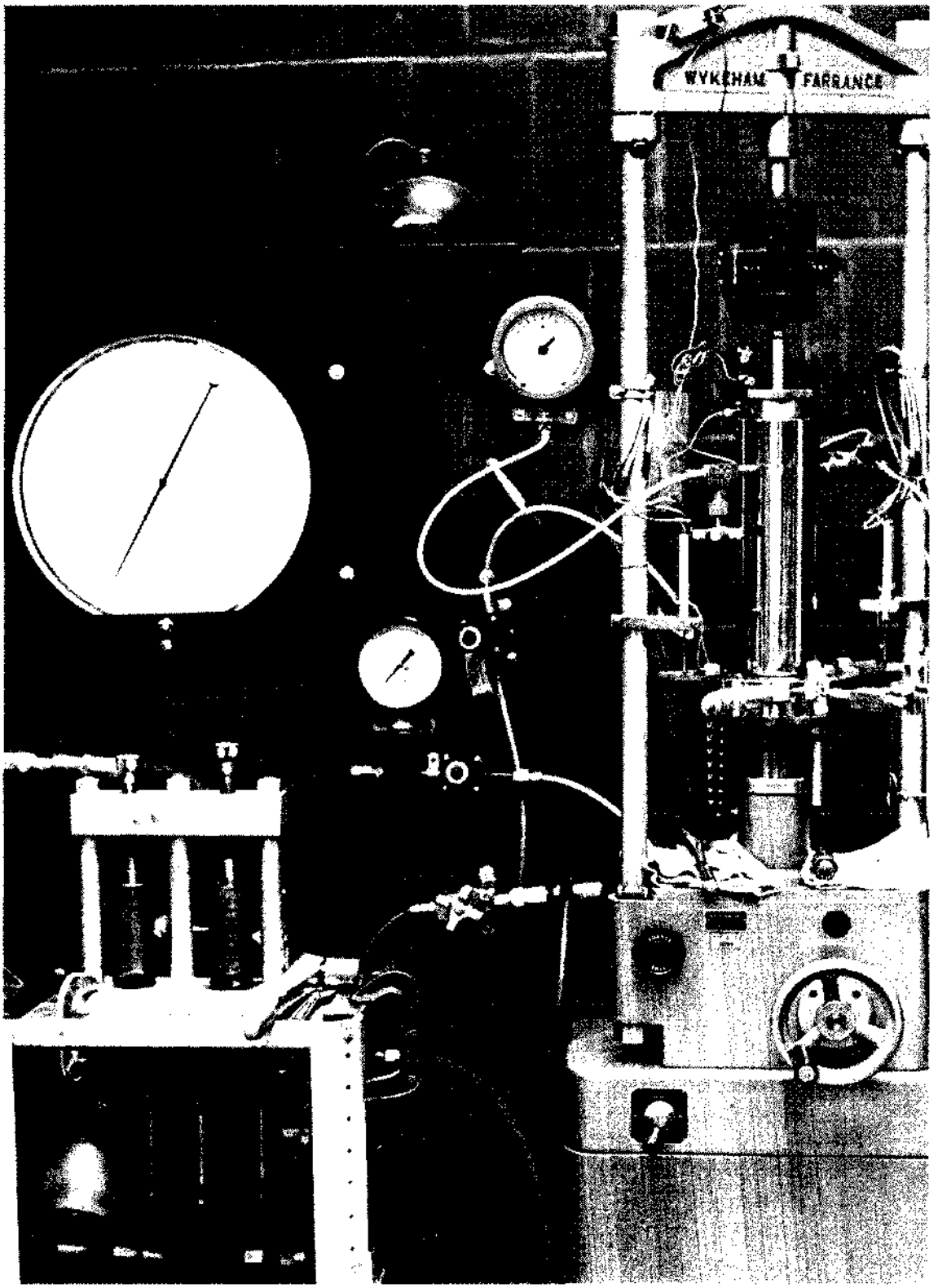

Figure 9. Loading Machine

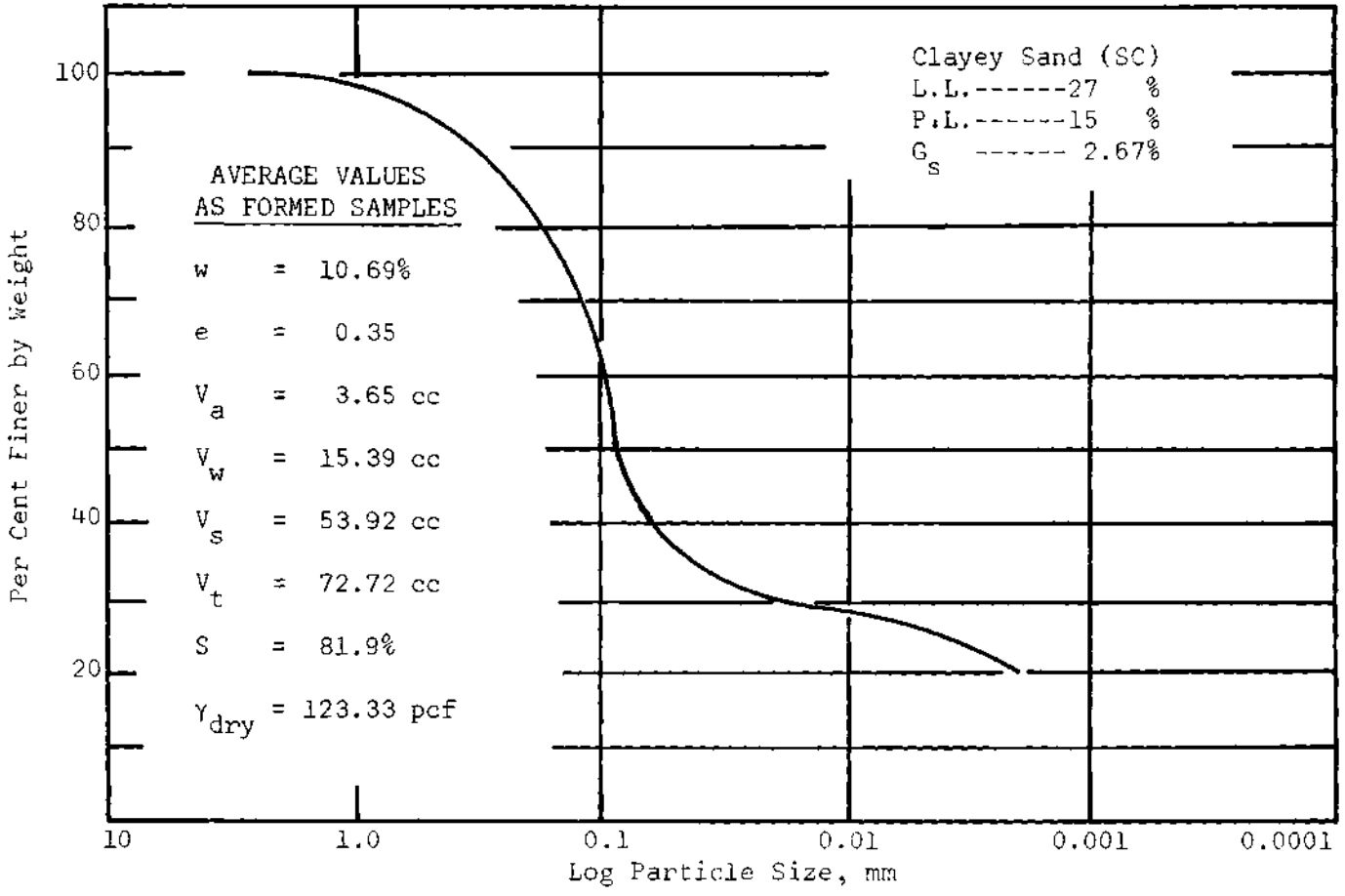

Figure 10. Grain Size Distribution--McCormick Ranch Soil

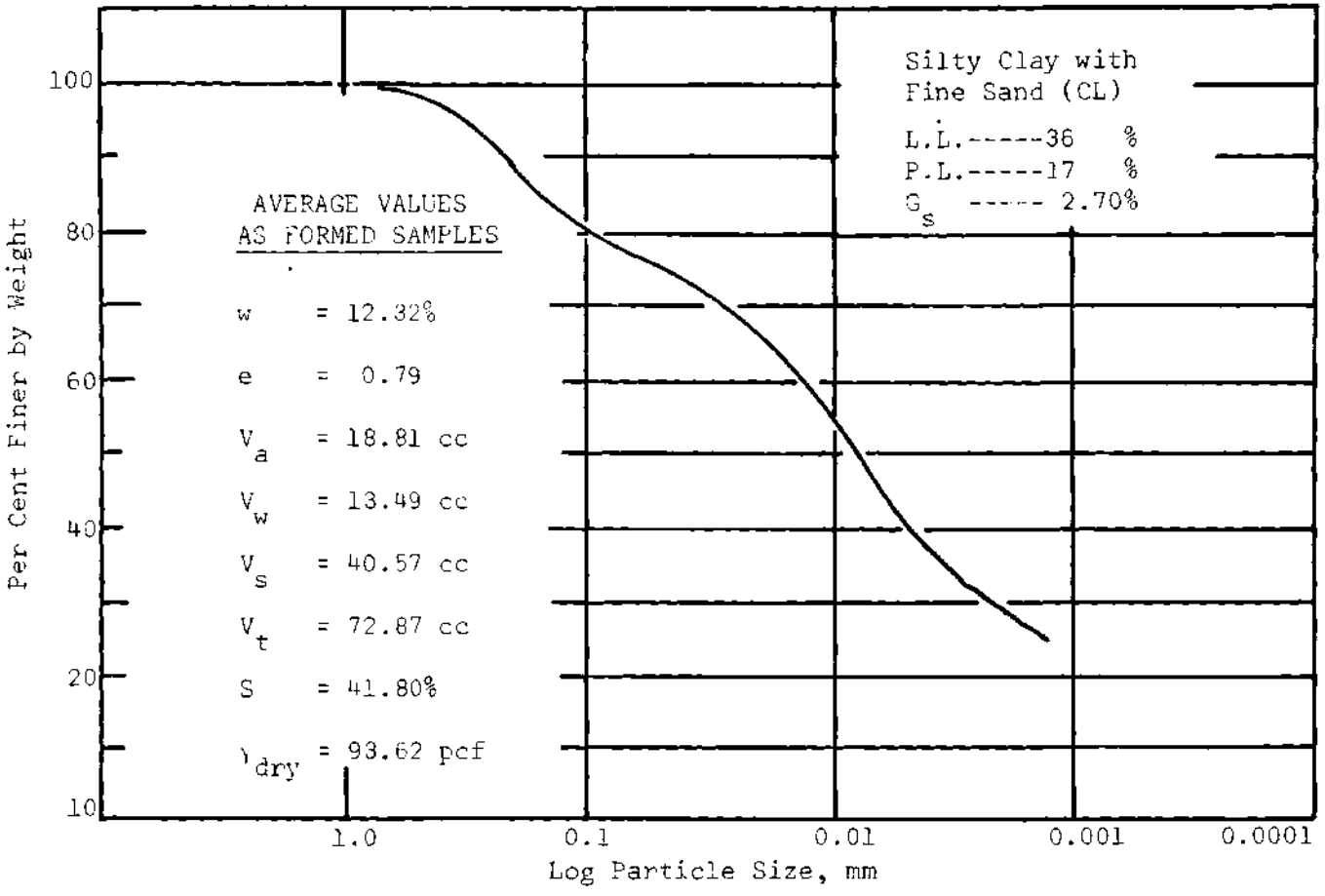

Figure 11. Grain Size Distribution--Watching Hill Soil

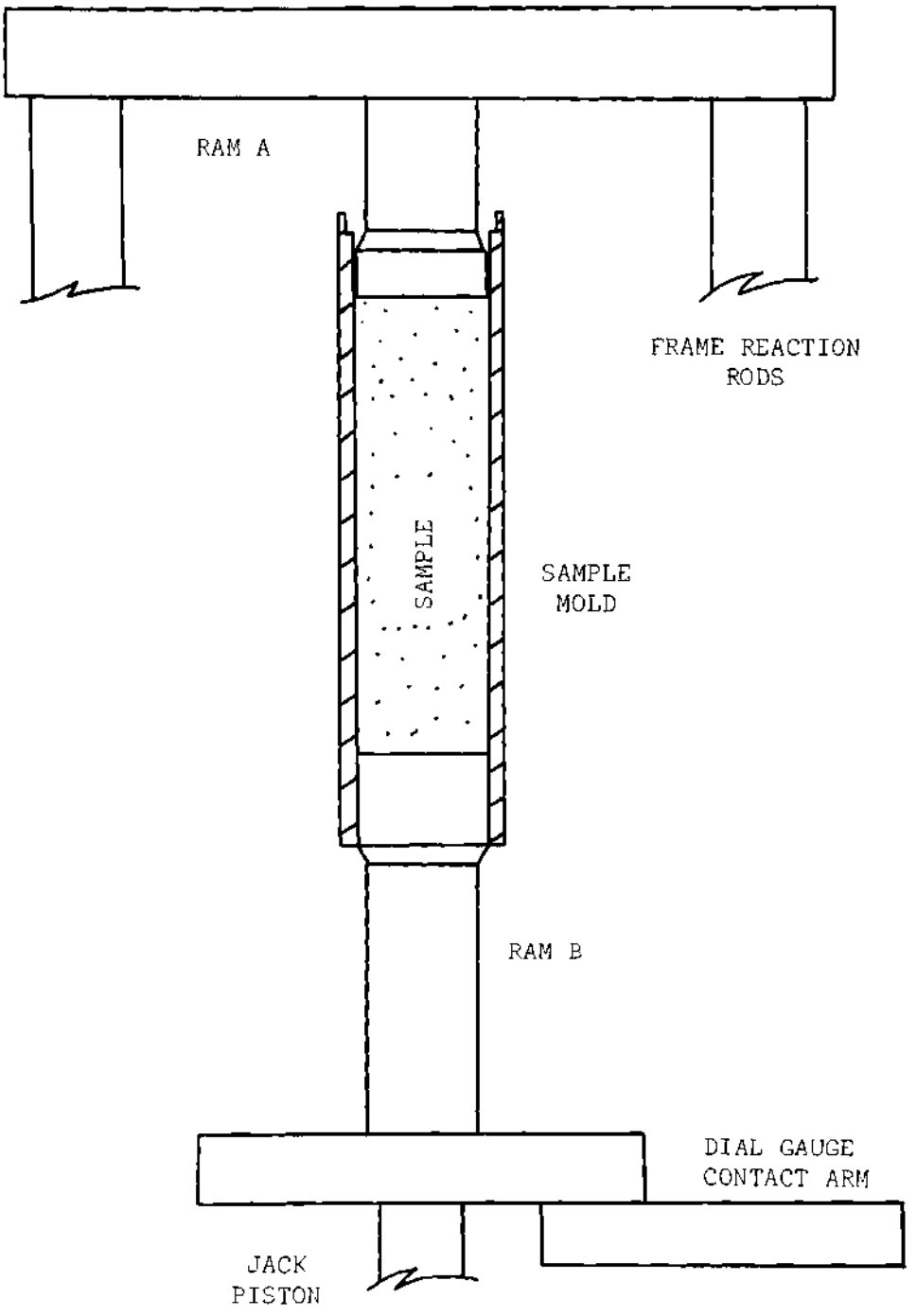

Figure 12. Loading Apparatus for Sample Forming

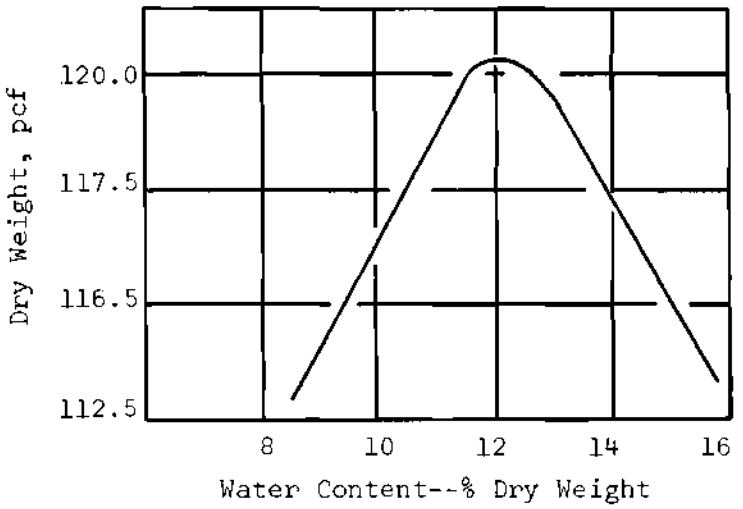

(a) McCormick Ranch Clayey Sand

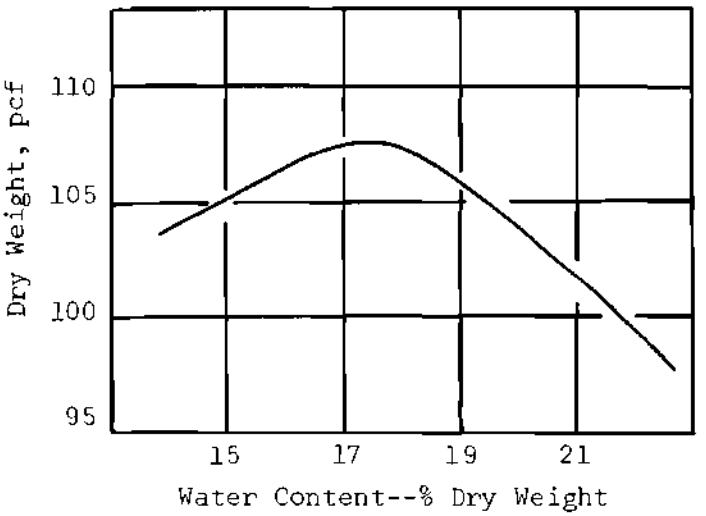

(b) Watching Hill Clay

Figure 13. Moisture-Density Relationships, Standard Proctor

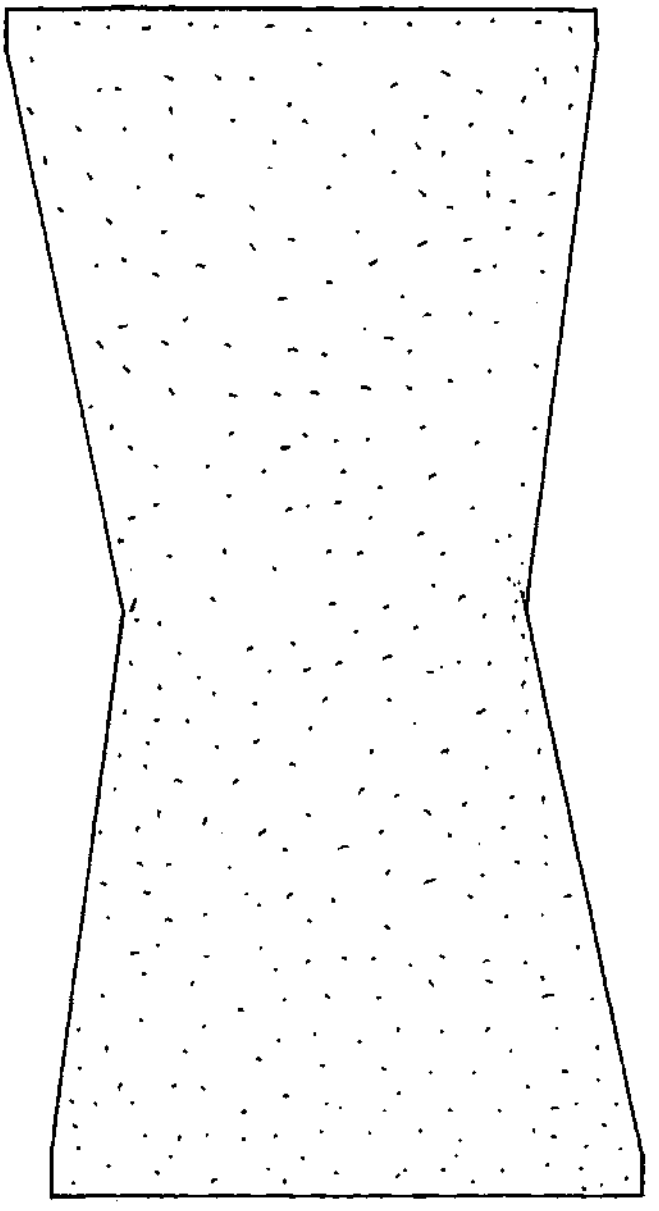

Figure 14. Sample Shape after Compression Under Hydrostatic Stress, McCormick Ranch Sand

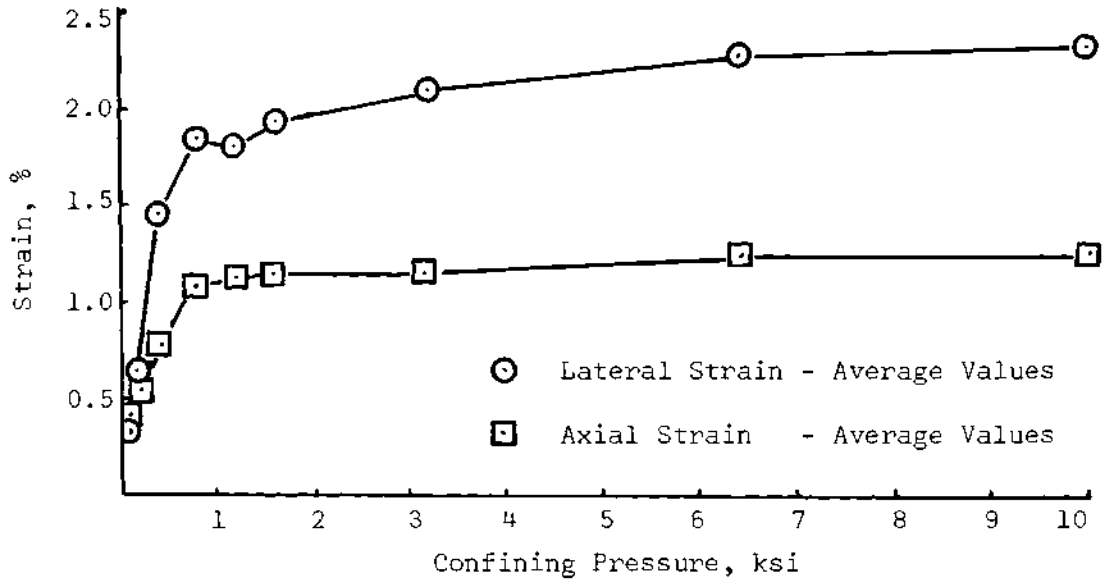

Figure 15. Hydrostatic Loading, Axial and Lateral Strain as a Function of Confining Pressure, McCormick Ranch Sand

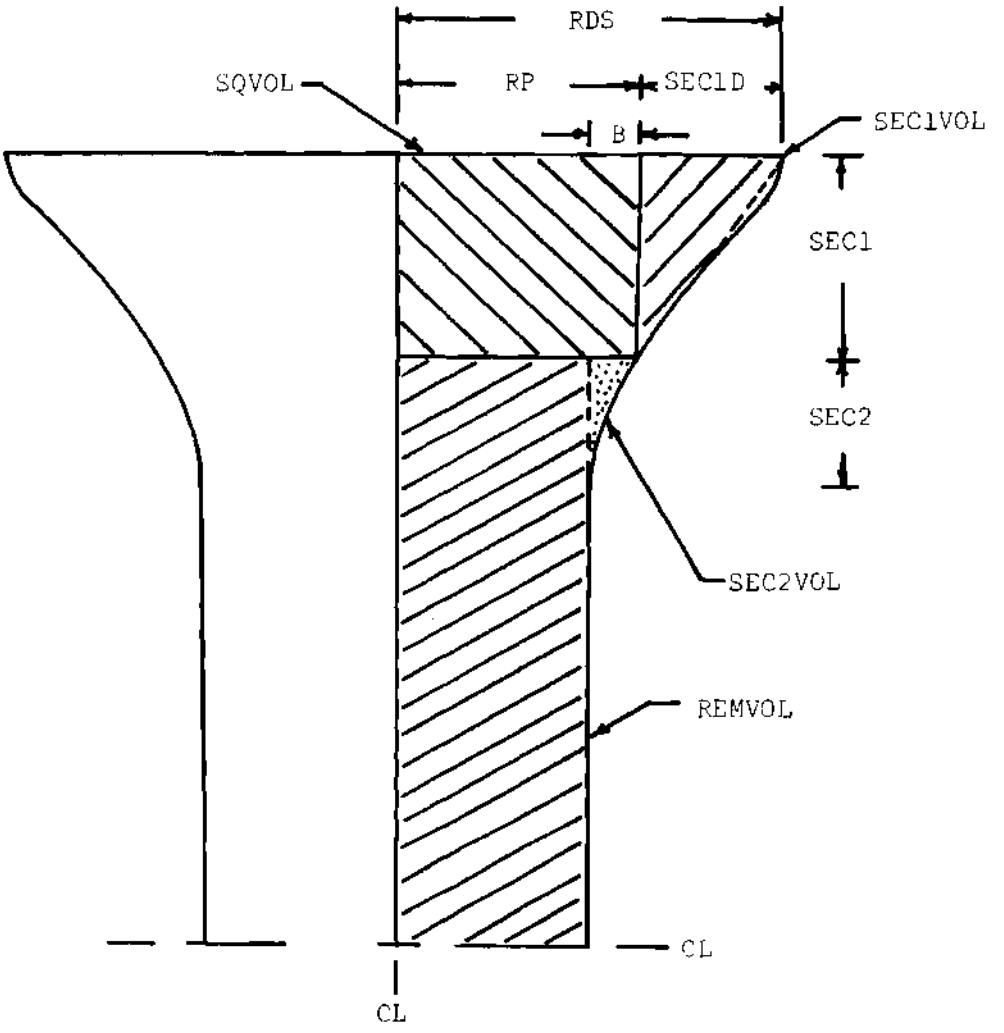

Sample Symmetrical About Centerline (CL)
(For Dimensions See Table 2)

Figure 16. Sample Shape after Hydrostatic Compression, Watching Hill Clay

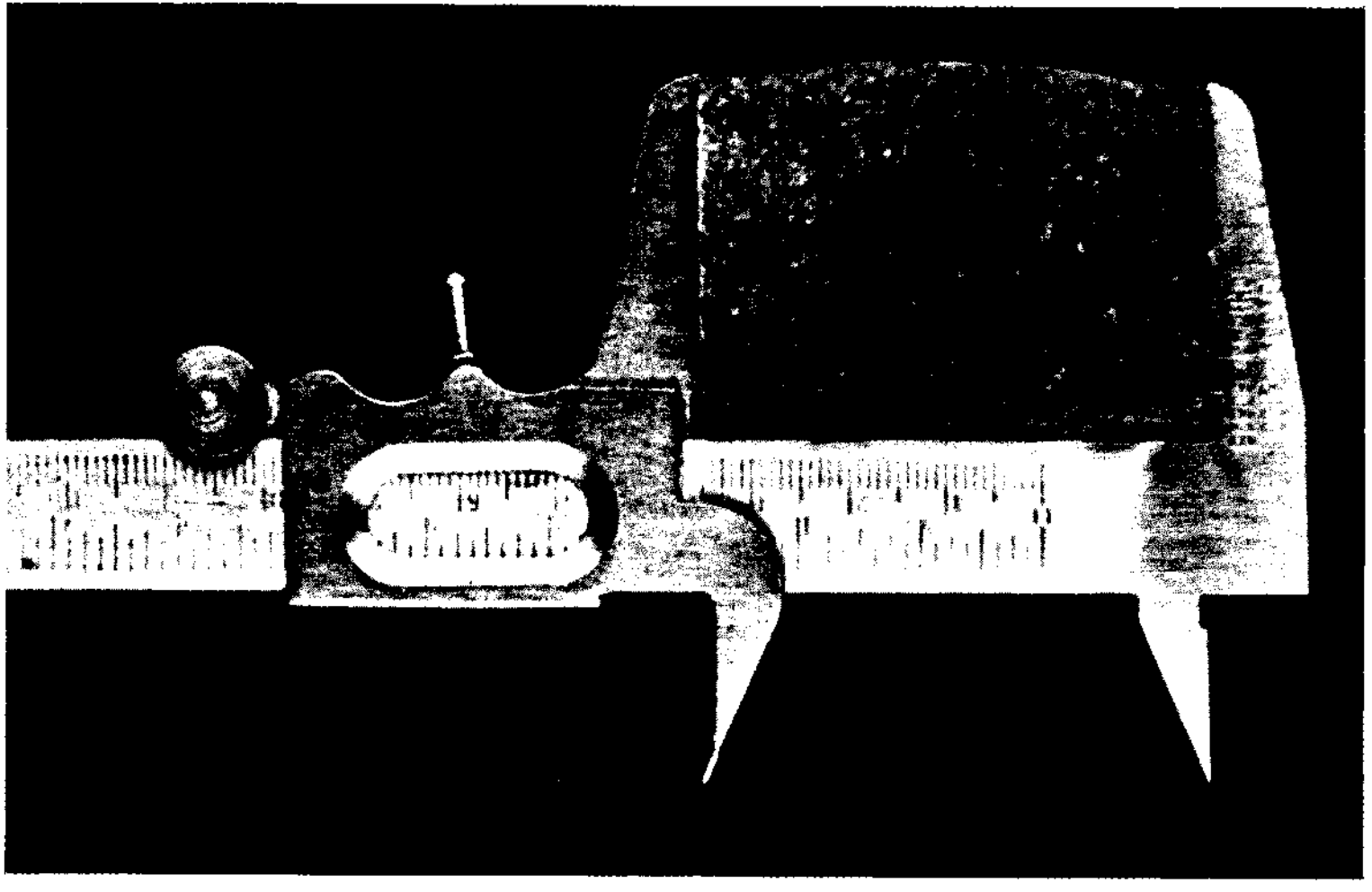

Figure 17. Watching Hill Clay Sample Following the Standard Triaxial Test at 6400 psi Confinement

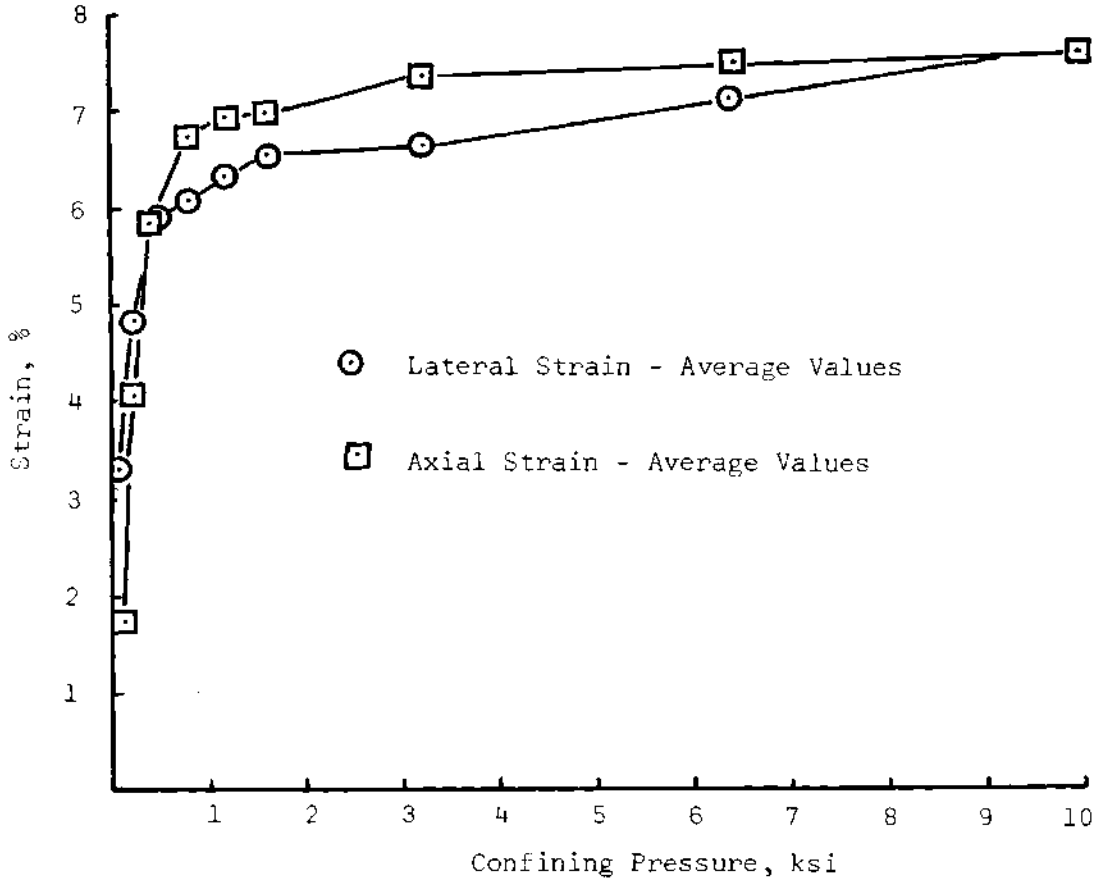

Figure 18. Axial and Lateral Strain as a Function of Confining Pressure, Hydrostatic Loading, Watching Hill Clay

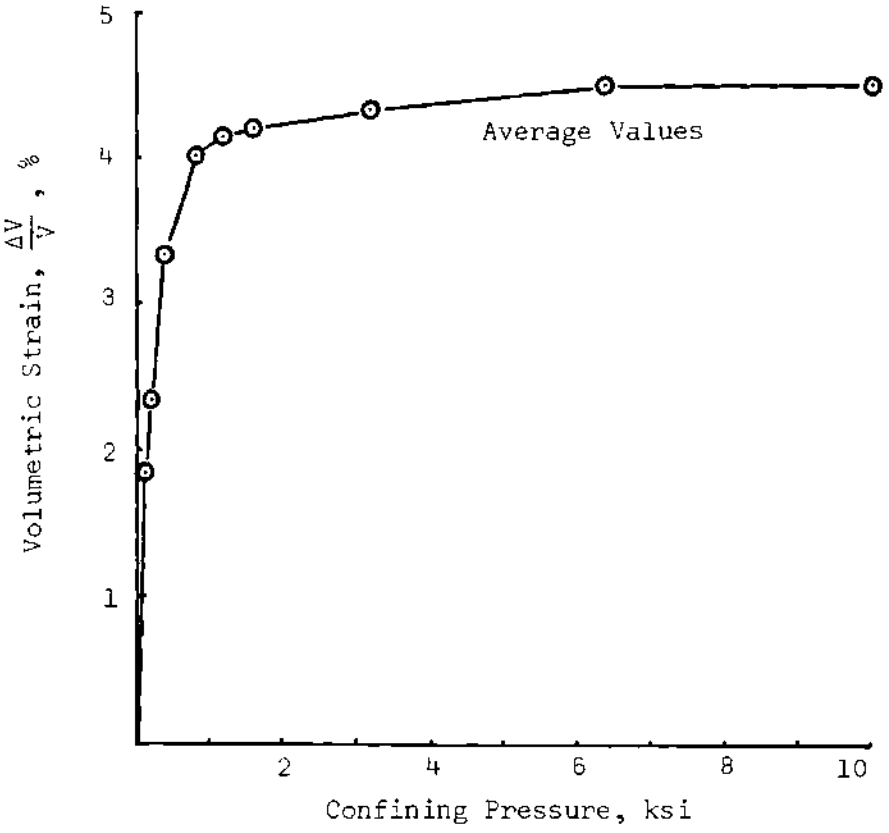

Figure 19. Volumetric Strain as a Function of Confining Pressure, McCormick Ranch Sand

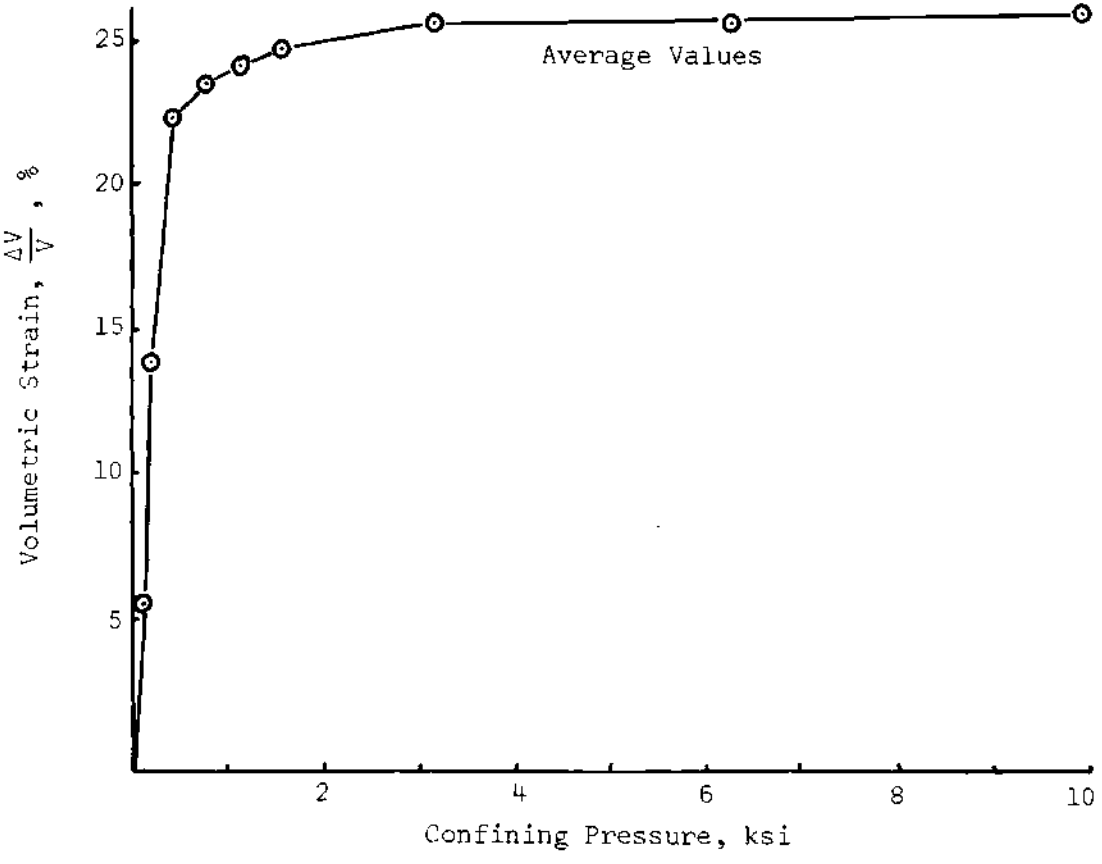

Figure 20. Volumetric Strain as a Function of Confining Pressure, Watching Hill Clay

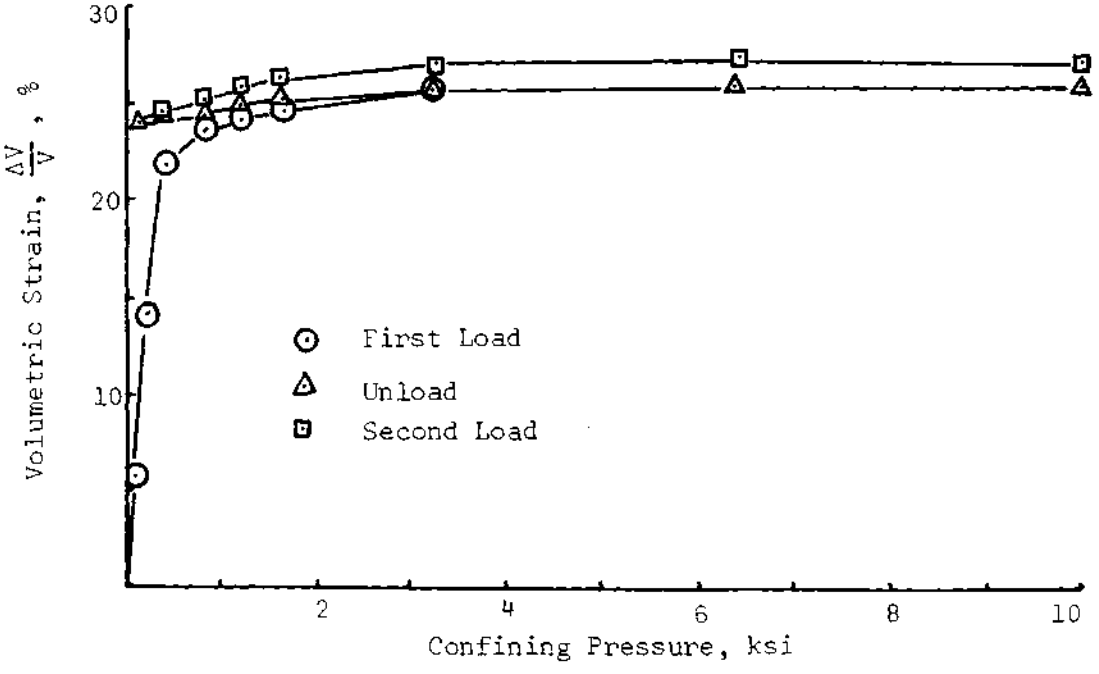

Figure 21. Volumetric Strain as a Function of Confining Pressure, Cycle Hydrostatic Stress, Watching Hill Clay

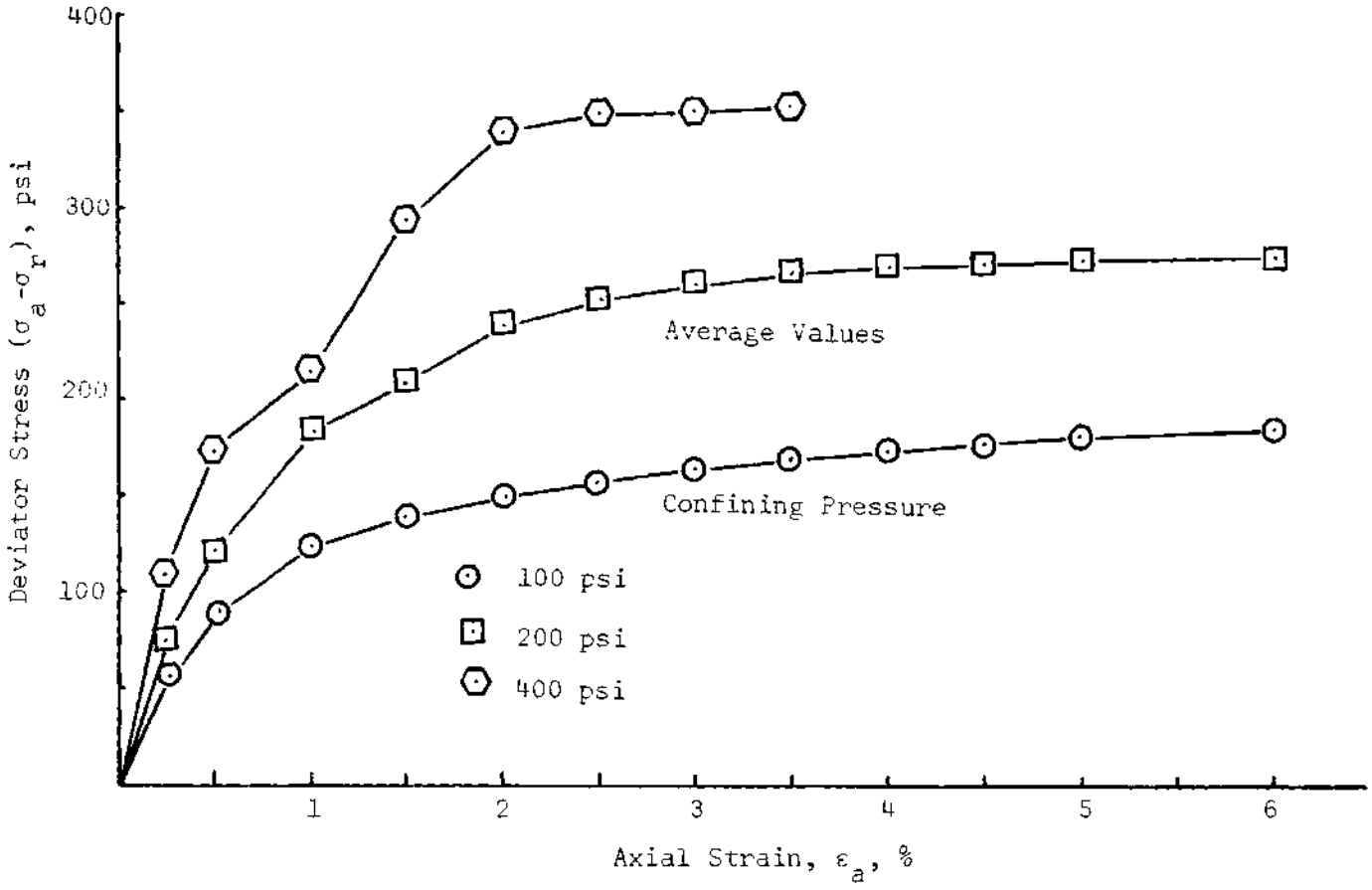

Figure 22. Deviator Stress as a Function of Axial Strain, Standard Triaxial Test, McCormick Ranch Sand

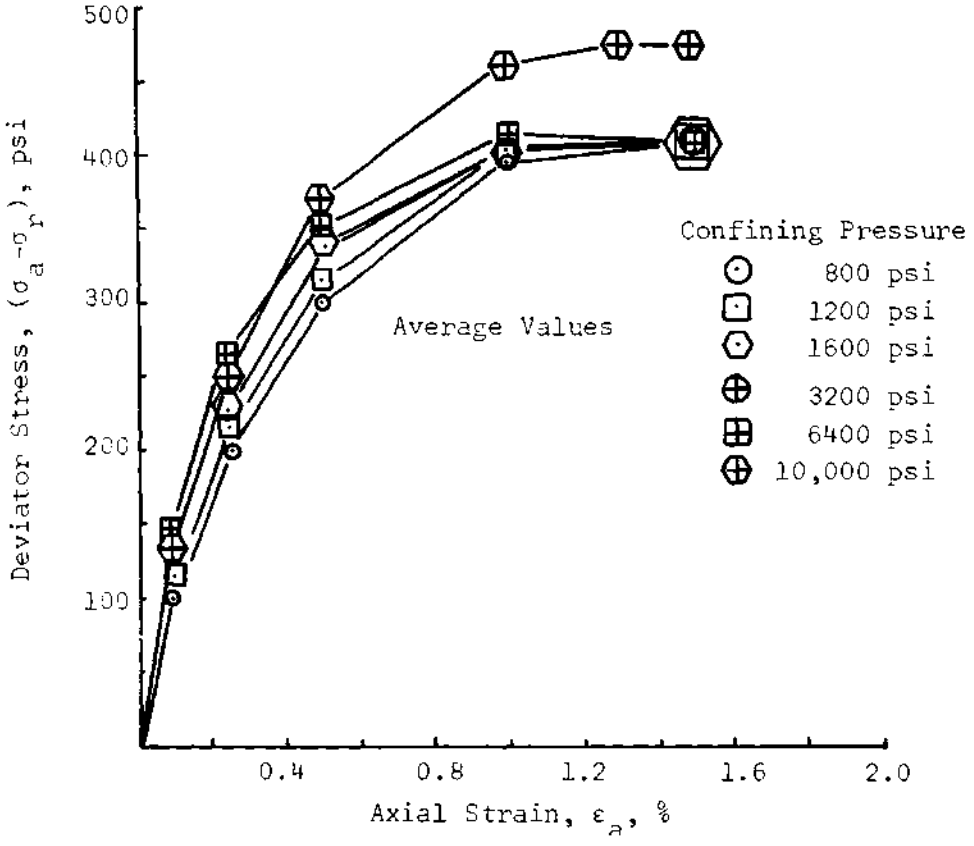

Figure 23. Deviator Stress as a Function of Axial Strain, Standard Triaxial Test, McCormick Ranch Sand

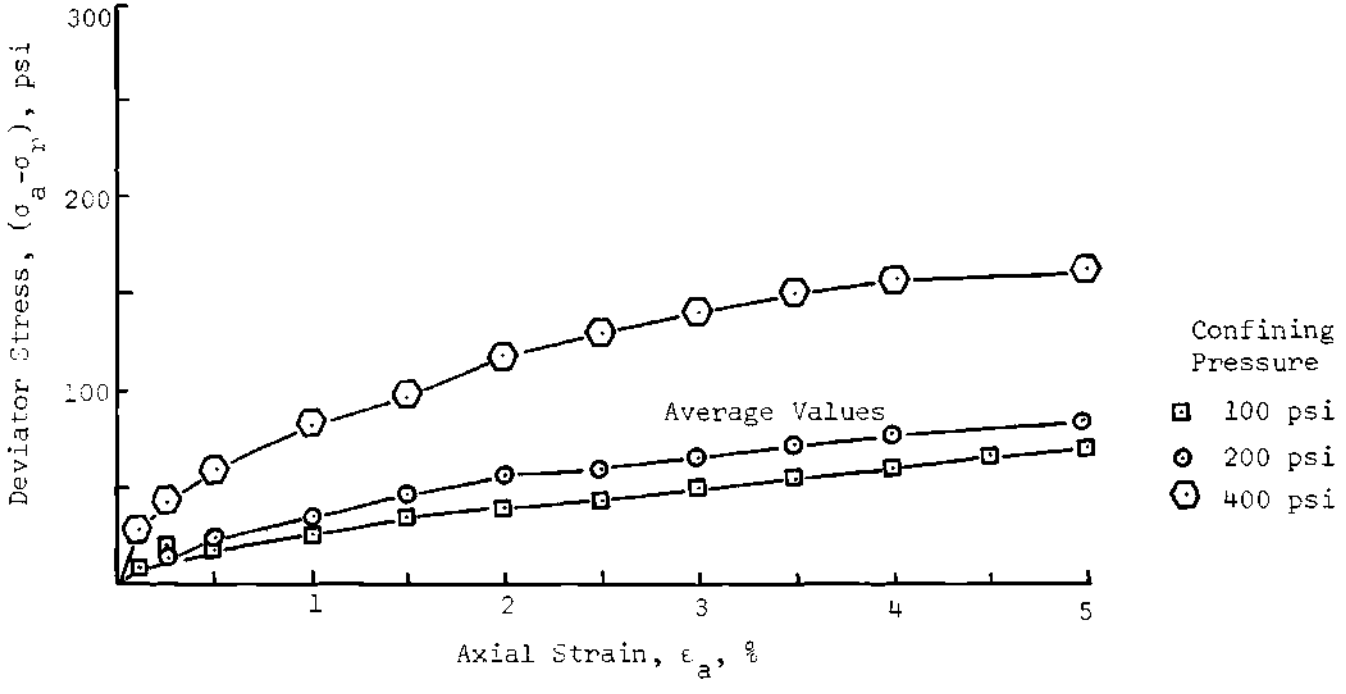

Figure 24. Deviator Stress as a Function of Axial Strain, Standard Triaxial Test, Watching Hill Clay

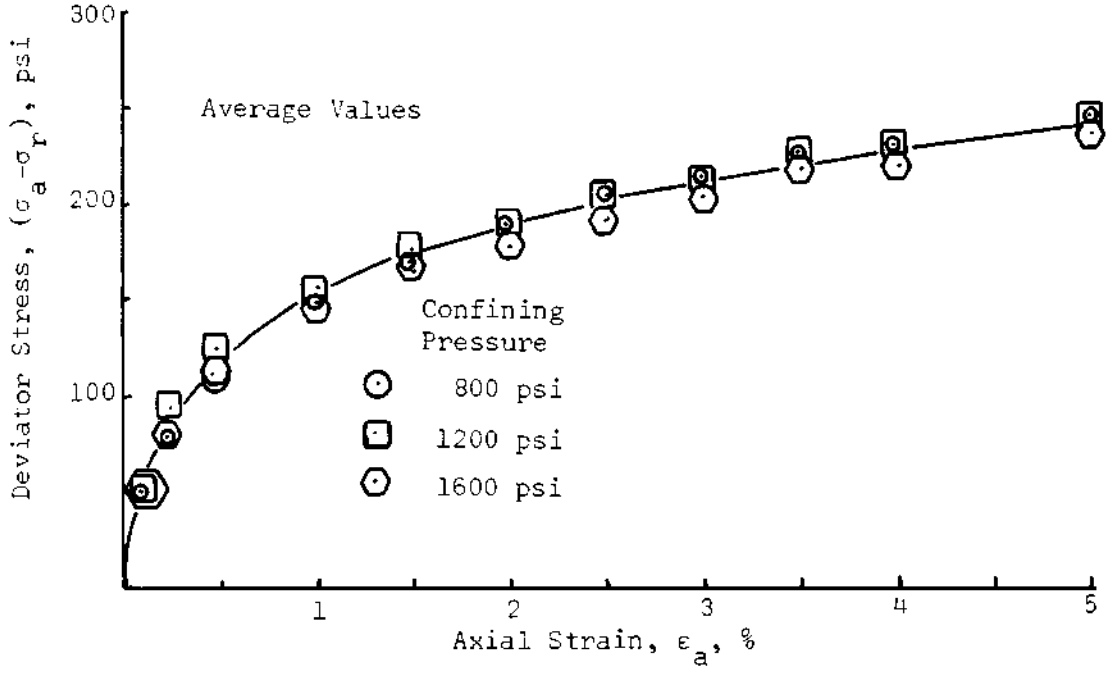

Figure 25. Deviator Stress as a Function of Axial Strain, Standard Triaxial Test, Watching Hill Clay

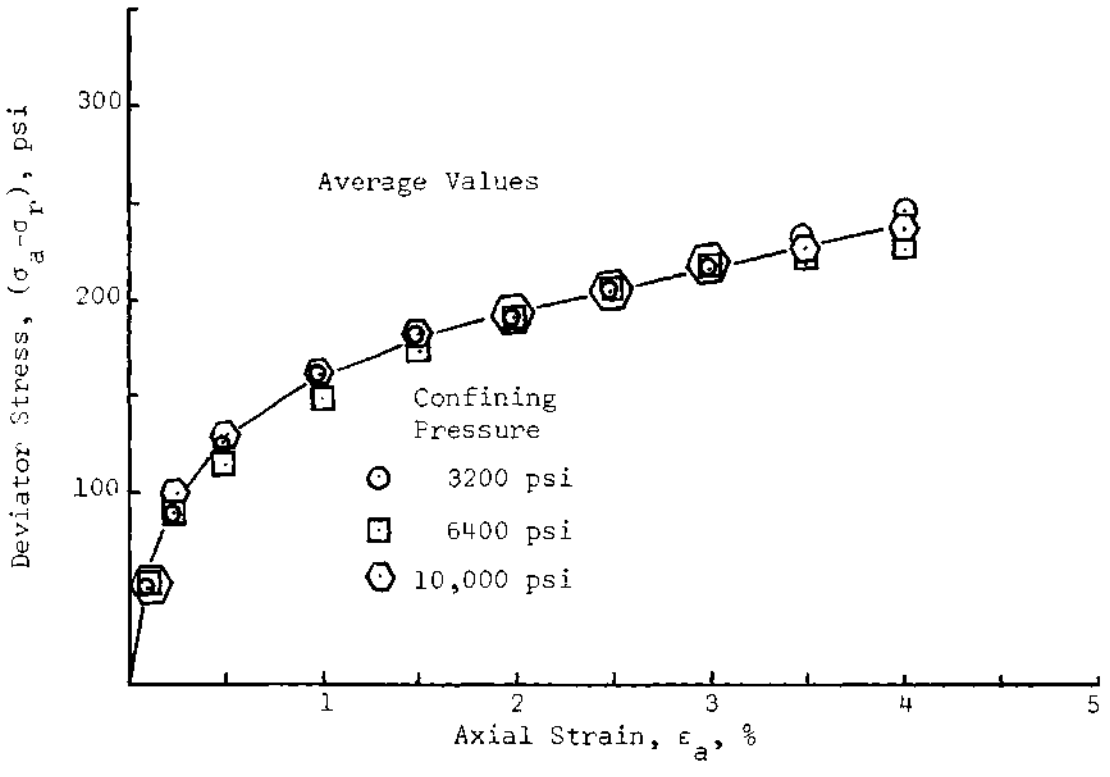

Figure 26. Deviator Stress as a Function of Axial Strain, Standard Triaxial Test, Watching Hill Clay

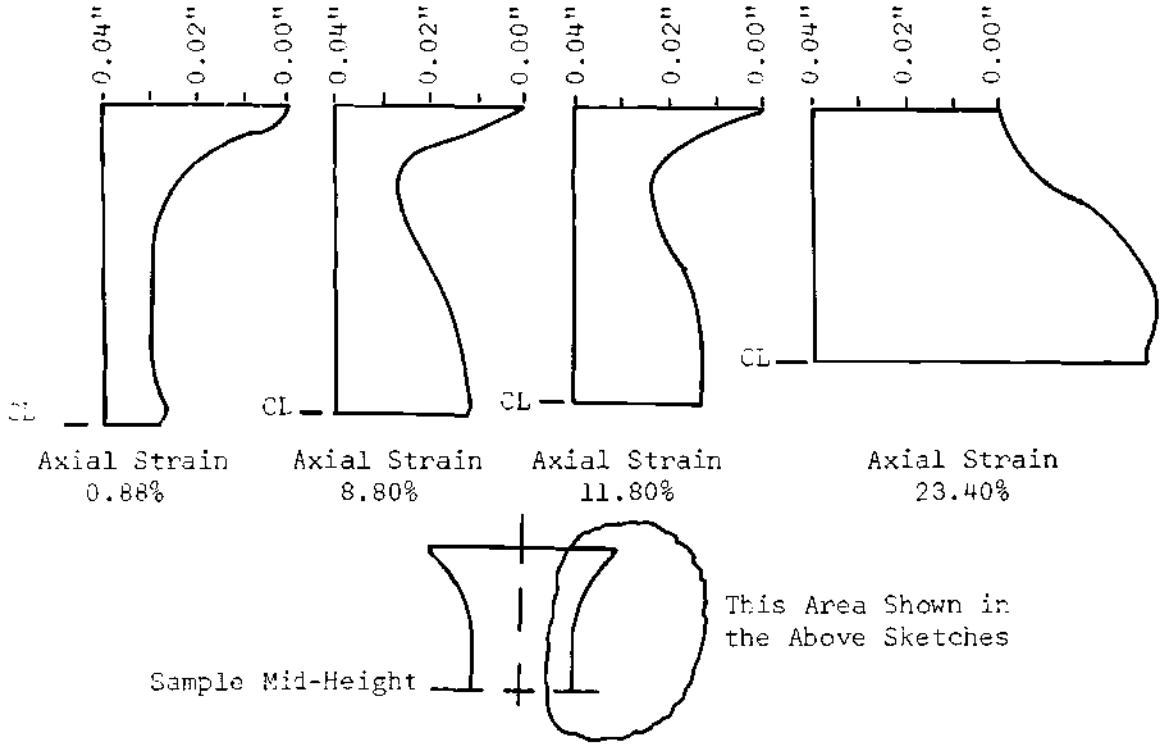

Figure 27. Deformed Sample, Standard Triaxial Test at a Confining Pressure of 3200 psi, Watching Hill Clay

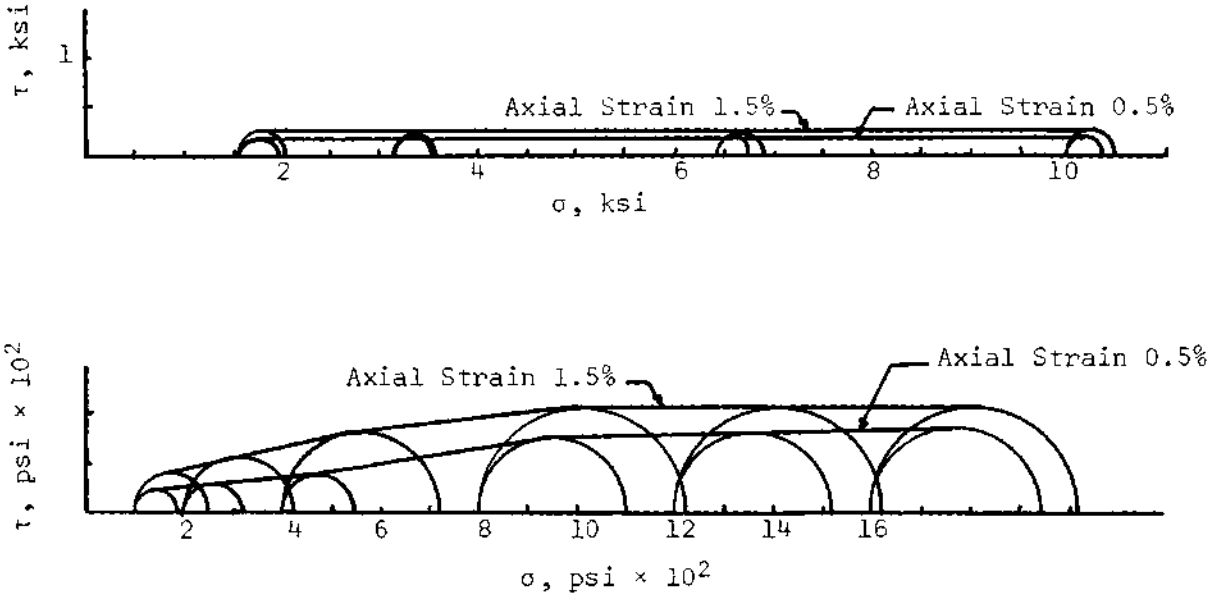

Figure 28. Mohr's Circles--Total Stress, McCormick Ranch Sand

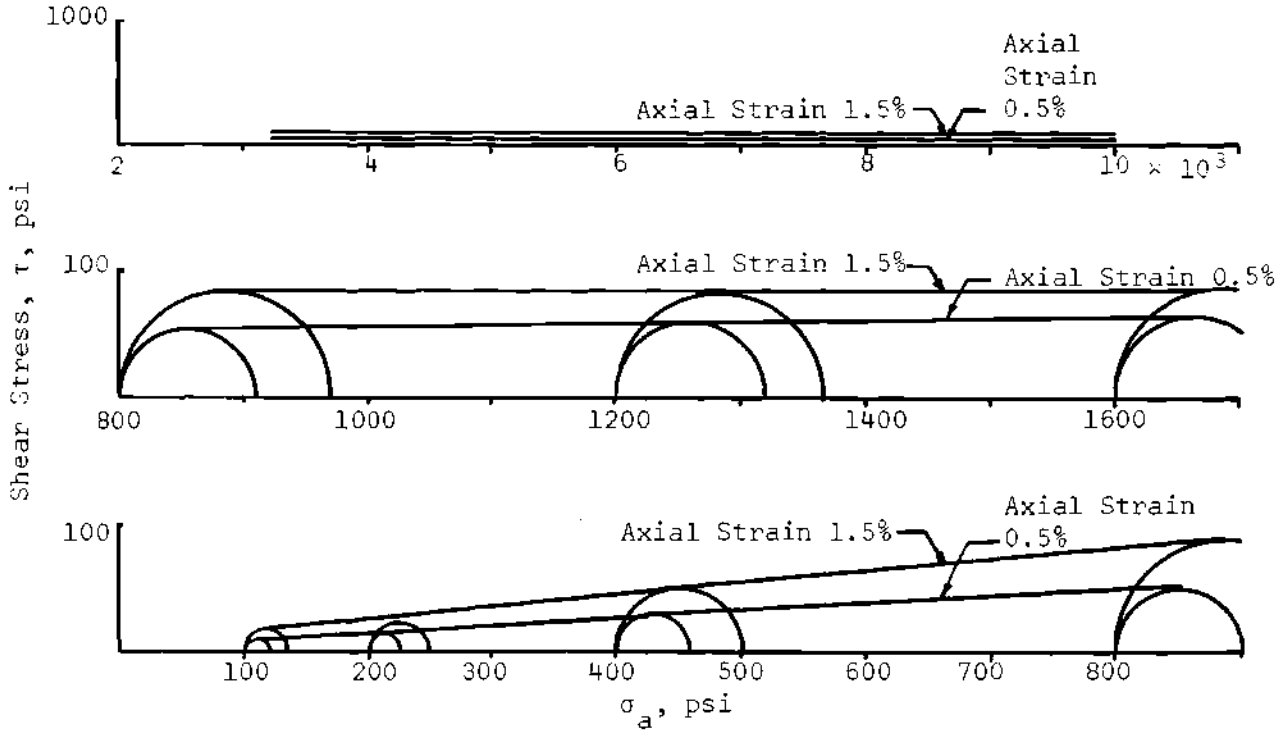

Figure 29. Mohr's Circles--Total Stress, Watching Hill Clay

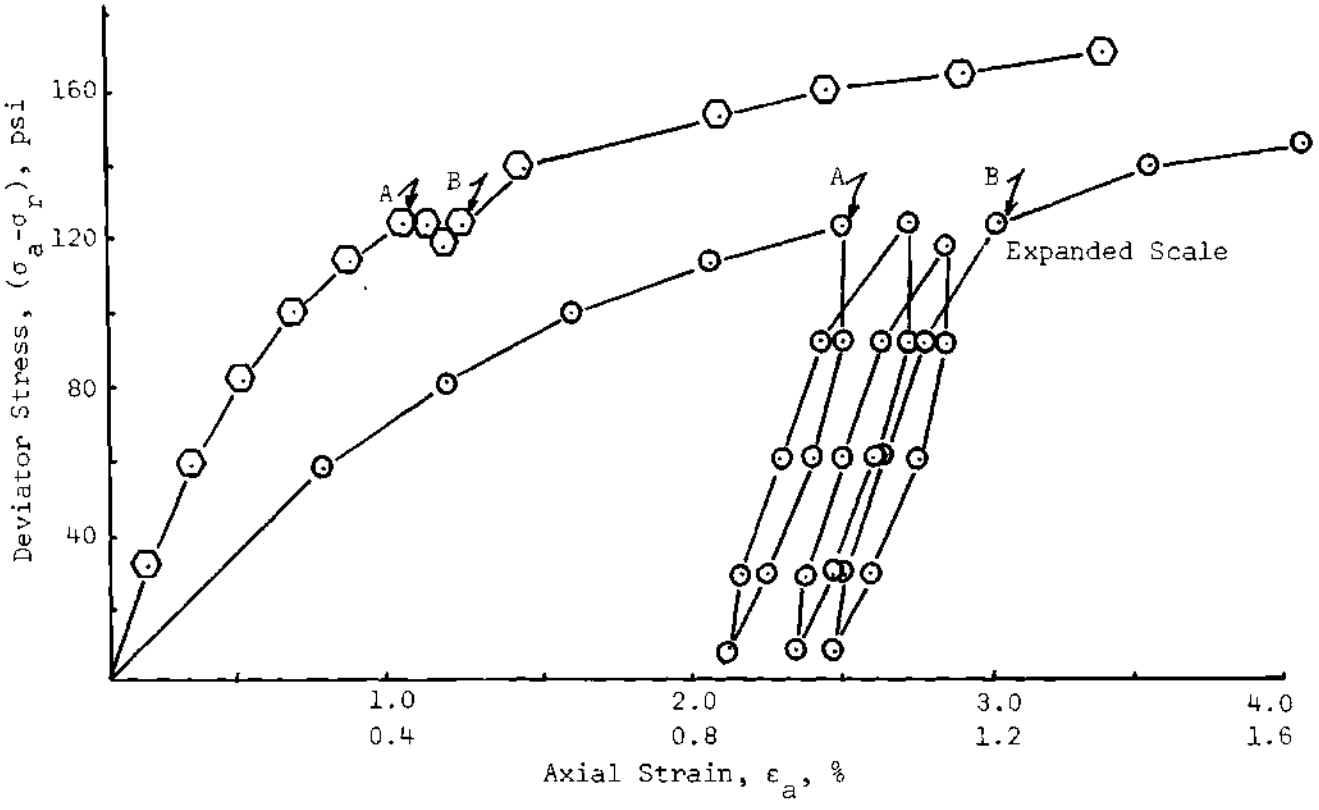

Figure 30. Deviator Stress as a Function of Axial Strain, 100 psi Confinement, McCormick Ranch Soil

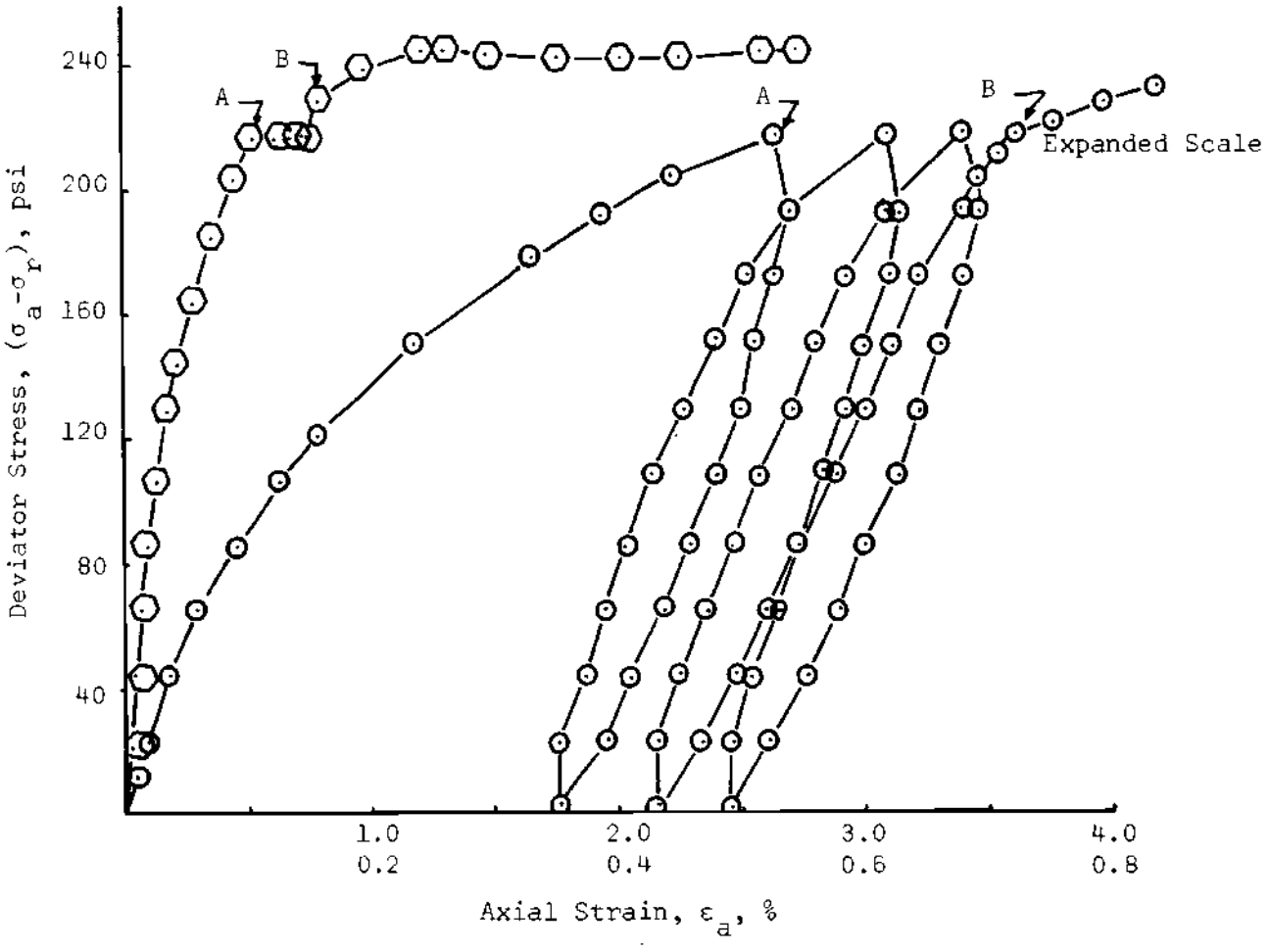

Figure 31. Deviator Stress as a Function of Axial Strain, 800 psi Confinement, McCormick Ranch Sand

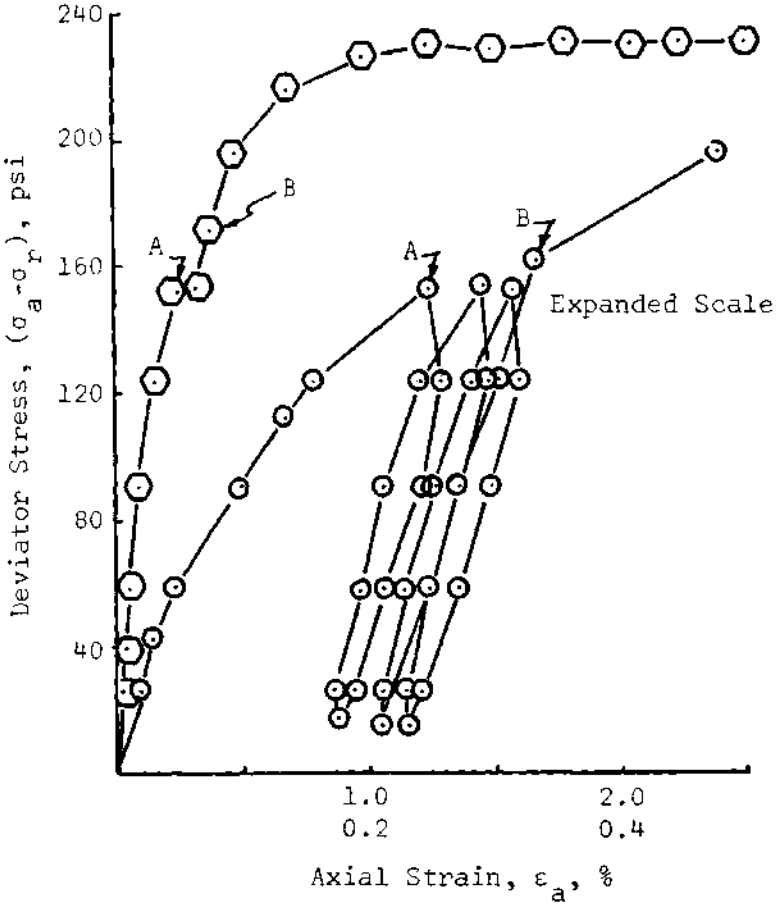

Figure 32. Deviator Stress as a Function of Axial Strain, 1600 psi Confinement, McCormick Ranch Sand

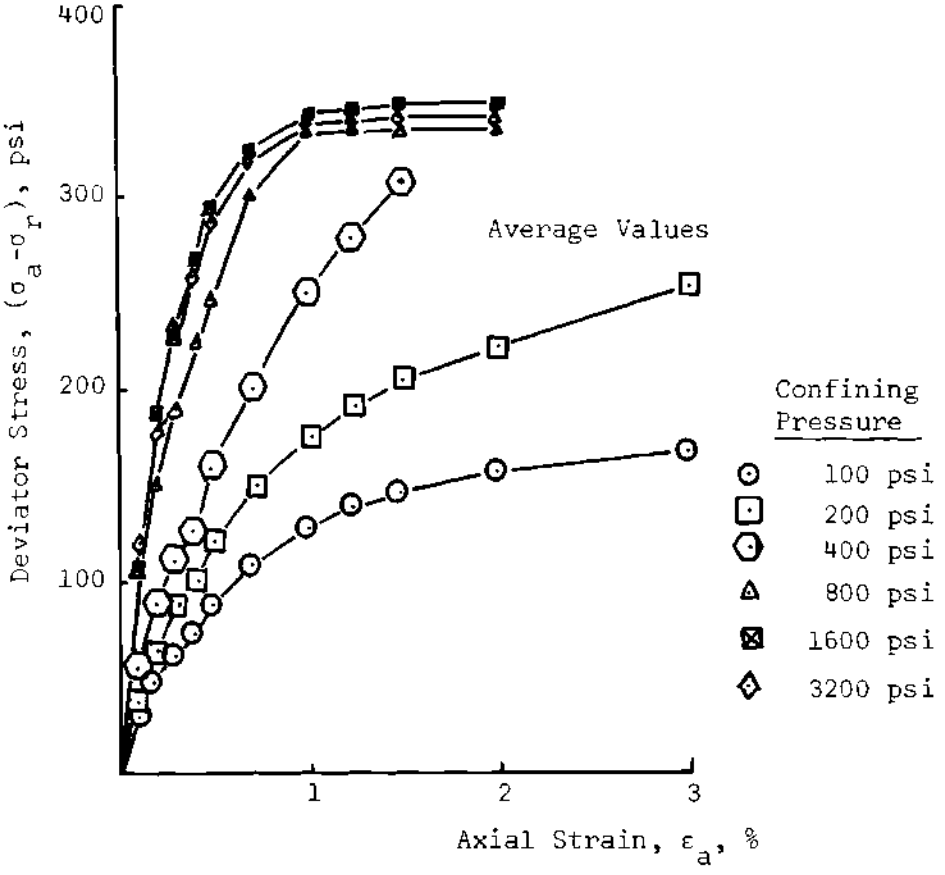

Figure 33. Deviator Stress as a Function of Axial Strain, Deviator Stress Cycled at 35% of Deviator Stress at Failure, McCormick Ranch Sand

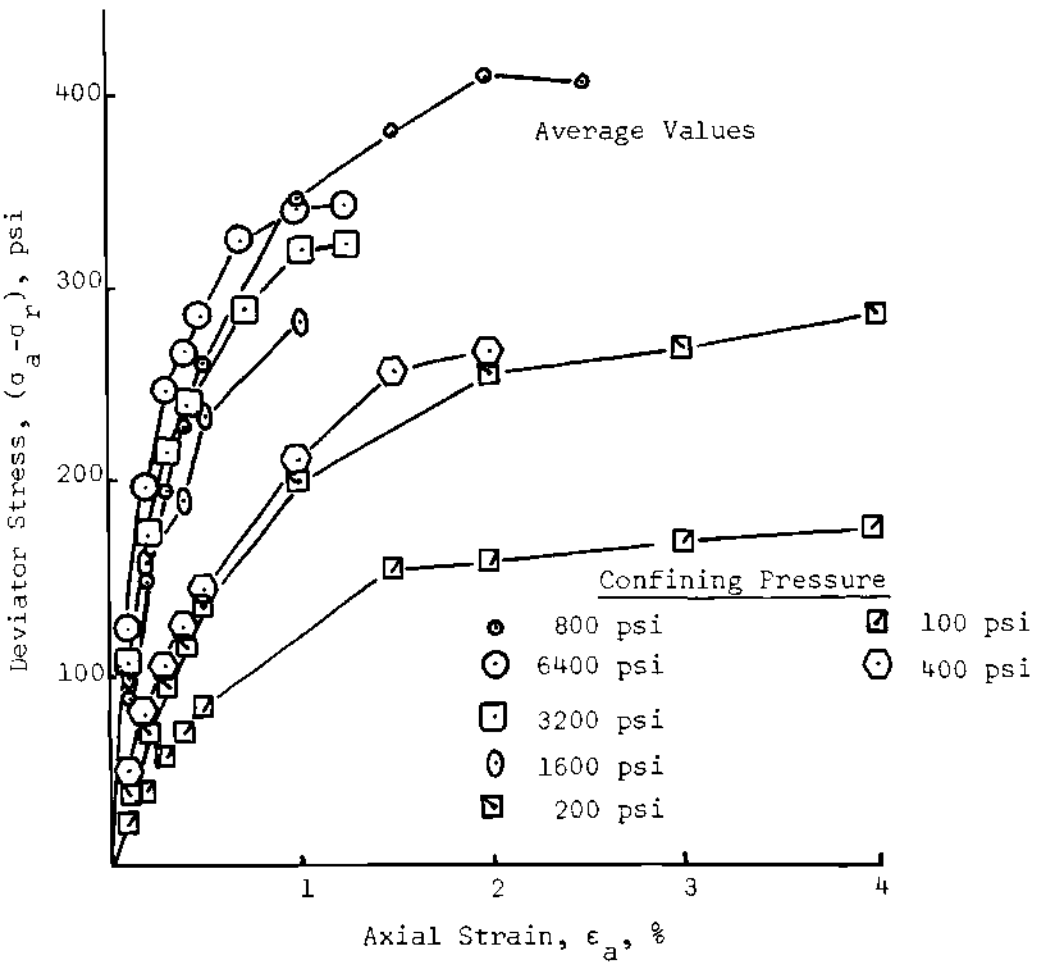

Figure 34. Deviator Stress as a Function of Axial Strain, Deviator Stress Cycled at 75% of Deviator Stress at Failure, McCormick Ranch Sand

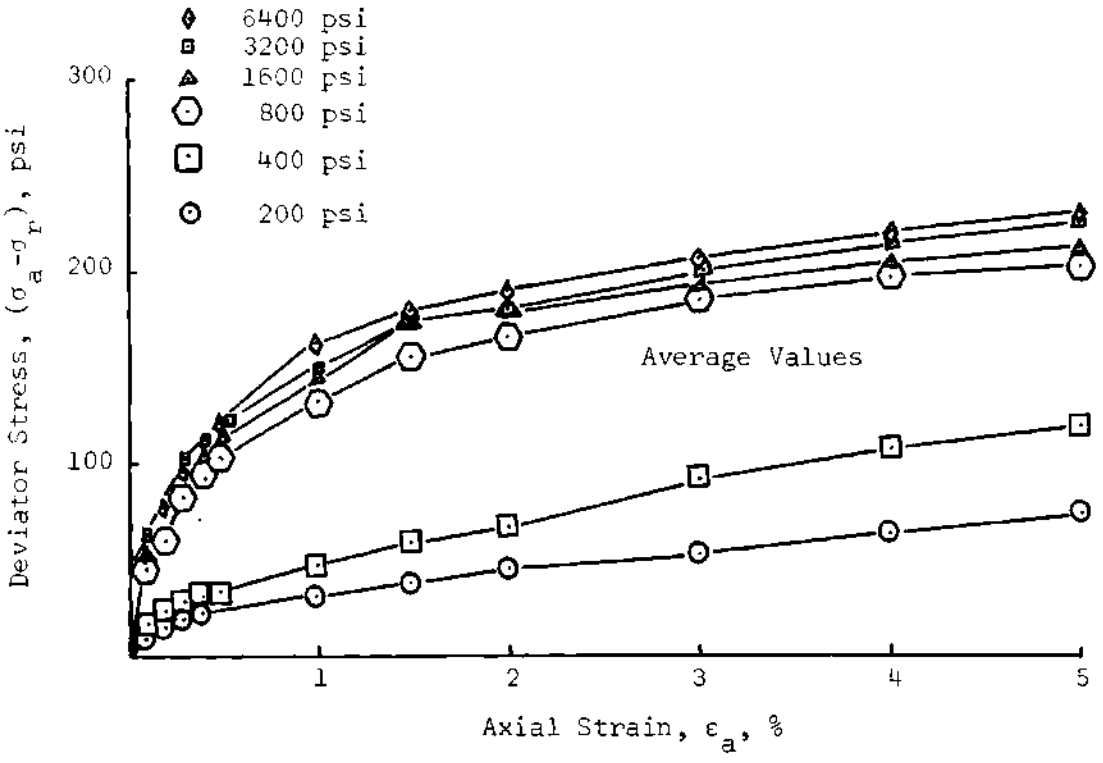

Figure 35. Deviator Stress as a Function of Axial Strain, Cycle Hydrostatic and Deviator Stress, Watching Hill Clay

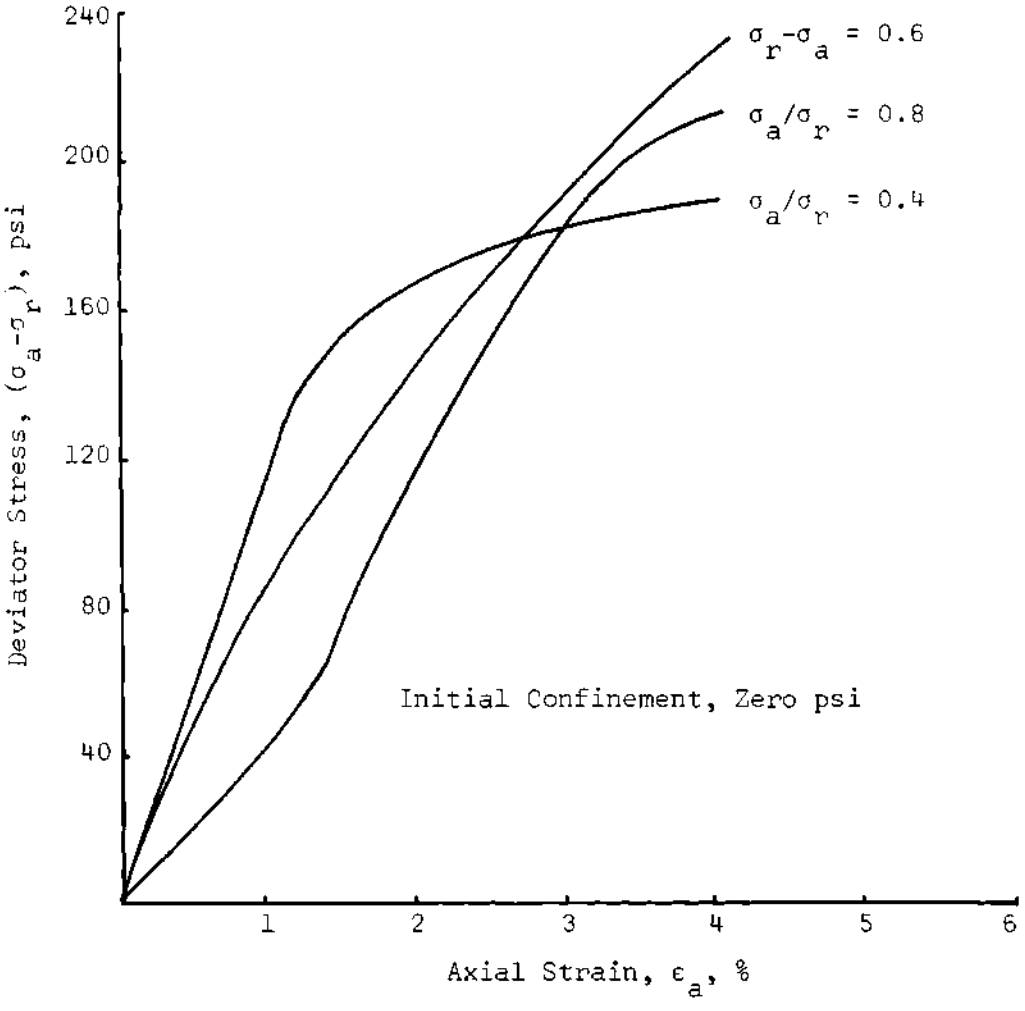

Figure 36. Deviator Stress as a Function of Axial Strain, Constant Stress Ratio, McCormick Ranch Sand

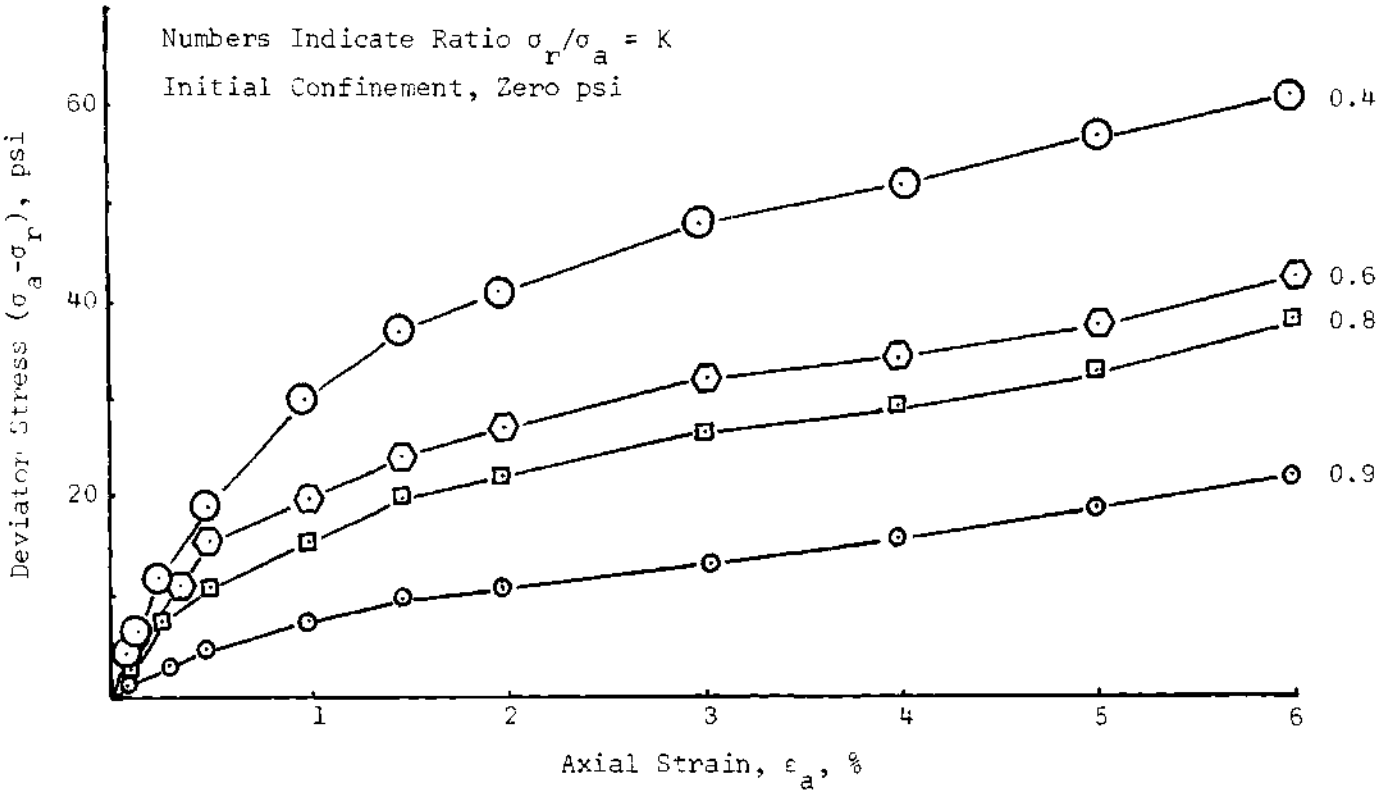

Figure 37. Deviator Stress as a Function of Axial Strain, Constant Stress Ratio, Watching Hill Clay

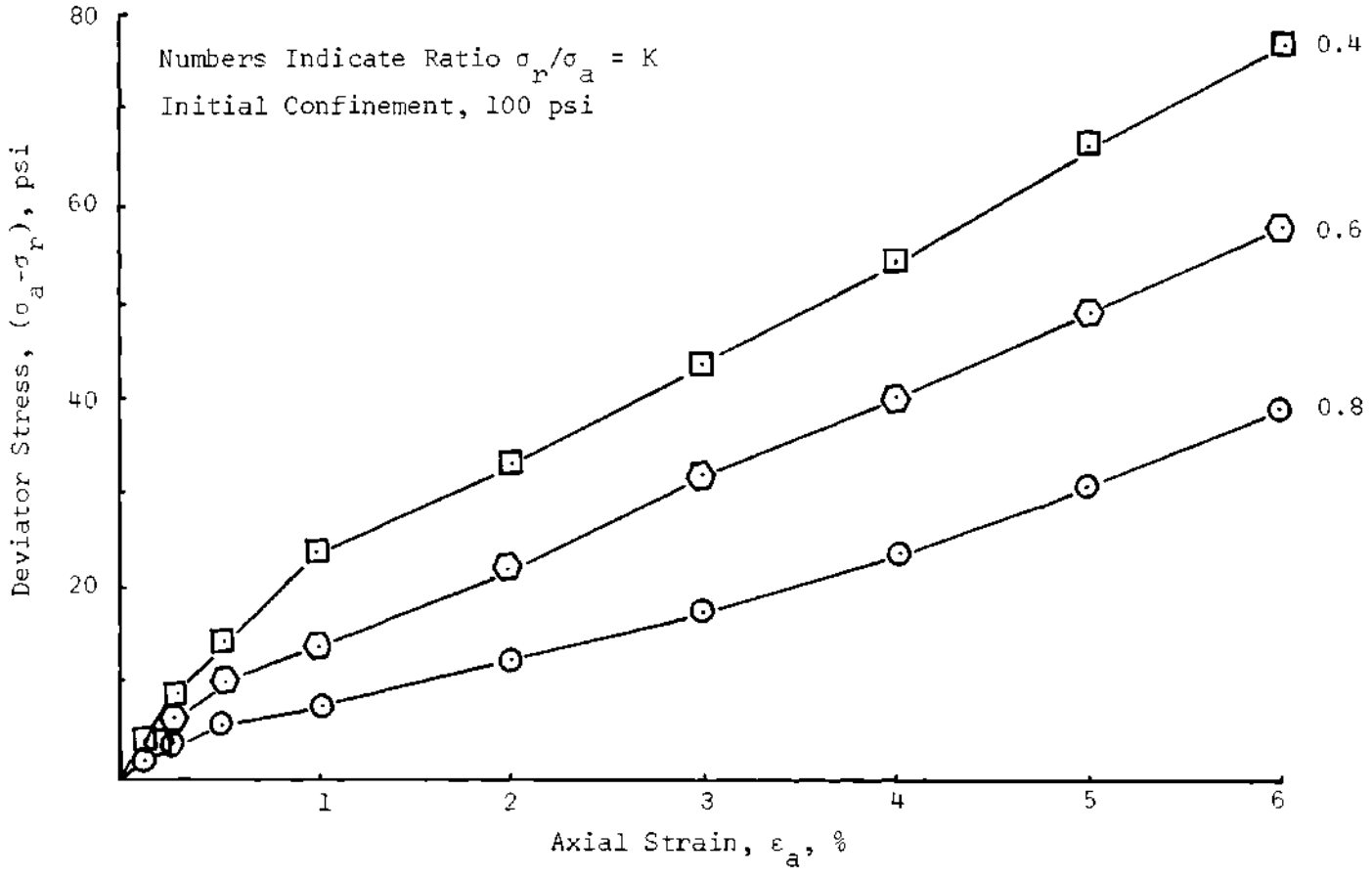

Figure 38. Deviator Stress as a Function of Axial Strain, Constant Stress Ratio, Watching Hill Clay

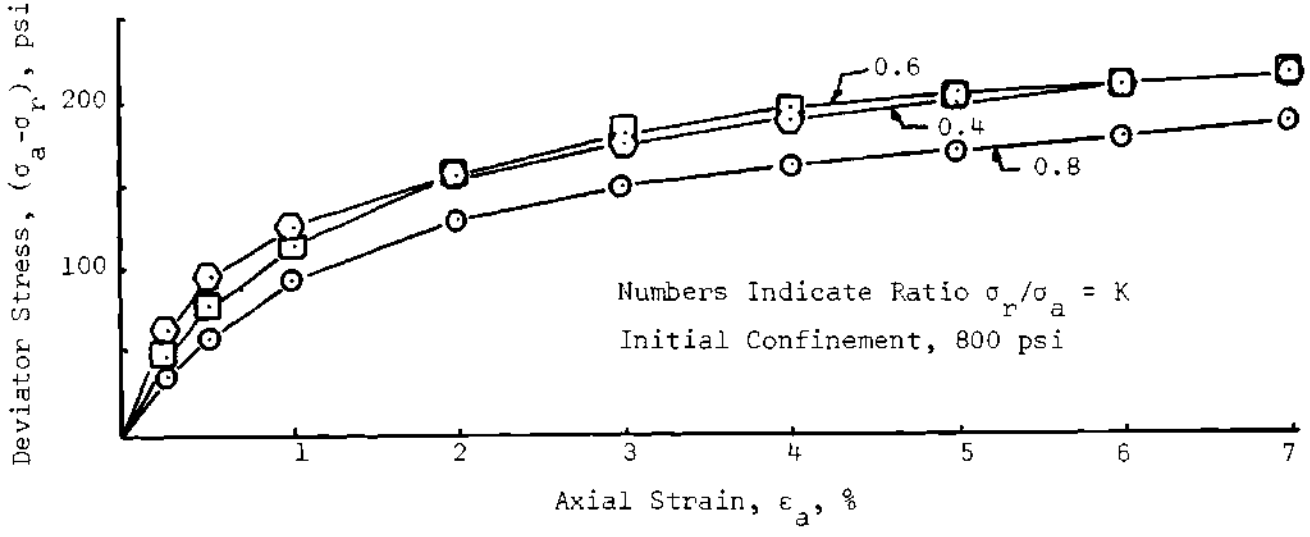

Figure 39. Deviator Stress as a Function of Axial Strain, Constant Stress Ratio, Watching Hill Clay

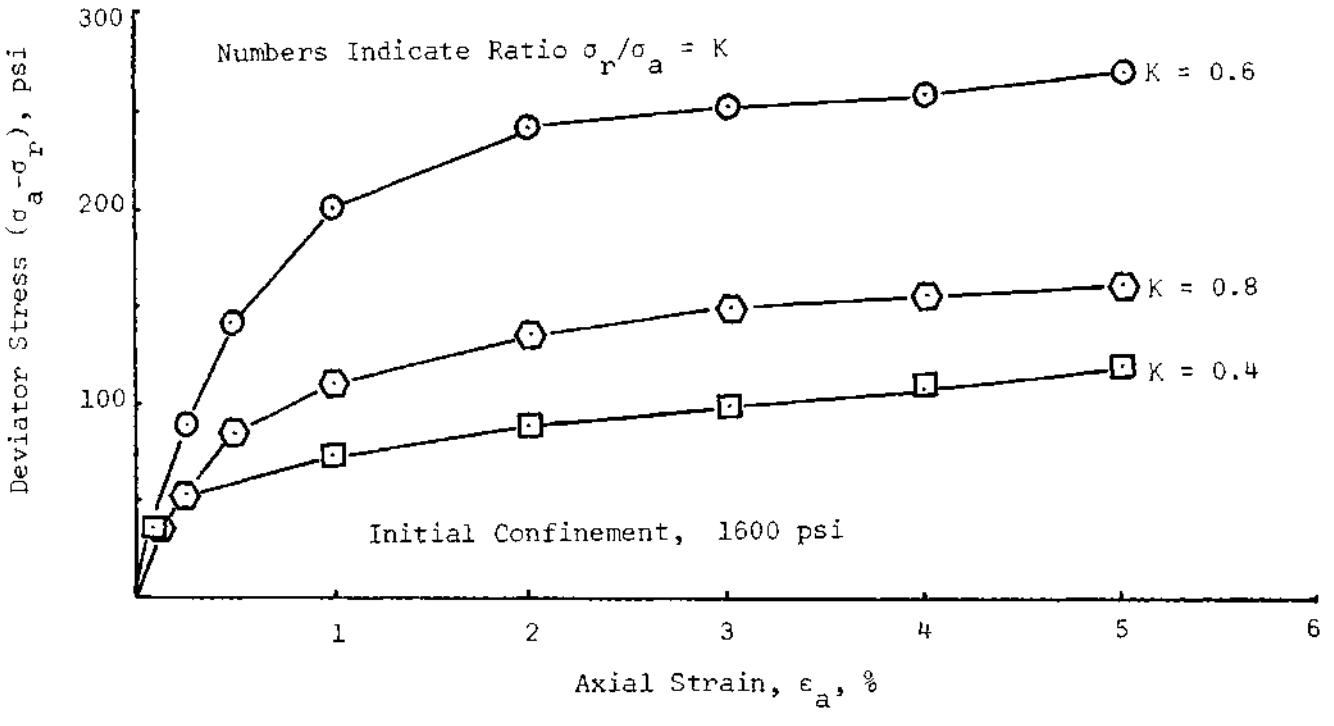

Figure 40. Deviator Stress as a Function of Axial Strain, Constant Stress Ratio, Watching Hill Clay

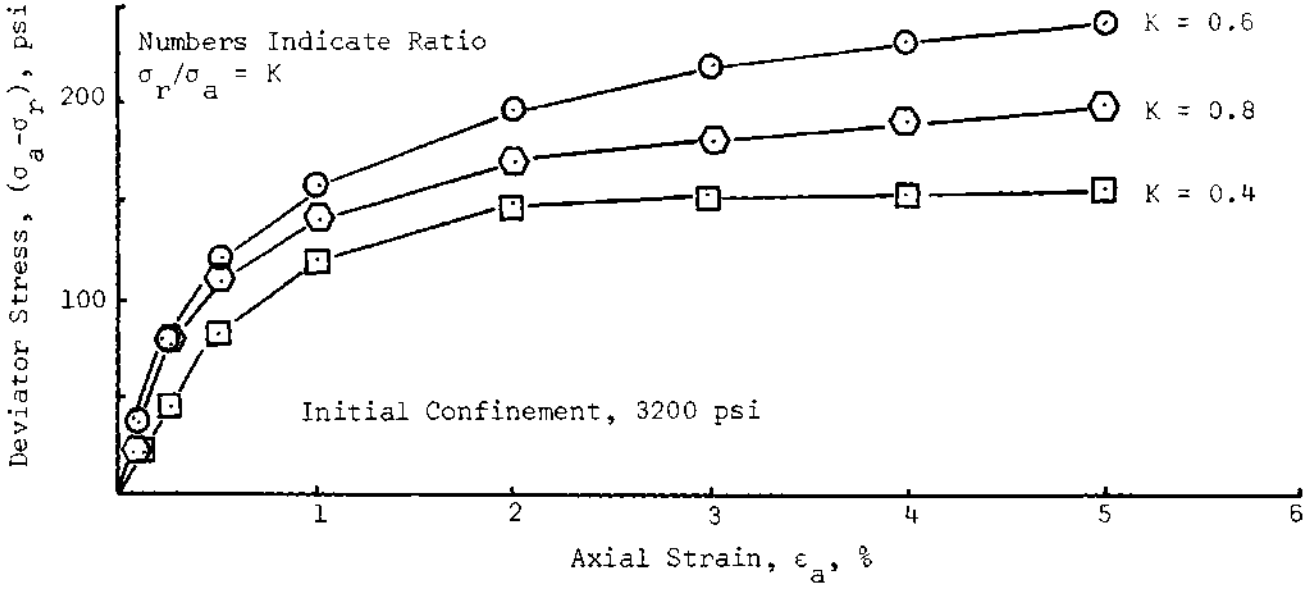

Figure 41. Deviator Stress as a Function of Axial Strain, Constant Stress Ratio, Watching Hill Clay

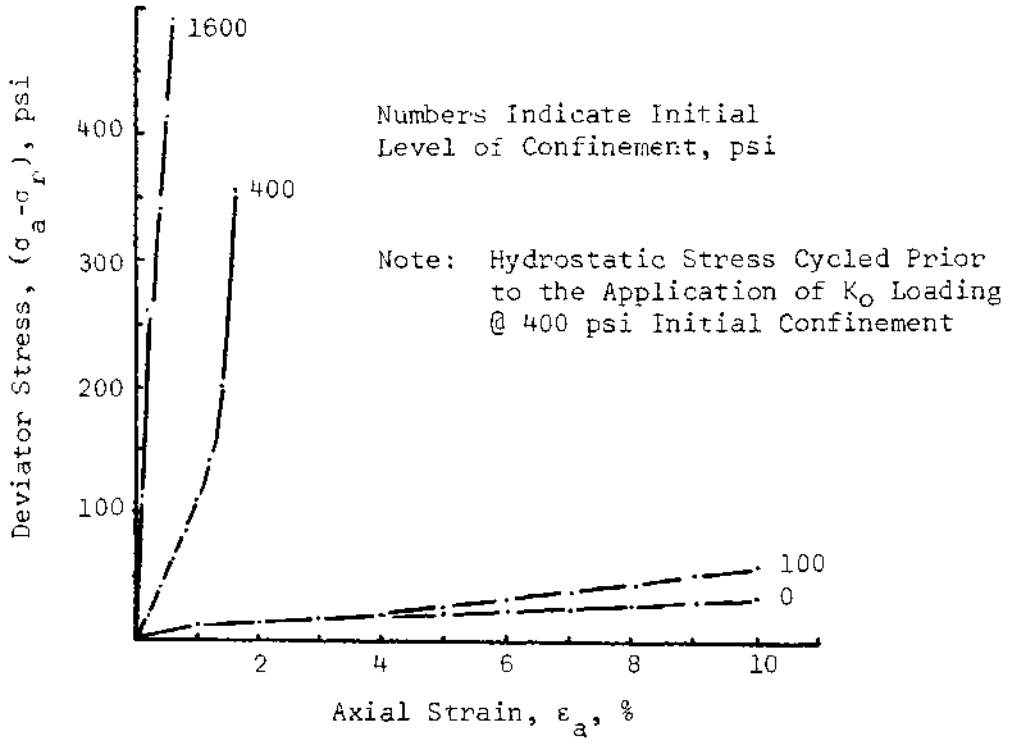

Figure 42. Deviator Stress as a Function of Axial Strain, No-Lateral-Strain Test, Watching Hill Clay

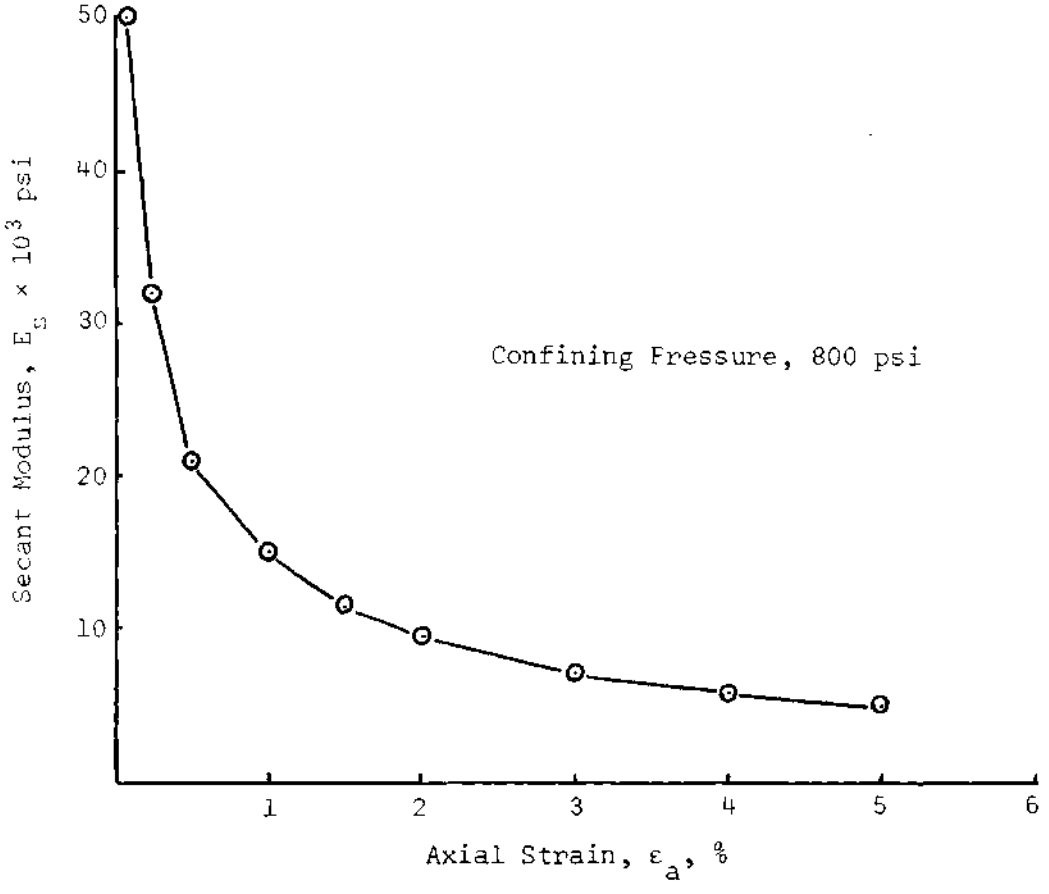

Figure 43. Secant Modulus as a Function of Axial Strain, Watching Hill Clay

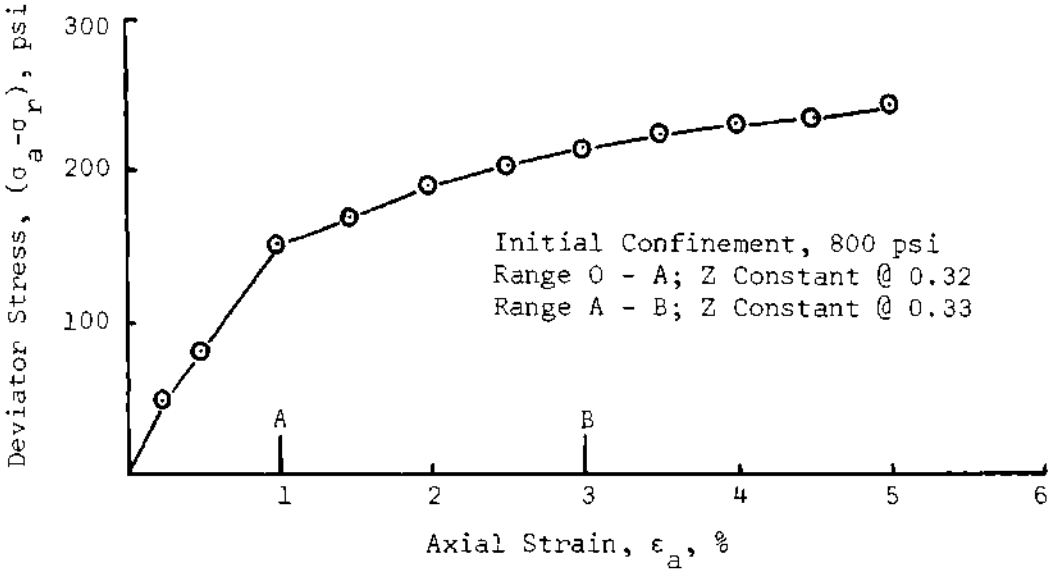

Figure 44. Deviator Stress as a Function of Axial Strain Illustrating the Range of Constant Z, Watching Hill Clay

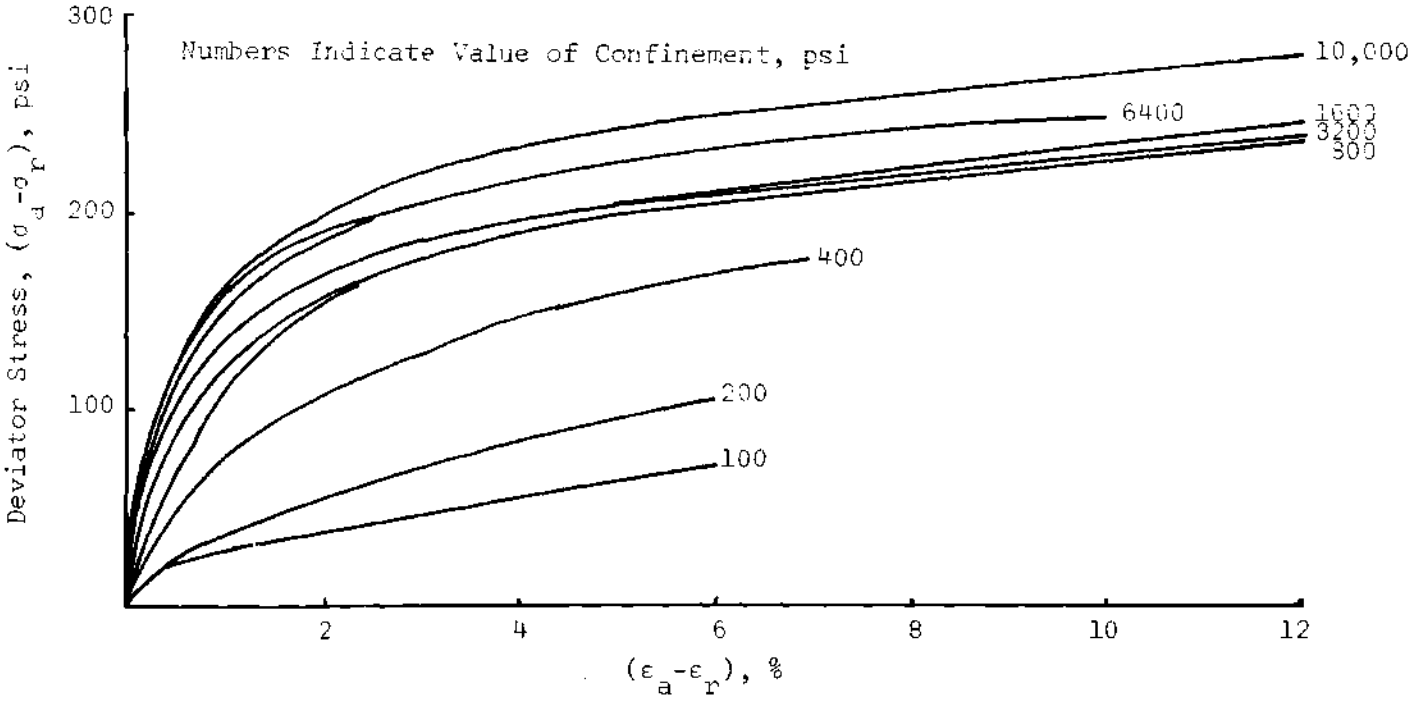

Figure 45. Deviator Stress as a Function of Strain Difference, Standard Triaxial Test, Watching Hill Clay

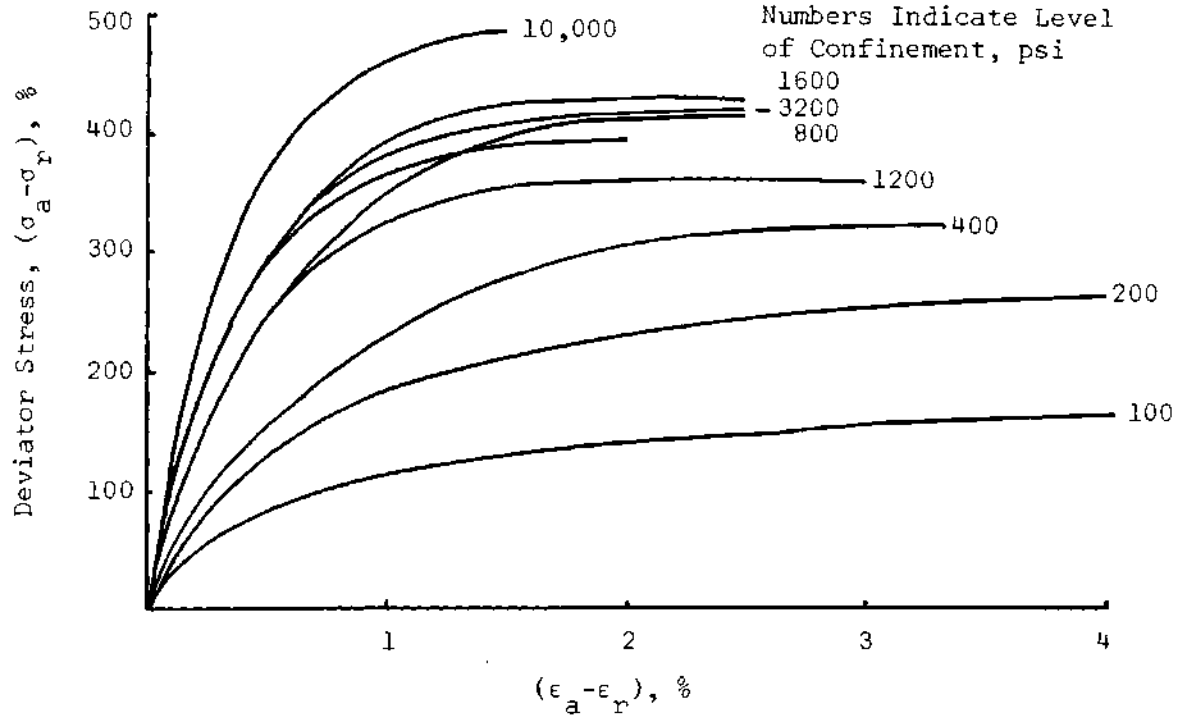

Figure 46. Deviator Stress as a Function of Strain Difference, Standard Triaxial Test, McCormick Ranch Sand

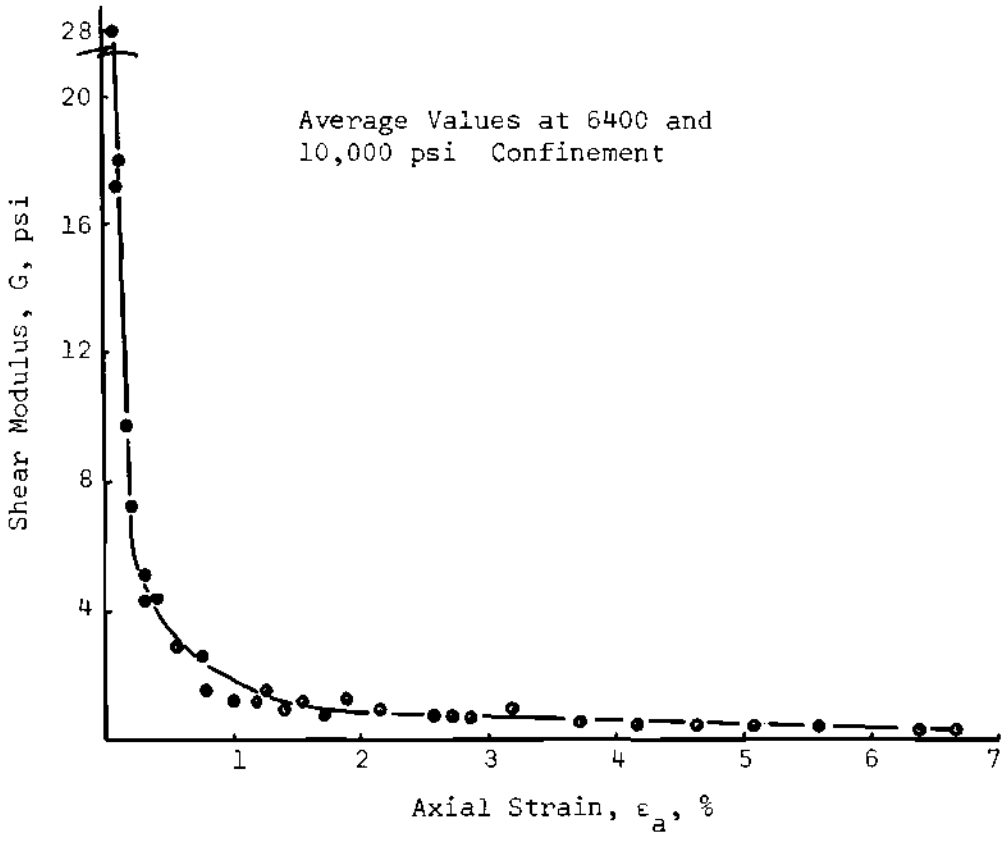

Figure 47. Shear Modulus as a Function of Axial Strain, Watching Hill Clay

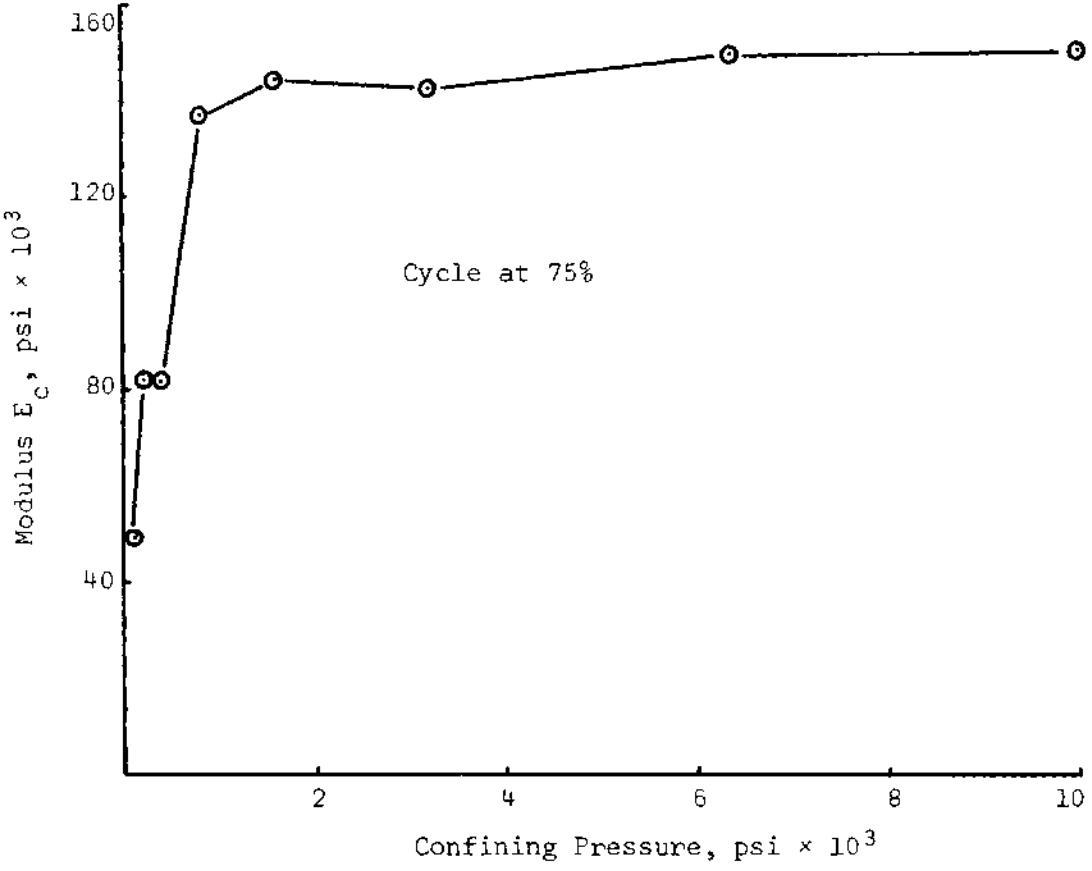

Figure 48. Modulus E_c as a Function of Confining Pressure, McCormick Ranch Sand

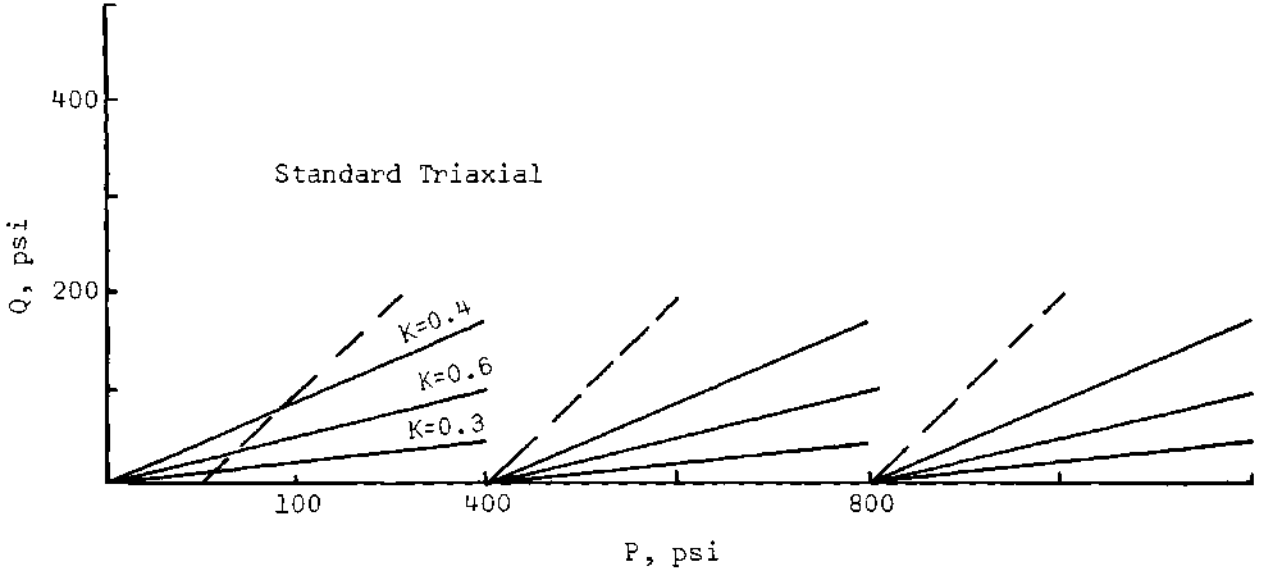

Figure 49. Standard Triaxial and Constant Stress Ratio Stress Paths

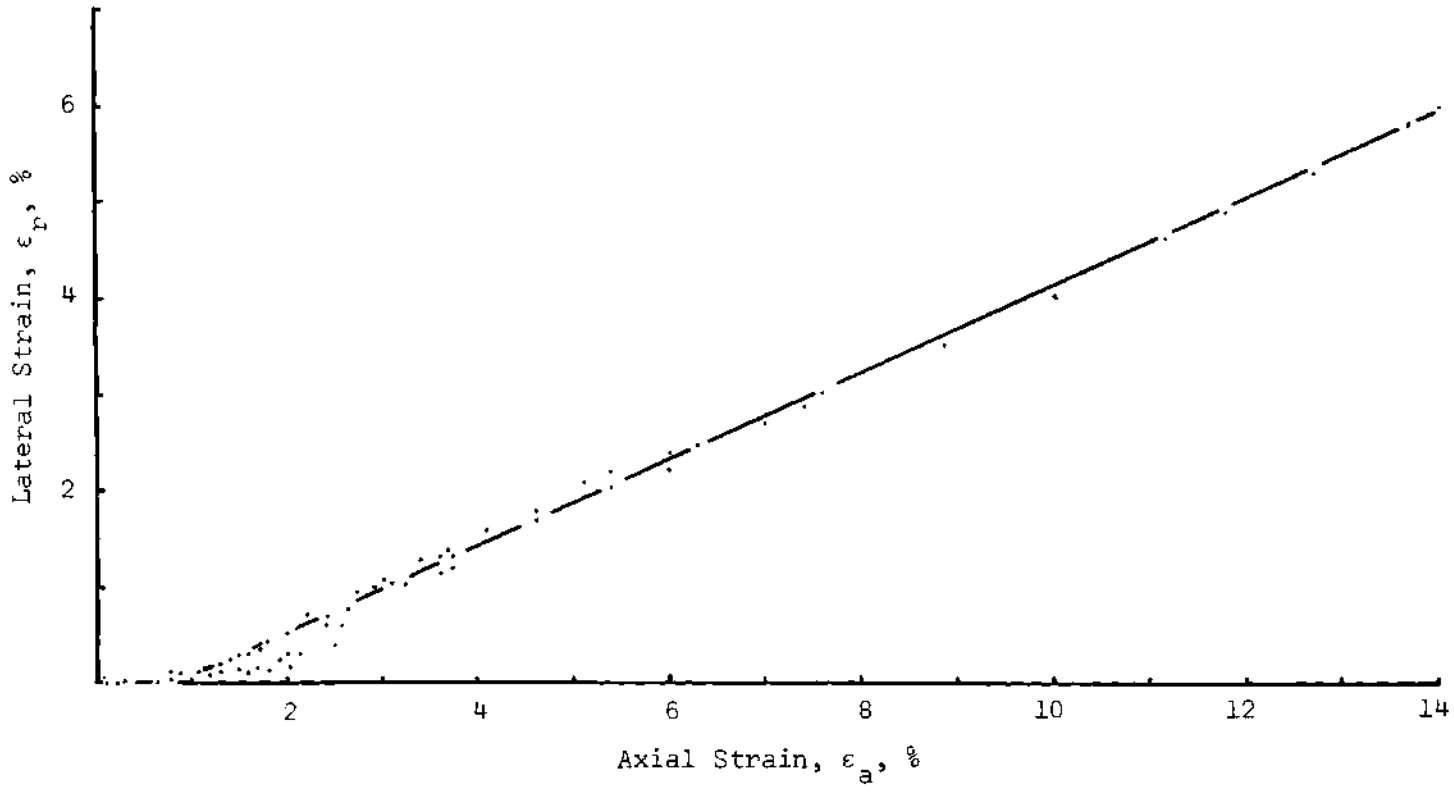

Figure 50. Lateral Strain as a Function of Axial Strain, Constant Stress Ratio of 0.4, McCormick Ranch Sand

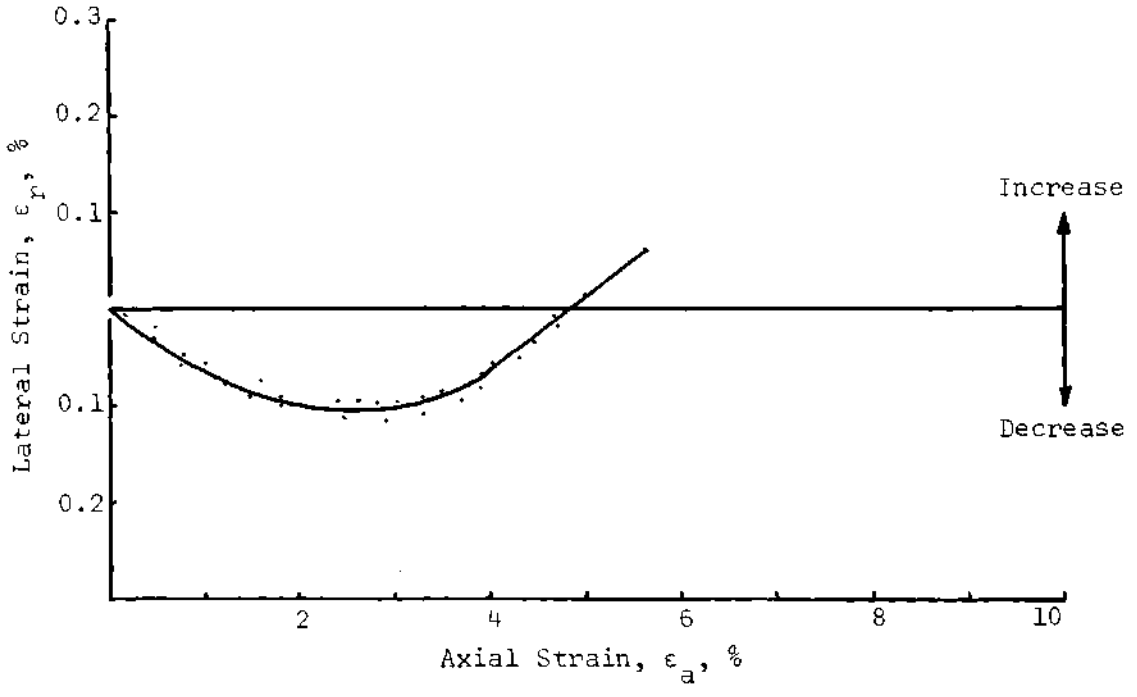

Figure 51. Lateral Strain as a Function of Axial Strain, Constant Stress Ratio of 0.8, McCormick Ranch Sand

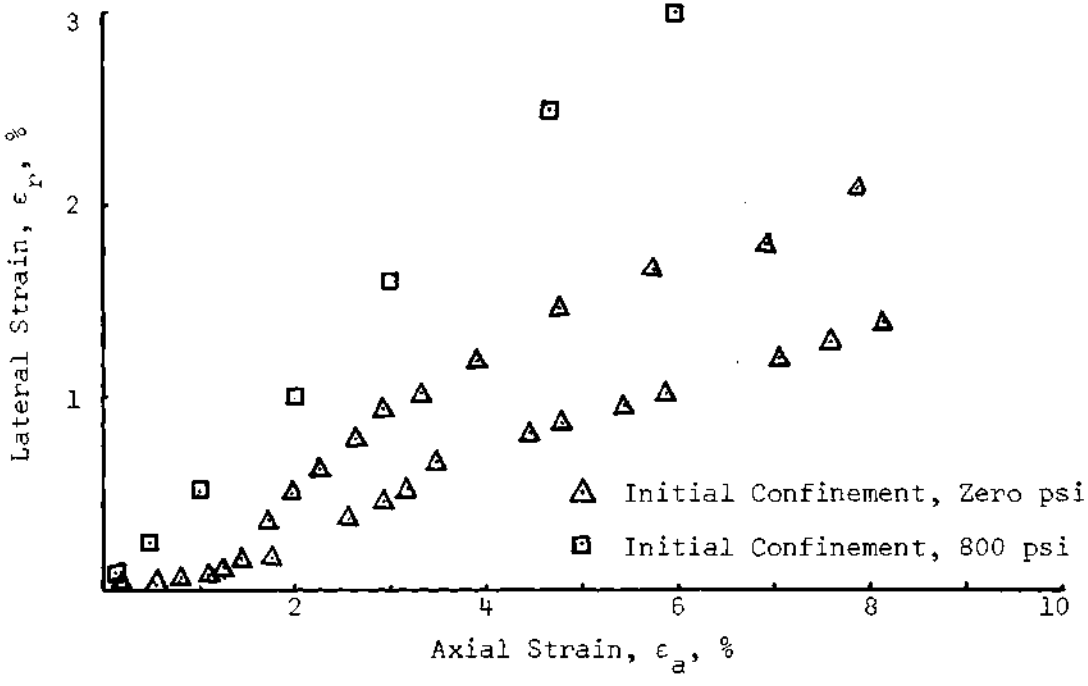

Figure 52. Lateral Strain as a Function of Axial Strain, Constant Stress Ratio of 0.4, Watching Hill Clay

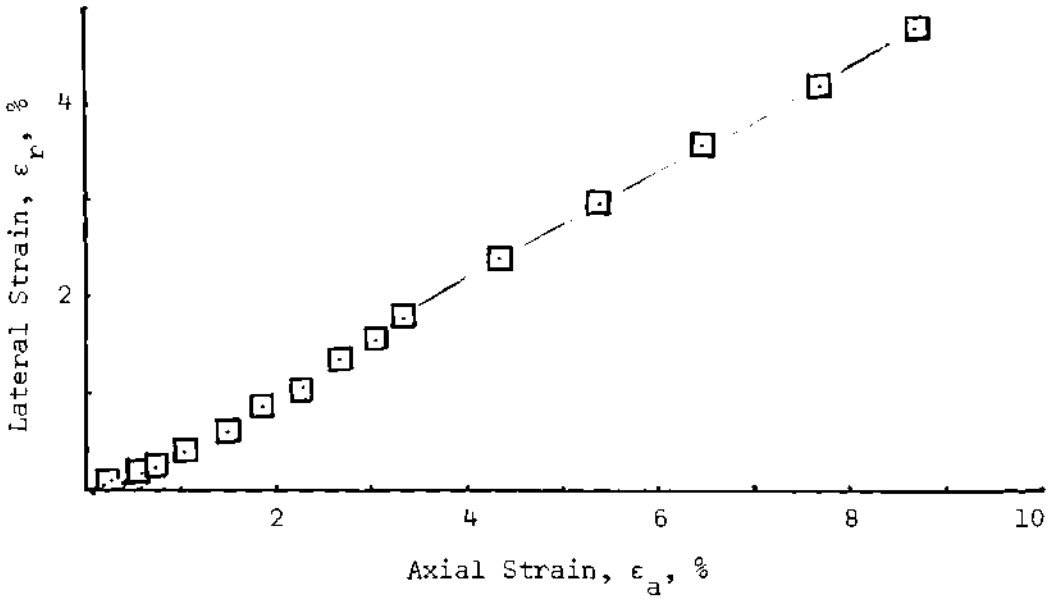

Figure 53. Lateral Strain as a Function of Axial Strain, Constant Stress Ratio of 0.6, Watching Hill Clay

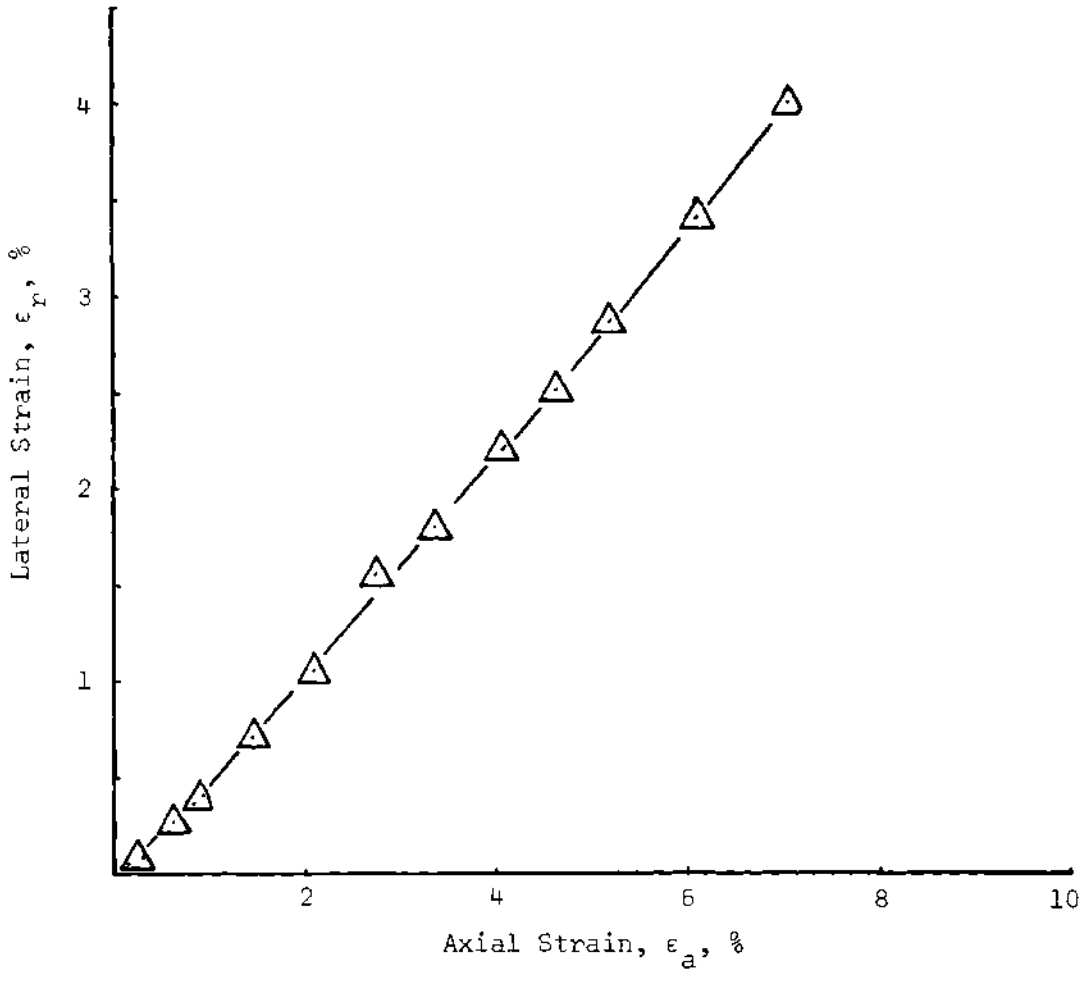

Figure 54. Lateral Strain as a Function of Axial Strain, Constant Stress Ratio of 0.8, Watching Hill Clay

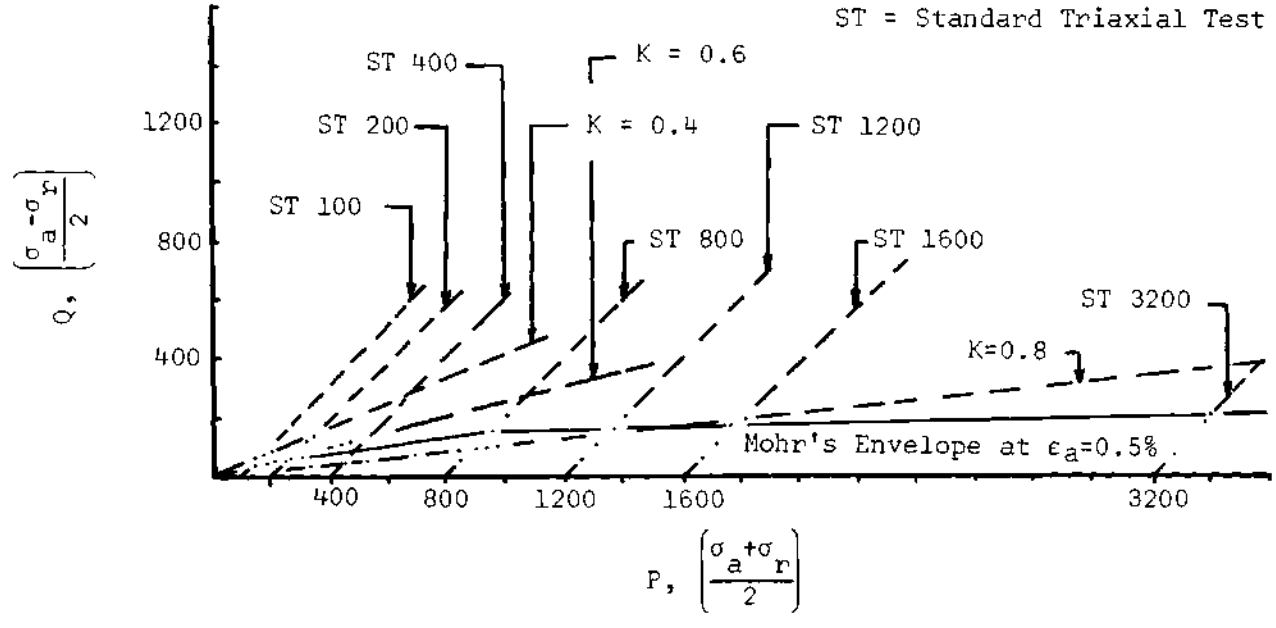

Figure 55. Stress Paths--Standard Triaxial and Constant Stress Ratio Tests, McCormick Ranch Sand

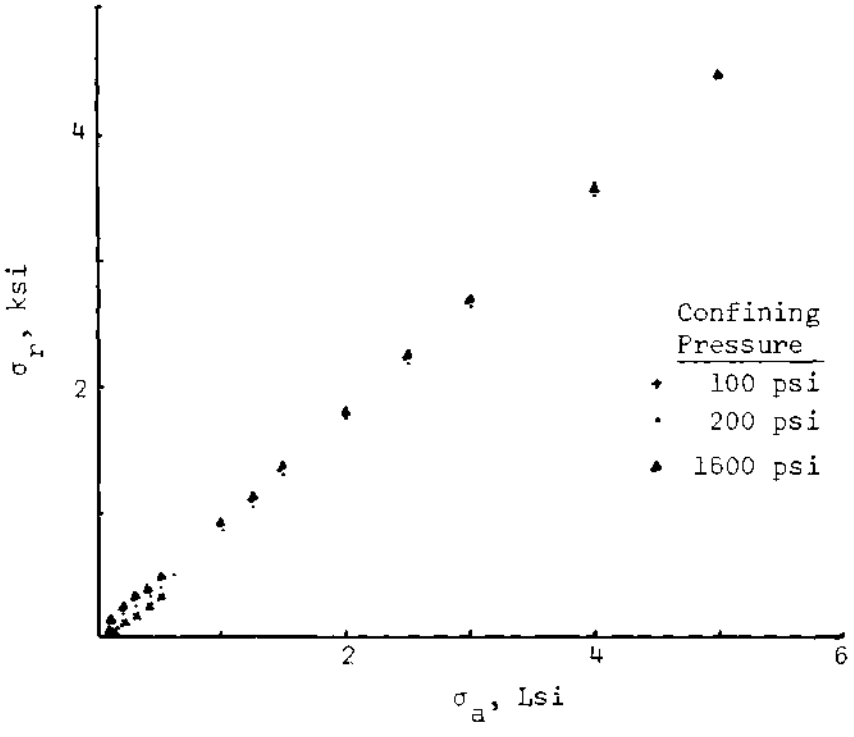

Figure 56. Radial Strain as a Function of Total Axial Stress, No Lateral Strain Test, Watching Hill Clay

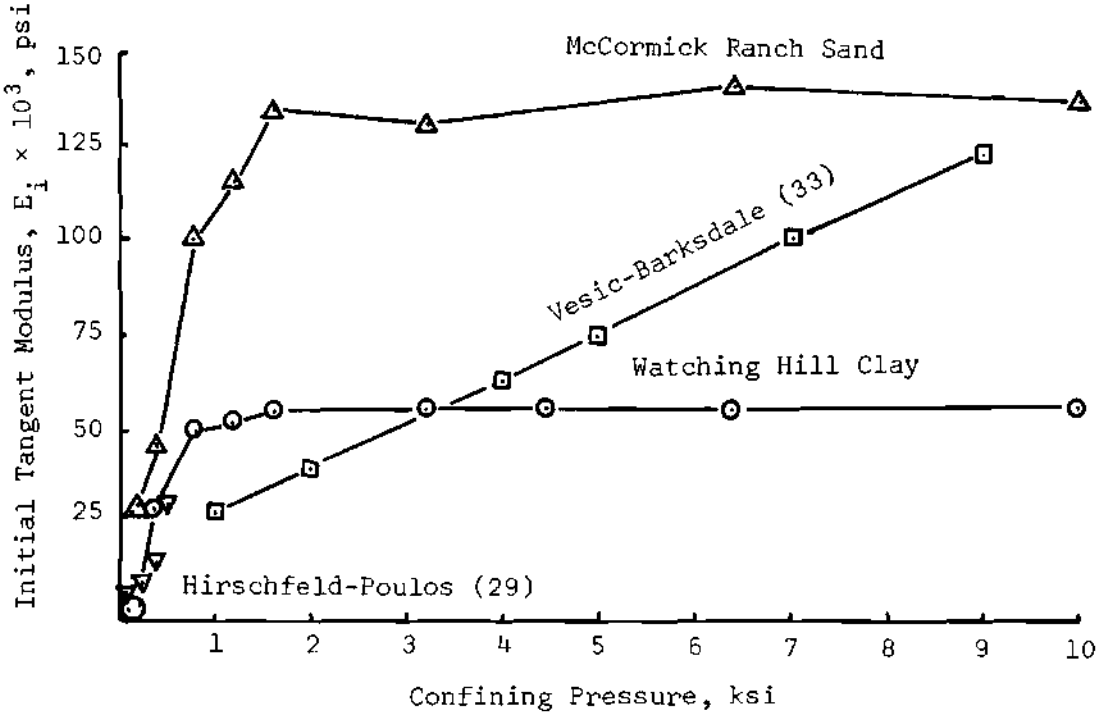

Figure 57. Initial Tangent Modulus, E_i, Standard Triaxial Tests

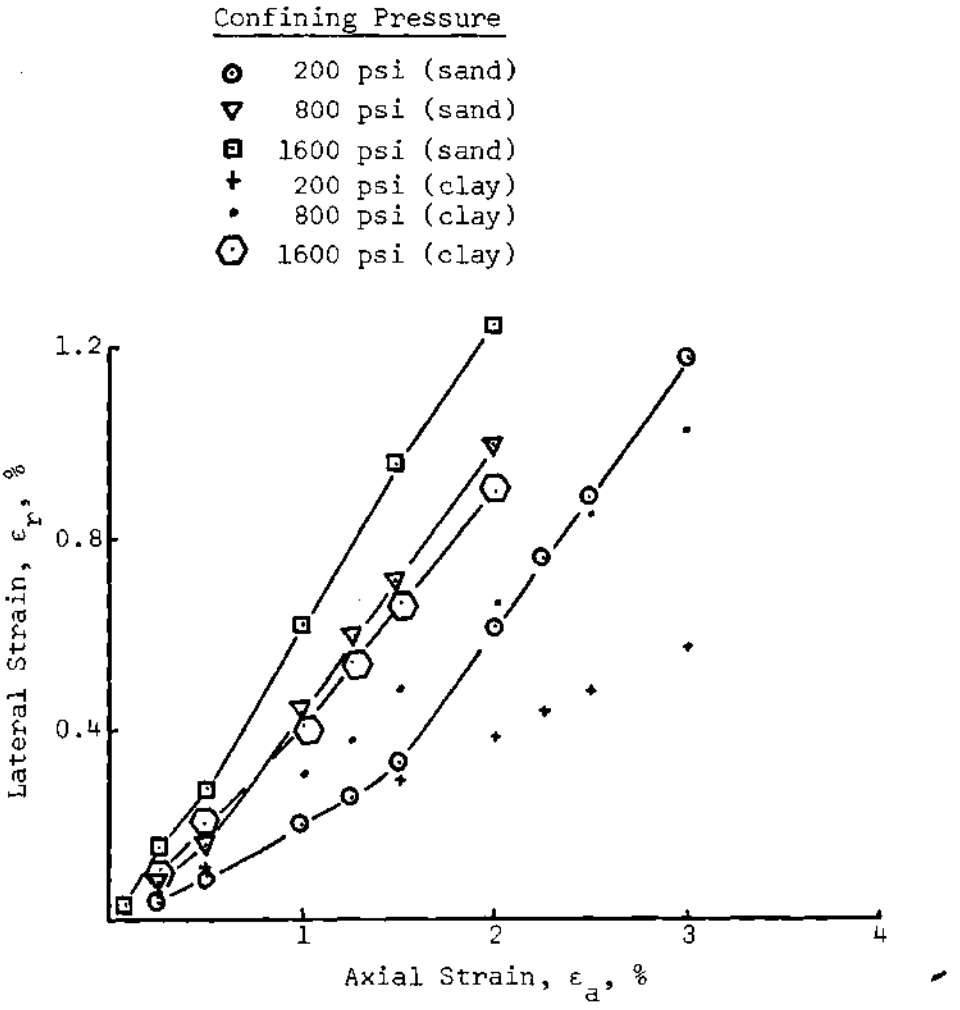

Figure 58. Lateral Strain as a Function of Axial Strain

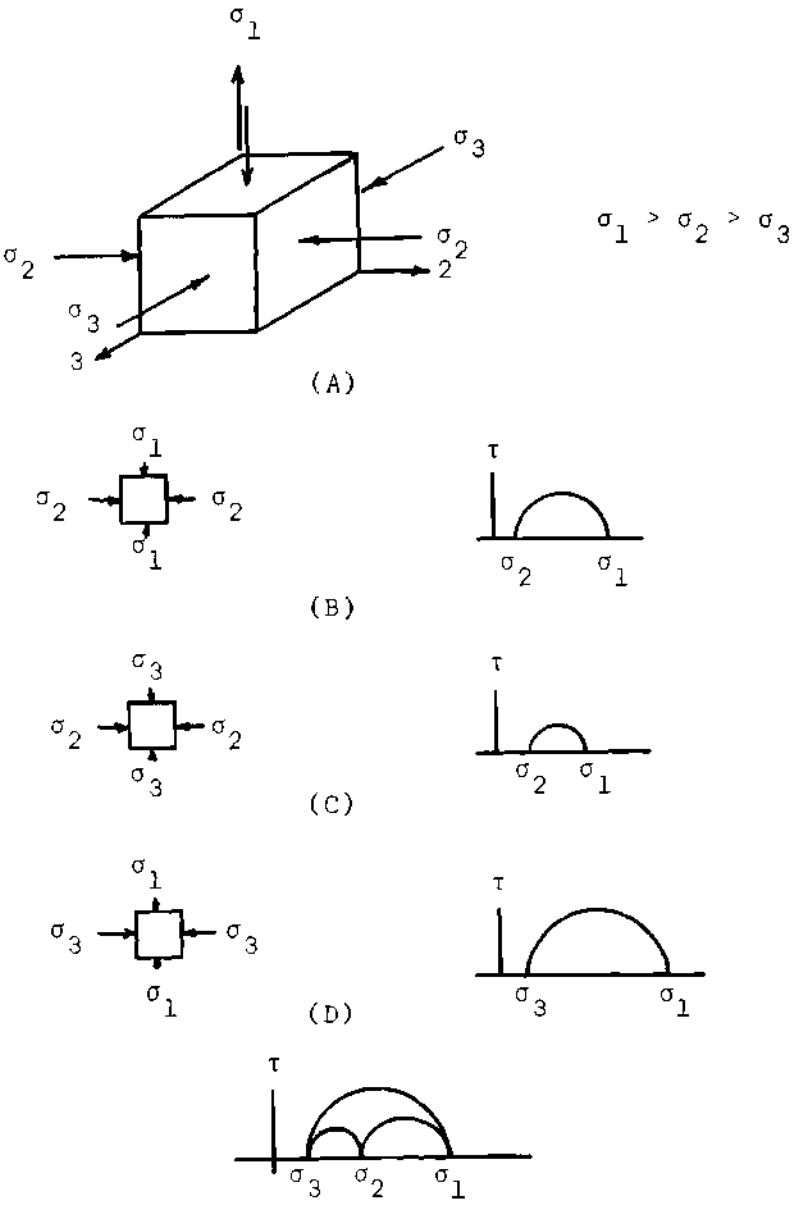

Figure 59. Mohr's Circles for the Triaxial Stress Condition

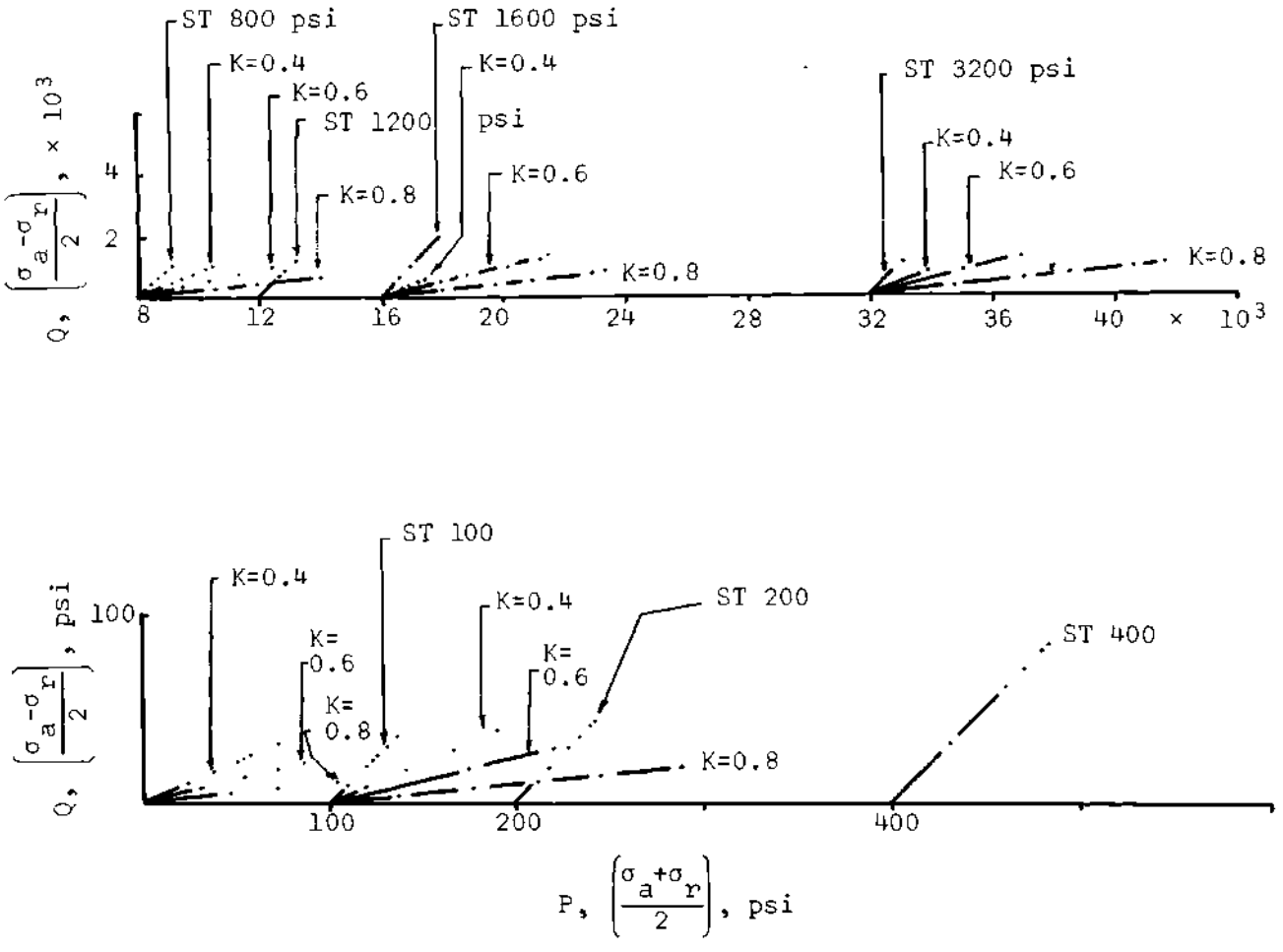

Figure 60. Stress Paths--Standard Triaxial and Constant Stress Ratio Tests, Watching Hill Clay

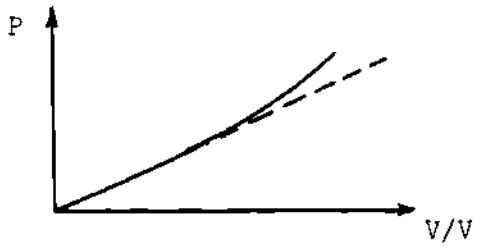

(a) Confining Pressure P as a Function of Volumetric Strain

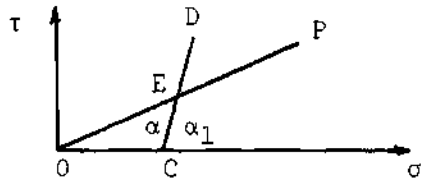

(b) Stress Paths--Standard Triaxial and Constant Stress Ratio Tests

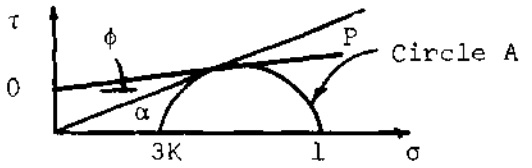

(c) Mohr Envelope and Constant Stress Ratio Stress Path

Figure 61. Volumetric Strain as a Function of Confining Pressure, Mohr Envelope and Constant Stress Ratio Path

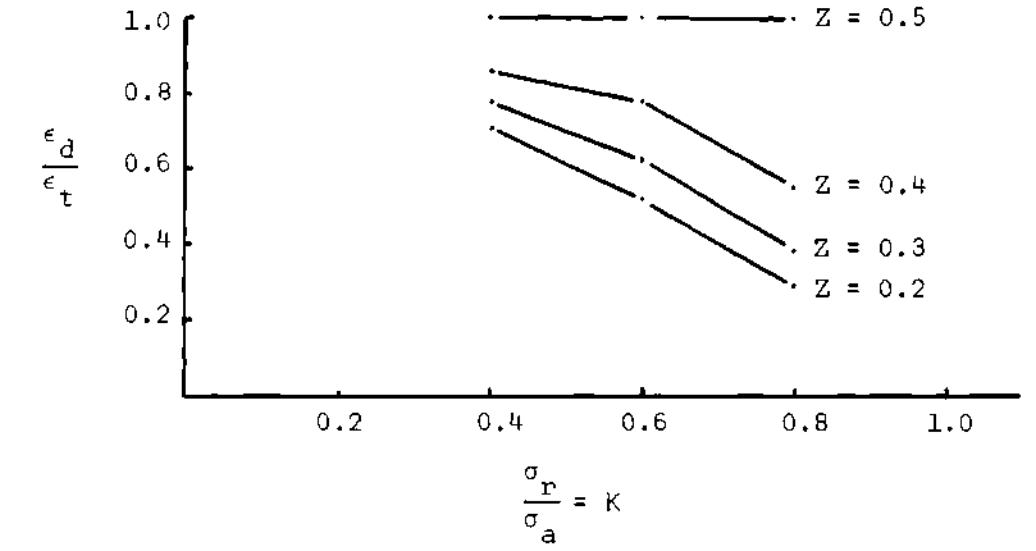

(A)

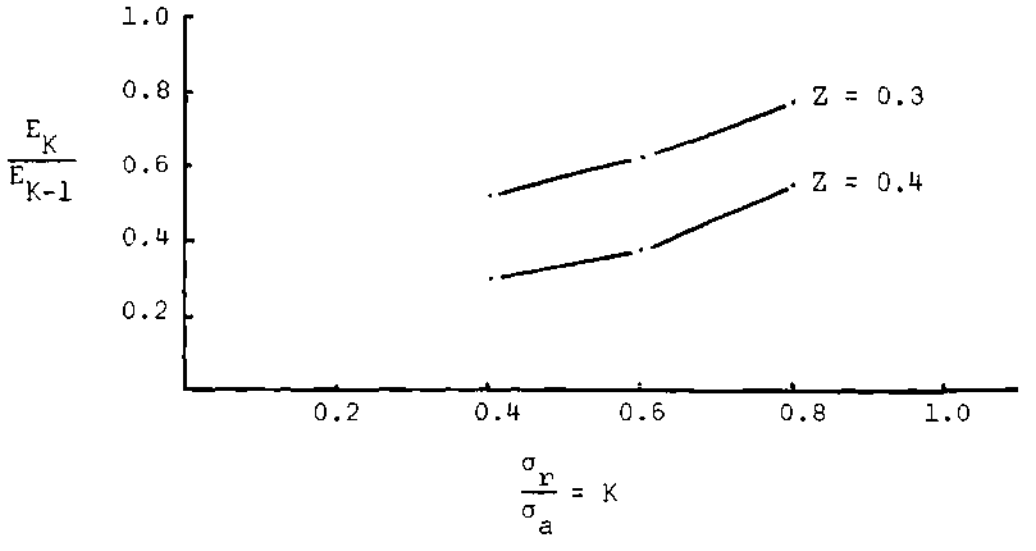

(B)

Figure 62. Constant Stress Ratio Relationships

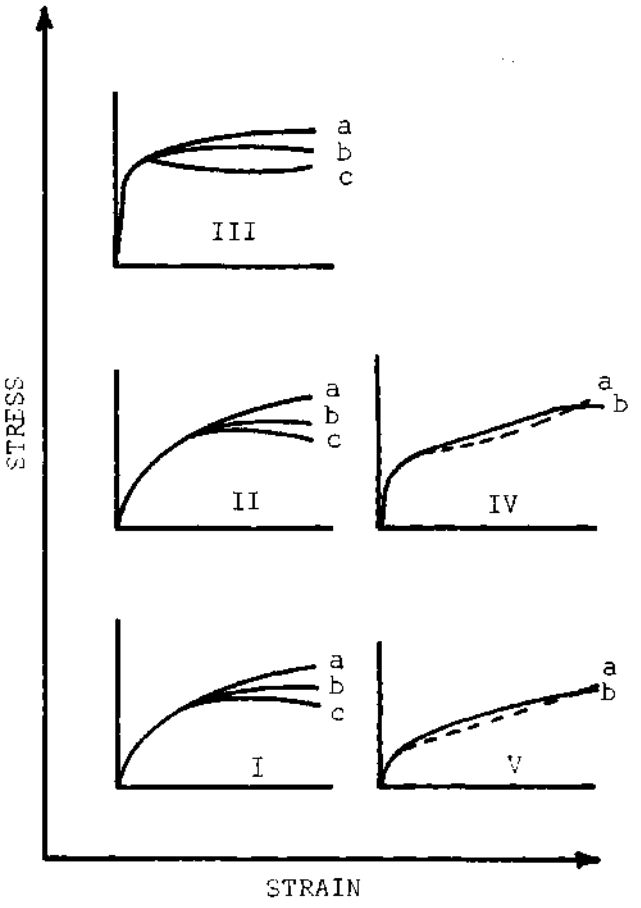

Figure 63. Typical Stress-Strain Curves as Reported by Casagrande and Hirschfeld (48)

Table 1. Maximum Expected Errors in Measurements

Measurement	Maximum Expected Error, %
Weight of Total Sample	± 0.07
Weight of Displaced Mercury for Volume Measurements	± 0.07
Manual Measurements of Sample Height	± 0.10
Height Measurements Inside Triaxial Cell	± 0.01
Manual Measurements of Sample Diameter	± 0.22
Diameter Measurements Inside Triaxial Cell	± 0.95

Table 2. Sample Dimensions Used for Volume Calculations During Hydrostatic Compression--Watching Hill Soil (Reference Figure 16)

AVERAGE VALUES			
Pressure psi	SecID (in)	Sec1 (in)	Sec2 (in)
100	0.035	1.00	0.20
200	0.018	0.25	0.50
400	0.036	0.25	0.50
800	0.036	0.25	0.50
1200	0.036	0.25	0.50
1600	0.036	0.25	0.50
3200	0.036	0.25	0.50
6400	0.036	0.25	0.50
10,000	0.036	0.25	0.50

Table 3. Bulk Modulus Values

Confining Pressure (psi)	McCORMICK RANCH SAND			WATCHING HILL CLAY	
	$\Delta\sigma$ (psi)	$\frac{\Delta V}{V}$ (%)	K_B 10^3 psi	$\frac{\Delta V}{V}$ (%)	K_B 10^3 psi
100	100	1.84	5.5	5.66	1.7
200	100	0.50	20.0	8.00	1.3
400	200	0.98	20.1	8.67	2.3
800	400	0.69	58.0	1.67	24.0
1200	400	0.13	308.0	0.75	53.4
1600	400	0.05	800.0	0.75	53.4
3200	1600	0.12	1333.0	0.1	1600.0
6400	3200	0.18	1775.0	-	-
10,000	3600	0.00	-	-	-

Table 4. Initial Tangent Moduli

Confining Pressure (psi)	McCormick Ranch Sand E_i (psi)	Watching Hill Clay E_i (psi)
100	25,000	3,000
200	30,000	4,200
400	45,000	28,000
800	100,000	50,000
1200	115,000	52,000
1600	135,000	54,000
3200	135,000	55,000

Values Calculated at an Axial Strain of 0.1%.

Table 5. Ratio of Lateral-to-Axial Strain (ϵ_r/ϵ_a=Z) (Reference Figure 44)

STANDARD TRIAXIAL TEST

Confining Pressure (psi)	Watching Hill Soil ϵ_a Range		Z Range	
	O-A	O-B	O-A	A-B
100	2.5 %	10 %	0.32	0.30
200	2.5 %	8 %	0.23	0.20
400	2.3 %	7.5%	0.21	0.33
800	1.0 %	3.0%	0.32	0.33
1200	0.75%	2.0%	0.36	0.42
1600	0.75%	2.0%	0.46	0.42
3200	0.75%	2.0%	0.46	0.42
6400	0.75%	2.0%	0.50	0.56
10,000	0.75%	2.0%	0.50	0.56
	McCormick Ranch Soil			
100	1.5 %	4.0%	0.30	0.65
200	1.5 %	3.5%	0.22	0.55
400	0.8 %	1.5%	0.30	0.55
800	0.5 %	1.0%	0.32	0.54
1200	0.5 %	1.0%	0.42	0.58
1600	0.5 %	1.0%	0.50	0.70
3200	0.5 %	1.0%	0.49	0.70
6400	0.5 %	1.0%	0.50	0.70
10,000	0.5 %	1.0%	0.50	0.70

Table 6. Shear Modulus G

Confining Pressure (psi)	G
100	3,500
200	3,500
400	6,250
800	7,750
1600	12,750
3200	21,500
6400	28,000
10,000	28,000

Watching Hill Soil at $(\varepsilon_a - \varepsilon_r)$ of 0.1%.

APPENDIX

APPENDIX A

FACTORS AFFECTING WATER AND AIR IN A PARTIALLY SATURATED SOIL

For the soils tested, after mixing with water and aging, the particles clung together into aggregates. To minimize the size of these aggregates, the soil was worked through a No. 20 sieve. As formed, the samples consisted of a series of individual acting lumps of soil, not as individual soil grains.

To form the McCormick Ranch Samples an axial load of 900 psi was required; for the Watching Hill Soil an axial load of 450 psi was used.

The formed samples were preconsolidated and consisted of a solid, liquid and gaseous phase. The liquid phase or soil water is considered to exist in a continuous film around the grains forming menisci near the points of grain contact. The remainder of the void space is assumed interconnected and filled with air. Because of the time lag between sample formation and sample testing, the air is under atmospheric pressure.

To investigate the response of such a mass to load, three cases will be considered: a perfectly dry sample, a saturated sample and a partially saturated sample.

Effective Stresses in Dry, Saturated and Partially Saturated Soil

In a saturated soil the total stress σ may be expressed as

$$\sigma = \bar{\sigma} - (1-a)u \tag{1}$$

where σ = total stress on a plane through the soil.

$\bar{\sigma}$ = the effective stress or the average intergranular stress per unit area of the plane.

a = the contact area between the grains per unit area of the plane.

u = pore water pressure.

To evaluate the stress values it is necessary to know the value of a. No means of directly measuring a has yet been developed. Indirect measurements indicate that (1-a) is very close to unity for both sands and clays (38). Equation 1 then becomes

$$\bar{\sigma} = \sigma - u \tag{2}$$

For dry soils Equation (1) reduces to

$$\bar{\sigma} = \sigma \tag{3}$$

If the soil air is allowed to excape, the effective stress increases in an amount equivalent to the increase in the total stress. Sealing a dry sample and loading without allowing air to escape results in the

air being compressed. If u_a is the air pressure, then Equation (2) is

$$\bar{\sigma} = \sigma - u_a \tag{4}$$

For partially saturated soils, sealed against the escape of both air and water, the total increase in pore gas and pore fluid pressure is

$$u = u_c + u_a$$

where u_c is the capillary pressure in the soil water and u_a is the pore air pressure. For these conditions Equation (2) is

$$\bar{\sigma} = \sigma - u \tag{5}$$

Dry Sample

Loading a dry soil sample enclosed in a membrane impervious to the passage of air would result in a volume change, a stress increase in the soil structure, and an increased air pressure. Calculation of the air pressure is possible if it is assumed that the compression of the individual grains is negligible compared to the compression of the soil structure, that the volume change of the sample is measured, and that the air obeys Boyle's law.

Let V_{ai} equal the initial volume of air in the soil, V_{af} the final volume of air, and (1+e) the total volume.

For an ideal gas

$$PV = NRT \tag{6}$$

where P = pressure in atmospheres.

V = volume in cubic centimeters.

N = number of mols (one mol - the weight of a substance in grams equivalent to the atomic weight).

T = absolute temperature in degrees Kelvin.

R = gas constant 82.06 $\frac{cm^3 - atm.}{^oK - mol.}$.

The density of air is 1.2928 grams/liter and the molecular weight in grams is (1.2928) × (22.4) or 28.96. If W_a is the weight of air, Equation (2) is then

$$PV_{ai} = W_a RT/28.96$$

If the air is compressed, then

$$\frac{W_a}{28.96} = \frac{P_a V_{ai}}{RT} = \frac{(P_a + u_a)V_{af}}{RT}$$

where P_a = atmospheric pressure.

u_a = air pressure above atmospheric.

$$P_a V_{ai} - P_a V_{af} = u_a V_{af}$$

$$u_a = P_a \frac{(V_{ai} - V_{af})}{V_{af}} \tag{7}$$

which relates the air pressure to the volume change in the sample. Equation (4) can be written as

$$\bar{\sigma} = \sigma - \frac{P_a(V_{ai}-V_{af})}{V_{af}}$$

Saturated Sample

Similar to the dry soil, the saturated soil involves a two-phase system. In the latter case the soil voids are completely filled with water.

Sealing and loading a saturated soil results in the soil water carrying the entire load or the water and soil structure sharing the load. At low confining pressures it is assumed that the load is carried by the soil water and there is no measurable volume change. This follows the fact that the water under loads normally used in soil testing is virtually incompressible and that the grain contact area is small.

The bulk modulus of water varies from 3.0×10^5 psi at low pressures to 3.74×10^5 psi at 10,000 psi confinement (39). In a saturated sample at high confining pressures the water may change in volume. Under such conditions there is a sharing of stress between the soil and the water phase. The relative percentage of the total load carried by the two phases will depend not only on the compressibility of the soil water, but also on the compressibility of the soil structure. In any case, the effective stress may be calculated by Equation (5).

Partially Saturated Soil

A partially saturated soil is a multi-phase system with the soil structure being surrounded by water, water vapor and air. Nature seldom provides a perfectly dry or a perfectly saturated soil; thus the partially saturated condition is representative of many natural deposits.

Soil water and its role in establishing soil behavior has been and is presently of great concern to the soils engineer. Depending on the controlling forces, soil water has been defined as gravitational water, capillary water and hygroscopic water (40). Hygroscopic water is the water attached to the surface of the soil grains that acts independent of gravity and capillary action. Gravitational water is that water in the soil voids whose movement is controlled by gravity. Capillary water is that water found in the soil voids which is controlled by capillary action. In partially saturated soils the phenomena of surface tension is of importance.

Surface tension is due to molecular forces. In a water-filled container with one or more surfaces exposed to the atmosphere, molecules in the interior of the mass are attracted equally in all directions by surrounding molecules. Molecules on the surface are not attracted equally in all directions since air exerts less of an attraction for water molecules than water. A resultant force exists; it is directed perpendicular to a line tangent to any point on the water surface. This phenomena is referred to as surface tension, the magnitude of which is independent of area but is a function of the form of contact through angle α and temperature.

The rise of water in a fine bore tube is due to surface tension. The height of rise of water in such a tube can be calculated by using statics and expressed as

$$h = \frac{2T_s \cos\alpha}{r} \tag{8}$$

where h = height of water rise in the tube measured from a water surface at atmospheric pressure.

T_s = surface tension.

r = radius of tube opening.

α = angle of contact between the tube wall and water.

γ = unit weight of water.

Taking atmospheric pressure as zero, then the water pressure at the meniscus is related inversely to the curvature of the meniscus regardless of whether the tube is vertical or horizontal. For either case the side walls of the tube are being compressed due to the water stresses. That is, since the capillary tube and the free water surface are exposed to atmospheric pressure, the pressure at the meniscus must be less than atmospheric or negative and equivalent to $-\gamma_\omega h$.
It is also to be noted that for the case of a constant diameter capillary tube the curvature of the meniscus is independent of atmospheric pressure.

If a free water system and a capillary tube were placed in a sealed container and the air pressure increased from atmospheric to u_a, the height of capillary rise h and the curvature of the meniscus would

not change. The pressure at all points in the capillary tube would change by an amount equivalent to the air pressure increase u_a. The pressure in the water at the meniscus would be $u_a - \gamma h$.

The relationship to soils is to consider that the void spaces between soil grains are analogous to the capillary tube. Water wets the grains and is held in the capillary spaces between them due to surface tension. If gravity is neglected; if the soil voids are interconnected and if equilibrium exists, then all the water will be at a pressure

$$u_c = -T_s\left(\frac{1}{r_1} + \frac{1}{r_2}\right) \tag{9}$$

where u_c = capillary pressure.

T_s = surface tension, generally taken as 72 dynes/cm^2 = 10.44×10^{-4}psi.

r_1, r_2 = radius of curvature of two sections formed by passing two planes normal to a plane tangent to a point and at right angles to each other.

Water surface tension is causing the soil grains to be pushed closer together. If for a particular soil skeleton the amount of water is decreased, the smaller the radius of the menisci the greater the capillary force. If for the same soil skeleton the amount of water is increased, curvature of the menisci increases and the capillary pressure decreases. Thus, capillary pressure may be decreased by adding water to the soil or by loading the soil and decreasing the void space.

A partially saturated soil contains air generally at atmospheric pressure. Sealing and loading a sample containing air and water results

in a change in the equilibrium which exists between the two mediums at atmospheric pressure. The major change in equilibrium between the air which contains water vapor and the water which contains air, results from a pressure change within the sample if the testing is done at a constant temperature.

The effect of air pressure on the vapor pressure of an air vapor pressure mixture is small for the pressures normally used in triaxial testing. At an air pressure of 10 atmospheres the ratio of vapor pressure to the vapor pressure of water with no gas except water vapor is 1.007 at 25°C. At the same temperature and a pressure of 700 atmospheres the ratio is 1.67 (41, p. 578).

The effect of temperature on water vapor in contact with a level water surface is as shown below (41, p. 564).

T - °C	Vapor Pressure MM of Hg
20	17.535
21	18.650
22	19.827
23	21.068
24	22.377
25	23.756

The variations in temperature during testing (±1°C) are not considered to alter the soil-water vapor pressure significantly.

The effect of the curvature of the water surface on the vapor pressure can be calculated as follows (41):

p = pressure of the vapor in contact with a flat surface.

P_o = pressures of the vapor in contact with a spherical surface of radius (r).

T_s = surface tension of the liquid, 72.75 at 20°C.

γ = density of the liquid, 0.9984 g/cm^3 at 20°C.

R = gas constant, 4.615 erg/g-°C.

T = temperature °K, 293.1°K at 20°C.

$$\frac{(P-P_o)}{P} = \frac{2T_s}{rRT\gamma} \tag{10}$$

For a temperature of 20°C Equation (6) becomes

$$\frac{r(P-P_o)}{P} = 1.07 \times 10^{-6} \text{ mm.}$$

If r is 0.002 mm, then the ratio of $(P-P_o)$ to P is 0.05 per cent approximately. Therefore, for the conditions of this testing, the vapor pressure of the soil water will be considered independent of the curvature of the meniscus, the temperature and the pressure.

Air is soluble in water. The most important factors influencing the solubility of a gas are temperature and pressure; compression of the gas will increase its solubility; increasing the temperature will decrease solubility. The quantitative relation between solubility and pressure is given by Henry's law which states that the mass of gas dissolved by a given volume of solvent at constant temperature is proportional to the pressure of the gas with which it is in equilibrium. Henry's Law may be expressed in the following way (42): The mass of gas dissolved per unit volume of solvent is really the concentration

in grams per ml and this is proportional to the concentration expressed in moles per liter of solvent or per liter of solution since there is no considerable volume change when the gas dissolves.

According to Henry's law (43),

$$P = HM \tag{11}$$

Where P = partial pressure of air (atmospheres).

H = Henry's constant (atmospheres per mol of air).

M = the number of gram formula weights of the gas in solution to the sum of that number and the number of gram formula weights of the water in which the air is dissolved.

Equation (11) is

$$\frac{P}{H} = M = \frac{\frac{W_d}{28.96}}{\frac{W_d}{28.96} + \frac{W_w}{18.02}}$$

Since the volume of water does not change significantly when air is dissolved (42), then

$$W_d = \frac{1.61\ pW_w}{H} \tag{12}$$

where W_d = weight of dissolved air.

W_w = weight of water.

If V_d is the volume of air dissolved in the water, then by Boyle's law (44)

$$\frac{W_d}{28.96} = \frac{pV_d}{RT} \tag{13}$$

From Equations (12) and (13) with V_w equal to the volume of water

$$\frac{V_d}{V_w} = \frac{RT}{18.015\ (H)} = h = \text{dimensionless.}$$

The variation of h with temperature is shown below:

°C	H(43)	h
15	60,700	0.0216
20	66,400	0.0201
25	72,000	0.0188

The time rate of solution of air in a fluid film unsaturated with air at a given pressure is determined (41) by

$$\frac{\Delta C}{C} = \frac{(C_\infty - C_o)}{C_o}\left(1 - e^{-\frac{\beta A t}{V}}\right) \tag{14}$$

where $\Delta C = C - C_o$.

C = contraction at any time t.

C_o = initial concentration of air in water (t=0).

t = time in minutes.

C_∞ = concentration at very large time.

A = area of water surface, cm^2.

V = volume of water film.

e = 2.71828.

β = coefficient with dimensions, cm/min.

Tabulated values (41, p. 555) of β for oxygen show that for $C_o = 0$ at 20°C, it will require 26 seconds for water to become saturated with oxygen.

It is then assumed that for general triaxial testing the time required for equilibrium of air in water is negligible.

Interaction of Air and Water in a Partially Saturated Soil

The curvature of the menisci has a negligible effect on the air-water interaction. The time required for the water to become saturated with air at a given pressure is small. At the temperature involved in this series testing the magnitude of the vapor pressure of water is approximately 3 per cent of one atmosphere. The effect of an air pressure of 700 atmospheres on the vapor pressure of water has been given as an increase (at 20°C) from 17.5 mm of mercury to 29.2 mm of mercury. The latter figure is less than 4 per cent of one atmosphere and will be neglected.

Water Pressure in a Partially Saturated Soil

Take a formed sample of soil of volume (1+e) with an air volume of V_{ai} at atmospheric pressure of P_a and compress at constant temperature T without drainage to a void ratio of e_1. Assume further that the void ratio change $(e-e_1)$ occurs in the air. The volume of soil water

remains constant at V_w but contains more dissolved air at a void ratio of e_1. The weight of free air is W_f and dissolved air is W_d. Then combining Boyle's and Henry's laws yields (44)

$$W_f(\text{initial}) = \frac{28.96\ P_a V_a(\text{initial})}{RT} \tag{15}$$

$$W_f(\text{final}) = \frac{28.96\ (P_a+u_a)}{RT} \times V_a(\text{final}) \tag{16}$$

$$W_d(\text{initial}) = \frac{28.96}{18.015H}\ P_a \gamma V_w \tag{17}$$

$$W_d(\text{final}) = \frac{28.96}{18.015H}\ (P_a+u_a)\gamma V_w \tag{18}$$

with no drainage

$$W_f(\text{initial}) + W_d(\text{initial}) = W_f(\text{final}) + W_d(\text{final})$$

$$\frac{P_a V_a(\text{initial})}{RT} + \frac{P_a \gamma V_w}{18.015H} = \frac{(P_a+u_a)}{RT}\ V_a(\text{final}) + \frac{(P_a+u_a)\gamma V_w}{18.015H}$$

Setting

$$h = \frac{RT\gamma}{18.015H}$$

then

$$P_a\left(V_a(\text{initial}) + hV_w\right) = (P_a+u_a)\left(V_a(\text{final}) + hV_w\right)$$

$$u_a = P_a \left[\frac{V_a(\text{initial}) - hV_w}{V_a(\text{final}) + hV_w} - 1 \right]$$

and

$$u_a = \frac{P_a \Delta V_a}{V_a(\text{initial}) + hV_w - \Delta V_a} \tag{19}$$

The air pressure required to dissolve the air completely is

$$u_a(\text{saturated}) = \frac{P_a V_a(\text{initial})}{V_w(\text{initial})} \tag{20}$$

The pressure in the pore water of an unsaturated soil which is the pressure in the fluid in contact with the soil skeleton is given by the following formula:

$$u = u_a + u_c$$

where u_c is the water pressure due to surface tension. For normal triaxial testing in the unsaturated condition the air pressure is less than the pressure required for saturation and u_c is negative. Loading the soil with no drainage causes a void ratio change and a change in u_a and u_c. When u_a equals u_a (saturated) the curvature of the water menisci is zero and u_c is zero. The value of u_a can be approximated by Equation (19); u_c can be estimated by Equation (9). Combining Equations (9), (19) and (20) gives an expression for pore water pressure of a partially saturated soil loaded with no drainage.

$$U_w = \frac{P_a \Delta V_a}{V_a(\text{initial}) + hV_w - \Delta V_a} - T_s\left[\frac{1}{r_1} + \frac{1}{r_2}\right] \qquad (21)$$

Shear Strength

The pore water pressure for a three-phase system has two components (see Equation (21)): the pore air pressure and capillary pressure. The former is zero at atmospheric pressure but increases as a function of volume decrease in a sealed sample. The capillary pressure is dependent on the curvature of the meniscus and must be less than atmospheric pressure when the pore air pressure is at atmospheric pressure. When the meniscus has a radius of zero, then the capillary pressure is zero.

It is possible for the pore water pressure in a partially saturated soil to have a positive value. The total fluid pressure in a partially saturated soil is given by

$$u = u_a + u_c.$$

At low values of u_a then u_c is negative or less than atmospheric. However, if u_a exceeds u_c and if the water is saturated with air at the pressure u_a, then u_c must be positive or greater than atmospheric.

The shear resistance of a soil is dependent on the effective stresses. By the Mohr Theory and the effective stress principle, the maximum shear stress that occurs on any plane in a loaded soil mass is

$$\tau = \frac{\bar{\sigma}_1 - \bar{\sigma}_3}{2} \tag{22}$$

where $\bar{\sigma}_1$ and $\bar{\sigma}_3$ are effective normal stresses. Equation 22 may be written in terms of total stresses as

$$\tau = \frac{\sigma_1 - \sigma_3}{2} \tag{23}$$

The effective normal stresses between the soil particles is equal to the difference between the total stress and the pressure on the air and water in the soil voids (see Equation (4)).

The effect of positive pore water pressures on the shear strength of a soil is the same whether water fills the voids or not. That is, a positive increase in pore water pressure will reduce the ability of the soil mass to resist shear. It does not matter whether the soil voids are partially or completely filled with water, only that the water in the voids has a positive pressure. The effect of positive pore water pressures will have no effect on the magnitude of the shear stress in a soil mass (see Equations (22) and (23)).

APPENDIX B

CONSTANT STRESS RATIO TEST

The constant stress ratio loading was carried out by keeping the confining stress ($\sigma_3=\sigma_r$) a constant portion of the applied axial stress ($\sigma_a=\sigma_1$). Consider one extreme case where $\sigma_r = 0$ and $\sigma_a = \sigma$, the unconfined case. For this case the maximum shearing stress is

$$\tau_{uc} = \frac{\sigma}{2} .$$

On the same sample superimpose a confining stress $\sigma_r = \sigma_3$; for example, $\sigma_3 = 0.75\ \sigma_1$. The maximum shearing stress is then

$$\tau_T = \frac{\sigma_1 - \sigma_3}{2} = \frac{\sigma}{8}$$

By the application of the transverse stress σ_3, the shearing stress is reduced, the reduction for the case used being from $\frac{\sigma}{2}$ to $\frac{\sigma}{8}$.

The hydrostatic case previously discussed is another extreme; that is $K = 1$ where $K = \frac{\sigma_r}{\sigma_a}$. For this case the shear stress is zero. Therefore, the application of a transverse confining stress σ_r, simultaneous with an axial compressive stress σ_a, results in the transverse compressive stress combining with an equal part of the axial compressive stress to form a hydrostatic component. Theoretically, the hydrostatic component does not contribute to the shearing stress. The net result is

that in the latter case (σ_r=finite value) the axial compressive stress can be raised to higher values before yielding takes place and the sample has an increase in strength with decreasing yielding for a given stress. Assuming the maximum shear criteria as a failure condition, then compare the shear stress at failure for the unconfined case and the triaxial case where $\sigma_3 = K\sigma_1$ with K taking values from 0 to 1. For this comparison, then

$$\tau_{uc} = \tau_T$$

$$\frac{(\sigma_1)uc}{2} = \frac{\sigma_1 - K\sigma_1}{2}$$

$$\sigma_1 = \frac{(\sigma_1)uc}{1 - K} = \delta(\sigma_1)uc$$

where σ_1 is for the triaxial case and $(\sigma_1)uc$ for the unconfined case. The factor δ represents the amount that the triaxial compression case raises the failure stress above the unconfined case.

For the standard triaxial test, the hydrostatic stress $\sigma_3 = \sigma_r$ is applied and then kept constant while the axial stress $\sigma_a = \sigma_1$ increases. Prior to increasing σ_a, K is unity, but as the test progresses, σ_a increases and K reduces. During the test the hydrostatic component is constant and the shear stress increases as 1/2 the difference in σ_a and σ_r.

In the constant stress ratio test, $K = \frac{\sigma_3}{\sigma_1} = \frac{\sigma_a}{\sigma_r}$ = constant. For such a case the hydrostatic component is not constant and the shear

stress increases with σ_1 as $\tau = \frac{\sigma_1(1-K)}{2}$. Therefore, as K gets larger the shear component becomes smaller and approaches the hydrostatic case. As K becomes smaller the shear stress increases, the extreme being K = 0 or the unconfined case. The difference between the standard triaxial test and the constant stress ratio test essentially is in the portion of the applied stress which acts as the shear component.

In comparing the standard triaxial test with the constant stress ratio test as performed in this study, several limitations will be made. First, σ_r must be compressive and either increasing or constant while σ_a is increasing. With this limitation a stress path in the coordinate system where τ is the ordinate and σ the abscissa can be plotted for any given value of K. For K equal a constant, this stress path will be linear and at a constant inclination α with the σ axis. Taking any point on the K line as the maximum shearing stress on an element, there the normal stress is σ and

$$\tau = \sigma \tan\alpha$$

$$\tau = (\sigma_1 - \tau)\tan\alpha$$

$$\tau = \frac{\sigma_1 \tan\alpha}{1 + \tan\alpha}$$

but

$$\tau = \frac{\sigma_1(1-K)}{2}$$

then

$$\frac{\sigma_1 \tan\alpha}{1 + \tan\alpha} = \frac{\sigma_1(1-K)}{2}$$

and

$$K = \frac{1 - \tan\alpha}{1 + \tan\alpha} .$$

For values of α greater than 45°, K is negative or infinity. For values of α less than 45°, K is positive or zero, which is the limitation previously described. Second, since in the standard triaxial test K is reducing as σ_r is constant and τ and σ_1 increase, while in the constant stress ratio test K is constant as σ_3, σ_1 and τ increase, the initial stress state must be identified for any comparison to be made between the two methods of loading.

In Figure 61(b) a stress path (total stress) for the standard triaxial test with an initial confining pressure of σ_3 is shown as CD, the stress path K_α for a constant stress ratio test is shown as O-P at angle α. Assume the circle is the critical circle and that the stress paths intersect at E where the shearing stress is $\tau_{max.}$ At this intersection the K value for the constant stress ratio test is equivalent to the K value for the standard triaxial test. If a horizontal Mohr envelope passes through E, and α greater than α_1, then for the value of σ_3 used in the standard triaxial test, it would be impossible for the stress paths to intersect. However, if α is less than α_1, then the stress paths would intersect at a τ value less than τ_{max}. For this

case the constant stress ratio loading at failure would have values of σ_3 and σ_1 exceeding those in the standard triaxial test within the initial σ_3 used in this example.

In Figure 61 circle A is the critical circle for constant stress ratio test with $K = K_\alpha$; σ_3 is the confining stress on the critical circle; OP is the Mohr envelope at angle ϕ. For the standard triaxial test, if σ_3 is less than σ_{3K} and $K = K_\alpha$, the constant stress ratio condition will fail at normal stresses greater than those for the standard triaxial loading. If $\sigma_3 > \sigma_{3K}$ and $K = K_\alpha$, then the standard triaxial loading will fail with normal stresses greater than those in the constant stress ratio test. While these statements apply to a particular situation, the results of varying α and the initial conditions for either the standard triaxial or constant stress ratio test can be obtained by showing the conditions on Figure 61(c). Thus it is possible through the Mohr diagram for both laboratory and field loading to compare the constant stress ratio test and the standard triaxial test if the initial stresses and the stress paths are defined.

The relationship between the elastic constants E and Z previously defined, and the K value in the constant stress ratio tests will be discussed by considering an elastic material loaded with a total minor principal stress of $K\sigma$ and a major principal stress σ. By elastic theory the total strain in the sample is

$$\epsilon_t = \frac{1}{E}[\sigma - u(K\sigma + K\sigma)] = \frac{\sigma}{E}(1 - 2uK)$$

In the previous discussion the stresses were separated into total hydrostatic stresses and deviator stresses. By the same reasoning the strains will be separated into one component due to the hydrostatic stress, ε_h, and one component due to the deviator stress, ε_d. Thus, in the sample the stress $K\sigma$ will cause a strain of ε_h and the stress $\sigma(1-K)$ will result in a strain ε_d. Note that the total stress is $K\sigma + \sigma(1-K)$ or σ and the total strain is $\varepsilon_t = \varepsilon_h + \varepsilon_d$. In keeping with the assumption of an elastic material, then $\varepsilon = \frac{\sigma}{E} = \frac{\sigma(1-K)}{E}$. The ratio of ε_d to ε_t is then

$$\frac{\varepsilon_d}{\varepsilon_t} = \frac{\frac{\sigma}{E}(1-K)}{\frac{\sigma}{E}(1-2ZK)} = \frac{(1-K)}{(1-2ZK)}$$

Figure 62 is a plot of the ratio $\frac{\varepsilon_d}{\varepsilon_t}$ as a function of K and different values of Poisson's ratio Z. From Figure 62(a) it is seen that with small values of Poisson's ratio the relationship between $\frac{\varepsilon_d}{\varepsilon_t}$ and K is approximately linear. As Poisson's ratio increases, the relationship is nonlinear and the slope of the plot increases as K increases. The greatest increase in the slope occurs at K values greater than 0.6.

For the same elastic material tested under K constant conditions the axial stress versus axial strain plot is linear and the modulus

$$E_K = \frac{\sigma}{E} = \frac{\sigma}{\frac{\sigma}{E}(1-2ZK)} = \frac{E}{(1-2ZK)} ,$$

indicating that the modulus E_K is directly proportional to Young's modulus E and inversely proportional to the value (1-2ZK). For the

condition of K equivalent to unity, then

$$E_{K-1} = \frac{E}{(1-2Z)}$$

for K less than unity, which is the test condition of interest here, then E_K is greater than E_{K-1}.

Taking the ratio E_K/E_{K-1} yields $\frac{(1-2Z)}{(1-2ZK)}$. As before, assuming values of Z and K and solving for the ratio $E_K/E_{K=1}$ gives the plot in Figure 62. From this plot it is seen that the relationship between E_K/E_{K-1} and K is nonlinear with the slope increasing as K increases. Considering K values above and below 0.6, it is seen that the rate of slope change in the plot of Figure 62(b) is greatest for K values greater than 0.6.

From these considerations it may be that a soil sample, which may only approach the purely elastic condition, would possibly display a more pronounced difference in mechanical properties when the K value is above or below 0.6.

APPENDIX C

SHEAR MODULUS G

Given that

σ_a = major principal stress

σ_r = minor principal stress

σ_θ = intermediate principal stress

ϵ_a = strain in the direction of σ_a

ϵ_r = strain in the direction of σ_r

ϵ_θ = strain in the direction of σ_θ

E = Young's modulus

Z = Poisson's ratio,

then

$$\epsilon_a = \frac{1}{E}[\sigma_a - Z(\sigma_r + \sigma_\theta)]$$

$$\epsilon_r = \frac{1}{E}[\sigma_r - Z(\sigma_a + \sigma_\theta)]$$

$$\epsilon_z = \frac{1}{E}[\sigma_z - Z(\sigma_a + \sigma_\theta)]$$

Assuming $\sigma_r = \sigma_\theta$; $\epsilon_r = \epsilon_z$ and taking the difference $(\epsilon_a - \epsilon_r)$, then

$$(\epsilon_a - \epsilon_r) = [\sigma_a(1+Z) - \sigma_r(1+Z)]\frac{1}{E} \qquad \text{(C-1)}$$

By the theory of elasticity it can be shown that the shear modulus G is

$$G = \frac{E}{2(1+Z)}$$

Solving for E in Equation (C-1) then

$$E = \frac{(\sigma_a-\sigma_r)(1+Z)}{(\epsilon_a-\epsilon_r)} \qquad (C-2)$$

Now

$$G = \frac{\dfrac{(\sigma_a-\sigma_r)(1+Z)}{(\epsilon_a-\epsilon_r)}}{2(1+Z)}$$

and

$$G = \frac{(\sigma_a-\sigma_r)}{2(\epsilon_a-\epsilon_r)}$$

BIBLIOGRAPHY

BIBLIOGRAPHY

(1) Golder, H. Q., "Coulomb and Earth Pressure," *Geotechnique*, 1948.

(2) Collin, A., *Landslides in Clay*, Translated by W. R. Schriever, University of Toronto Press, 1956.

(3) Rankine, W. J. M. "On the Stability of Loose Earth," *Philosophical Transactions*, Royal Society, Part I, Vol. 147-1857, pp. 9-27.

(4) Atterberg, A., "On the Investigation of the Physical Properties of Soils and the Plasticity of Clays," *Int. Mitt. Bodenkunde, 1*, pp. 10.

(5) Burmister, D. M., "The Place of the Direct Shear Test in Soil Mechanics," Symposium on Direct Shear Testing of Soils, ASTM Special Technical Publication 131, 1953.

(6) Bishop, A. W. and Henkel, D. J., "The Measurement of Soil Properties in the Triaxial Test," Edward Arnold, London, 1957.

(7) Hvorslev, M. J., "A Ring Shear Apparatus for the Determination of the Shearing Resistance and Plastic Flow of Soils," *Proceedings International Conference on Soil Mechanics and Foundation Engineering*, Cambridge, Massachusetts, 1936, Vol. II.

(8) "Vane Shear Testing of Soils," *Special Technical Publication 193*, ASTM, 1957.

(9) Canton, J., "Experiments to Prove that Water is Not Incompressible," *Transactions Royal Society*, 1762, pp. 640-643.

(10) Perkins, J., "On the Compressibility of Water and Some Other Fluids," *Transactions Royal Society*, 1764, pp. 261-262.

(11) Parsons, C. A., "Experiments on Carbon at High Temperatures and Under Great Pressures, and in Contact with Other Substances," *Proceedings Royal Society, XLIV* (1888), pp. 320-323.

(12) Richards, T. W., and Stull, W. N., "New Method for Determining Compressibility," Carnegie Institute, Washington (1903), No. 7.

(13) "Bibliography of Publications of P. W. Bridgman," Engineering Supervision Company, January, 1961.

(14) Von Karman, T., "Festigkeitsversuche Unter Allseitigem Druck," *Zeitschrift des Vereines Deutscher Ingenieure, LV,* No. 42 (1911), pp. 1749-1757.

(15) Griggs, D. T., "Deformation of Rocks Under High Confining Pressures," *The Journal of Geology, XLIV* (1936), pp. 541-577.

(16) Handin, J., and Hager, R. V., Jr., "Experimental Deformation of Sedimentary Rocks Under Confining Pressure: Tests at High Temperature," *Bulletin American Association of Petroleum Geologists, XLII,* No. 12 (1958).

(17) Heard, H. C., "Transition from Brittle Fracture to Ductile Flow In Solenhofen Limestone as a Function of Temperature, Confining Pressure, and Interstitial Fluid Pressure," *Geological Society of America,* Memoir 79.

(18) Schwartz, A. E., "An Investigation of the Strength of Rock," Ph.D. Thesis, Georgia Institute of Technology, 1963 (unpublished).

(19) Mazanti, B. B., "The Effect of the Intermediate Principal Stress on the Strength of Rock," Thesis (unpublished) at Georgia Institute of Technology, Atlanta, Georgia, 1967.

(20) Ural, M. V., "An Experimental Study of the Compressibility of Remoulded Clay at HIgh Pressure," M.S. Thesis, University of Illinois, 1945.

(21) Terzaghi, K. and Peck, R. B., *Soil Mechanics in Engineering Practice,* John Wiley and Sons, Inc. (1948).

(22) Smith, C., "Soil Properties of Fort Union Clay Shale," *Proceedings of the Third International Conference on Soil Mechanics, VI* (1953), p. 66.

(23) Esrig, M. E., Davison, M. T., and Peck, R. B., "Report on Consolidation of Soils Under High Pressures," University of Illinois Engineering Experiment Station (unpublished report).

(24) Chilingar, G. V., and Knight, L., "Relationship Between Pressure and Moisture Content of Kaolinite, Illite, and Montmorillite Clays," *Bulletin American Association of Petroleum Geologist, XLIV* (January, 1960) pp. 101-106.

(25) DeBeer, E. E., "The Scale Effect in the Transposition of the Results of Deep-Sounding Tests on the Ultimate Bearing Capacity of Piles and Caisson Foundations," *Geotechnique, XIII* (1963), pp. 39-75.

(26) Blanks, R. F., and McHenry, O., "Large Triaxial Testing Machine Built by Bureau of Reclamation," *Engineering News Record, CXXXV* (1945), p. 6.

(27) Golder, H. O., and Akroyd, T., "An Apparatus for Triaxial-Compression Tests at High Pressures," *Geotechnique, IV* (1954), No. 4.

(28) Hirschfeld, R. C., "Report on Investigation of Permeability, Consolidation and Strength Characteristics of Soil from Foundation of Cannonsville Dam," (unpublished) Cambridge, Massachusetts. Harvard University, 1961.

(29) Hirschfeld, R. C., and Poulos, S. J., "High Pressure Triaxial Tests on a Compacted Sand and an Undisturbed Silt," Laboratory Shear Testing of Soil, ASTM-STP, No. 361, 1963.

(30) Hall, E. B., and Gordon, B. B., "Triaxial Testing with Large-Scale High Pressure Equipment," Laboratory Shear Testing of Soils, ASTM-STP No. 361, 1963.

(31) "Tester 'Buries' Soil 500 Feet Deep," *Engineering News Record,* July 18, 1963.

(32) Barksdale, R. D., "High Pressure Testing of Sands," (unpublished) Test Performed at the Georgia Institute of Technology, Atlanta, Georgia (1963).

(33) Vesic, A. B., and Barksdale, R. D., "On Shear Strength of Sand at Very High Pressures," Prepared for the Symposium on Laboratory Shear Testing of Soils, Ottawa, Canada (September, 1963) (unpublished).

(34) Clough, G., "An Investigation of the Shear Strength of Sand at High Pressures," Thesis (unpublished), Georgia Institute of Technology, Atlanta, Georgia.

(35) Patterson, M. S., "Triaxial Testing of Materials at Pressures up to 10,000 Kg/Sq.Cm.(150,000 lb/sq.in.)," *The Journal of the Institution of Engineers, XXXVI,* No. 1-2, Australia (January-February, 1964), pp. 23-27.

(36) Bishop, A. W., Webb, D. L., and Skinner, A. E., "Triaxial Tests on Soil at Elevated Cell Pressures," *Proceedings of the Sixth International Conference on Soil Mechanics and Foundations Engineering, VI* (1965), p. 170.

(37) Vesic, A. S. and Clough, G. W., "Behavior of Granular Materials Under High Stresses," *Proceedings of the American Society of Civil Engineers, Journal of the Soil Mechanics and Foundations Division*, Vol. 94, SM3, May, 1968.

(38) Bishop, A. and Eldin, A., "Undrained Triaxial Tests on Saturated Sands and Their Significance in the General Theory of Shear Strength," *Geotechnique*, Vol. 2, No. 1, p. 13-32.

(39) Yong, R. and Warkentin, B., *Introduction to Soil Behavior*, Macmillan Publishing Co., 1966.

(40) Briggs, L. J., "The Mechanics of Soil Moisture," *Bull. 10, U. S. Department of Agriculture, Division of Soils*, Washington U. S. Gov. Printing Office, 1897.

(41) Dorsey, N. E. (Compiler), *Properties of Ordinary Water Substances*, New York, Reinhold Publishing Co., 1949.

(42) Glasstone, D., *Textbook of Physical Chemistry*, Van Nostrand Co., Inc., p. 696-97, 1946.

(43) Perry, J. E. (ed.), *Chemical Engineers Handbook*, 2nd Edition, McGraw-Hill Co.

(44) Hilf, J. W., "An Investigation of Pore-Water Pressure in a Compacted Cohesvie Soil," *Tech. Memo 654*, U. S. Dept. of Interior Bureau of Rec., Denver, Colo., 1956.

(45) Ladd, C. C., "Shear Strength of Cohesive Soils," *Chicago Sect., ASCE, Soil Mech. Lecture Series*, 1966.

(46) Terzaghi, K. and Peck, R., *Soil Mechanics in Engineering Practice*, John Wiley, 1969, 2nd Edition.

(47) Bishop, A. and Bjerrum, L. "The Relevance of the Triaxial Test to the Solution of Stability Problems," *ASCE Research Conference on Shear Strength of Cohesive Soils*, 1960.

(48) Casagrande, A., and Hirschfeld, R., *Harvard Soil Mech. Series #65*, pp. 31-36.

(49) Sowers, G. B., and Sowers, G. F., *Introduction Soil Mechanics and Foundation*, Macmillan Pub. Co., 1970, 3rd Ed.

(50) Casagrande, A. and Hirschfeld, R., *Harvard Soil Mechanics Series #61*, 1960.

(51) Chen, "An Investigation of Stress-Strain and Strength Characteristics of Cohesionless Soils by Triaxial Compression Tests," *Proceedings 2nd Int. Conf. on Soil Mech. and Found. Engr.*, V5, 194B.

(52) Bridgeman, P. W., "Studies in Large Plastic Flow and Fracture with Special Emphasis on the Effects of Hydrostatic Pressure, 1st ed. (Metallurgy and Metallurgical Engineering Series), McGraw-Hill Book Co., Inc., New York, 1952.

(53) Skempton, A. W., "The Pore Pressure Coefficients A and B," *Geotechnique*, Vol. 4, No. 4, p. 143-147.

(54) Bishop, A. and Henkel, D., *The Triaxial Test*, Edward Arnold Publishing Co., London, 1962.

(55) Lee, K. and Haley, S., "Strength of Compacted Clay at High Pressure," *JSMFD, Proc. ASCE*, Nov., 1968.

VITA

Clyde Nelson Holland was born on June 30, 1933, in Boyce, Virginia. He graduated from Clark County High School, Berryville, Virginia, in 1952. After studying pre-engineering at Emory and Henry College, Emory, Virginia, he entered Virginia Polytechnic Institute in Blacksburg, Virginia, in 1954. He received a Bachelor of Science in Civil Engineering from Virginia Polytechnic Institute in 1957, and a Master of Science with a major in Civil Engineering from Duke University in 1961. Mr. Holland is a registered civil engineer and has for a number of years acted as a private consultant in soil mechanics and foundations engineering. He has also held the position of Assistant Professor of Civil Engineering at Duke University, Instructor and Research Associate at the Georgia Institute of Technology, and Associate Professor of Civil Engineering at the University of Tennessee at Knoxville, Tennessee. Presently Mr. Holland is Associate Professor of Civil Engineering at Northern Arizona University, Flagstaff, Arizona.